Modelling, Estimation and Optimization of the Methanol Synthesis with Catalyst Deactivation.

Ingvild Løvik

A thesis submitted in partial fulfilment of the degree of Doktor Ingeniør

Norwegian University of Science and Technology
Department of Chemical Engineering

March 2001

Summary

This thesis studies dynamic modelling, estimation and optimization of the methanol synthesis with catalyst deactivation. Conversion of natural gas is of special interest in Norway for both economic and political reasons. In June 1997 Statoil opened a methanol plant at Tjeldbergodden. It is among the largest in the word with a capacity of 830 000 metric tons per year, which equals 1/4 of Europe's capacity. Methanol is today mainly used as a building block to produce chemical intermediates, and it is also a promising fuel for fuel cells.

The overall theme for this thesis is to find the optimal operation of the methanol synthesis when undergoing catalyst deactivation by dynamic optimization. There has been an increase in method development, tool development and industrial use of dynamic optimization in the past decade. Few realistic, large-scale applications with nonlinear, first principle models, exist apart from this thesis.

A rigorous pseudo-steady state model of the total methanol synthesis loop is developed. The model has been verified against a design flow sheet and to some extent, validated against process data. Overall, good agreement was found.

Optimal operation policy of the methanol synthesis is found by dynamic optimization. Both the reactor and the reactor system with recycle are studied, and it is shown that the total reactor system with recycle must be considered to find the optimal operating policy. It is also shown that a heterogeneous reactor model gives different optimal policy and more accurate results than a pseudohomogeneous reactor model. Optimization of the loop leads to USD 3 165 000, or 0.75 per cent, increased profit over four years compared to a selected reference case with a constant operation policy. Optimal operation policy is compared with an operating procedure recommended for the Tjeldbergodden methanol plant. The calculated optimal operation policy gives higher profit. However, there are two important advantages of optimization: The ability to find the optimal operation if some of the variables in the optimization problem change, and the ability to track changes in the process by model updating and repeated optimization.

During modelling and optimization, it became evident that a good industrial-scale deactivation model is needed for the methanol synthesis. The sensitivity in the dynamic optimization of the methanol synthesis is analysed with regards to the deactivation model by a first order error propagation - approach. It is found that 20 per cent standard deviation in the deactivation parameters is sufficient for optimization purposes.

A deactivation model for the methanol synthesis catalyst is estimated from historic process data from a methanol plant. A model on the generalized power law form was successfully fitted to process data from a limited period of time. The estimated model is of second order. No measurable effect of water was found, probably because the variations in the feed compositions were too small. The model parameters found are confidential, and are not valid for the total catalyst lifetime because the deactivation process is fast in the beginning and slower after some time. It is necessary to use data from a longer period of time to obtain a model that is valid over the total catalyst lifetime.

The work presented in this thesis serves as a framework for the implementation of dynamic optimization in the control system of a methanol synthesis plant. The dynamic optimization should be implemented in the optimization layer of the control system with feedback to update the activity. A new catalyst deactivation model should be estimated whenever the commercial catalyst type is changed. A shrinking horizon algorithm with repeated optimization is proposed.

The main contribution in this thesis is a realistic, large-scale case study on modelling, estimation and dynamic optimization. Several researchers have studied optimal operation of fixed bed reactors experiencing catalyst deactivation. This work adopts an approach which is more realistic. A rigorous model of the total reactor system with recycle, with varying model parameters and thermodynamic properties is used. A thorough analysis of the process is enployed to formulate the optimization problem. The actual time varying control variables in the reactor system, the recycle rate and coolant temperature, are optimized with regards to an economic objective, and path constrains on the reactor temperature are considered. An optimal operation strategy for the methanol synthesis has not been published before. Similar studies have probably been performed in industry without being published.

Acknowledgements

I wish to thank my supervisor Professor Terje Hertzberg, Department of Chemical Engineeing, Norwegian Univerisity of Science and Technology (NTNU), for his support, advice and positive attitude.

The project woud have been less interesting without the collaboration with Statoil Research Centre. I appreciate this, and thank Magne Hillestad for contribution to the focus and problem analysis in this work, Ola Olsvik, Morten Rønnekleiv and Margrete Hånes Wesenberg for their assistance on deactivation model estimation, and Roger Hansen for interesting discussions.

I acknowledge the assistance of Stewart Clark from the Administration, NTNU for his comments and advice on the English language in this thesis.

I received a three-year scholarship from the Research Council of Norway's programme *Chemical conversion of natural gas*. In addition, I received financial support from Statoil, the Department of Chemical Engineering and the strong point centre in Process Systems Engineering. I am grateful for all these sources for their financial support.

Most of all, I thank Thomas for his encouragement and understanding, and all my friends in Trondheim for a good time.

Contents

List of Figures

List of Tables

Notation

Symbol	Definition	Unit
A	Heat transfer area in heat exchanger	m^2
A_i	Parameter in correlation for heat capacity	$J/molK$
a	Catalyst activity	
a_0	Initial catalyst activity	
a_{eq}	Limiting catalyst activity	
a^1_{init}	Parameter in Equation 6.3	
a^2_{init}	Parameter in Equation 6.3	
$\tilde{a}$	Effective catalyst activity	
B_i	Parameter in correlation for heat capacity	$J/molK^2$
C_i	Parameter in correlation for heat capacity	$J/molK^3$
C	Total concentration	mol/m^3
C_{p_g}	Heat capacity in gas phase	kJ/kgK
$Cov(f,g)$	Covariance between variables f and g	
$D_b^{i,j}$	Binary diffusion coefficient, components i and j	m^2/s
D_e^i	Effective diffusion coefficient in pellet, component i	m^2/s
D_i	Parameter in correlation for heat capacity	$J/molK^4$
D_k^i	Knudsen diffusion coefficient, component i	m^2/s
D_m^i	Multicomponent molecular diffusion coefficient, component i	m^2/s
E_d	Activation energy for deactivation	J/mol
F	Process stream, separator feed	$kmol/s$
F_{MeOH}	Production of methanol from reactor or loop	ton/day
$F_{Steam,MP}$	Net production of MP steam	kg/h
$F_{Steam,LP}$	Net production of LP steam	kg/h
f_i	Fugacity of component i	bar
$f(x,y)$	Differential equations	
$g(y)$	Algebraic equations	
g_z	Jacobian matrix of g	
H	Molar enthalpy	J/mol
H^i_{ref}	Molar enthalpy, component i	J/mol
$-\Delta H^j_{rx}$	Heat of reaction, reaction j	J/mol
$h_{i,g}$	Heat transfer coefficient on the inside of the tube wall, gas phase	kW/m^2K
$h_{i,s}$	Heat transfer coefficient on the inside of the tube wall, solid phase	kW/m^2K
$h_{o,c}$	Heat transfer coefficient on the outside of the tube wall to cooling water	kW/m^2K
K_d	Deactivation rate constant	day^{-1}
K^j_{eq}	Equilibrium constant, reaction j	$bar^{\Sigma\nu_j}$
K_i	Equilibrium constant, elementary reaction i or Equilibrium adsorption constant, component i	$bar^{\Sigma\nu_j}$
k_{dyn}	Dynamic contribution to effective conductivity	kW/mK
k^i_g	Mass transfer coefficient from pellet to gas, component i	m/s
k_g	Conductivity, gas phase	kW/mK
k_j	Reaction rate constant, reaction j	$mol/kgsbar^{n_j}$
$k_{i,j}$	Binary interaction coefficient in SRK equations, components i and j	
k_a	Parameter in the kinetic model	$bar^{-1/2}$
k_b	Parameter in the kinetic model	bar^{-1}
k_c	Parameter in the kinetic model	
k_d	Parameter in the kinetic model	$mol/kg\ s\ bar^2$
k_e	Parameter in the kinetic model	$mol/kg\ s\ bar$
$k_{r,g}$	Effective radial conductivity, gas phase	kW/mK

Symbol	Definition	Unit
$k_{r,s}$	Effective radial conductivity, solid phase	kW/mK
k_s	Conductivity in pellet	kW/mK
k_{stat}	Static contribution to effective conductivity	kW/mK
k_w	Conductivity in tube wall	kW/mK
L	Liquid stream from separator	$kmol/s$
L_r	Reactor length	M
l_r	Axial reactor coordinate	M
M'	Mass flux	kg/sm^2
M	Mass stream	kg/s
Mw^i	Molar weight, component i	$kg/kmol$
m	Deactivation order	
n	Parameter in Equation 6.1	
n_c	Number of component	
n_{is}	Number of inlet streams	
n_j	Reaction order, reaction j	
n_r	Number of reactions	
n_t	Number of reactor tubes	
n_{us}	Number of outlet streams	
ne	Number of experiments	
nm	Total number of measurements	
nm_{ij}	Number of measurements of variable j in experiment i	
nv_i	Number of variables in experiment i	
P	Reactor pressure	bar
P	Objective function	\$ or $ton(metric)$
P_c^i	Critical pressure, component i	bar
Pr	Prandtl number	
Pr_c	Prandtl number in cooling water	
p_i	Partial pressure, component i	bar
p_{MeOH}	Price of methanol	$\$/ton(metric)$
p_{Steam}	Price of steam	$\$/ton(metric)$

Symbol	Definition	Unit
P_s	Pressure in pellet	bar
p_s^i	Partial pressure i pellet, component i	bar
$p_{s,s}^i$	Partial pressure on the pellet surface, component i	bar
Q	Heat transferred in heat exchanger	W
Q_{comp}	Compressor duty	W
Q_{comp}^{ref}	Compressor duty in reference case	W
$Q_{c,reactor}$	Heat removed from the reactor	W
R	Recycle rate	$kmol/kmol$
R_g	Gas constant	$kJ/kmolK$
R_p	Catalyst pellet radius	m
R_{pore}	Mean pore radius in catalyst	m
R_r	Reactor tube radius, inside	m
$R_{r,y}$	Reactor tube radius, outside	m
Re	Reynolds number	
Re_c	Reynolds number in cooling water	
r	Radial coordinate in reactor	m
r_p	Radial coordinate in pellet	m
r_j	Rate of reaction, reaction j	mol/kgs
$\tilde{r}_j$	Actual rate of reaction in gas phase, reaction j	mol/kgs
r_j^s	Rate of reaction in pellet, reaction j	mol/kgs
$r_j^{obs,global}$	Global observed rate of reaction in gas phase, reaction j	mol/m^3s
Sc^i	Schmidt number, component i	
T	Reactor temperature	K
$\overline{T}$	Reactor temperature averaged over r	K
T_0	Reference temperature in catalyst deactivation	K
T_c	Cooling water temperature	K

Symbol	Definition	Unit
T_c^i	Critical temperature, component i	K
$T_c(i)$	Discretized cooling water temperature, interval i	K
T_{eq}^j	Equilibrium temperature	K
ΔT_{eq}^j	Approach to equilibrium temperature	K
$T_{hutting}^i$	Hutting temperature, component i	K
T_m^i	Measurement number i of reactor temperature	K
$T_{melting}^i$	Melting point, component i	K
$T_{r,max}$	Maximum reactor temperature	K
T_{ref}	Reference temperature for enthalpy	K
T_s	Pellet temperature	K
T_{tamman}^i	Tamman temperature, component i	K
U	Heat transfer coefficient in heat exchanger	W/m^2K
U_{eff}	Effective heat transfer coefficient	
	from $\overline{r}$ to cooling water	KW/m^2K
$U_{w,g}$	Heat transfer coefficient from inside of the wall	
	to cooling water, gas phase	KW/m^2K
$U_{w,s}$	Heat transfer coefficient from inside of the wall	
	to cooling water, solid phase	KW/m^2K
u_g	Linear gas velocity	m/s
V	Vapour stream from separator	$kmol/s$
V^i	Diffusion volume, component i	m^3
$Var(f)$	Variance of variable f	
X_{MeOH}	Conversion of methanol	
x	Dimensionless radial coordinate in pelletr_p/R_p,	
	or state variable	
x_i	Mole fraction in liquid phase, component i	
y	Algebraic variable	
y_i	Mole fraction in gas phase, component i	
z	Dimensionless axial coordinate in reactor l_r/L_r	
z_i	Mole fraction in separator feed, component i	

Symbol	Definition	Unit
z_{ijk}	Measurement k of variable j in experiment i	
$\tilde{z}_{ijk}$	Estimate of measurement k of variable j in experiment i	
α	Step length	
δ	Newton step	
γ	Adiabatic coefficient	
ϵ	Void fraction in catalyst bed	
ϵ_s	Porosity of catalyst	
η	Effectiveness factor of catalyst	
η_m	Mechanic efficiency	
η_p	Polytropic efficiency	
θ_i	Fractional coverage on catalyst surface, component i	
θ	Parameters to be estimated	
μ	Viscosity	N/sm
ν_{ij}	Stoichiometric coefficient, component i, reaction j	
$\Sigma\nu_j$	Stoichiometric sum, reaction j	
σ_f	Standard deviation of variable f	
Φ	Maximum likelihood function	
Φ_{liq}^i	Fugacity coefficient in liquid phase, component i	Pa
Φ_{vap}^i	Fugacity coefficient in gas phase, component i	Pa
ρ_g	Gas density	kg/m^3
ρ_p	Catalyst density	kg/m^3
ρ_s	Catalyst bulk density	kg/m^3
$\rho_{f,g}$	Correlation coefficient between variables f and g	
τ	Turtuosity factor for catalyst	
ω	Acentric factor	

Chapter 1

Introduction

This thesis studies modelling, estimation and optimization of the methanol synthesis with catalyst deactivation. In this chapter, an introduction to natural gas conversion, methanol and dynamic optimization is given to explain the motivation fo this work. The aims of the work are presented, and finally an outline of the thesis is given.

1.1 Motivation

1.1.1 Natural gas conversion

Conversion of natural gas is of special interest in Norway for both economic and political reasons. Norway has large occurrences of natural gas under the seabed along its coast. The following data is taken from NFR (2000). The extractable gas reserves are estimated to 6 665 million m^3. The gas fraction of the total petroleum production will increase. The main options for the use of natural gas are; export to Europe by pipelines, power production and conversion to petrochemicals like methanol. Many of the new gas fields are located too far north for export of the gas to Europe by pipelines. Small occurrences of associated gas are currently being flared, contributing to 11 per cent of Norway's CO_2 emissions. Both types of gas occurrences are called 'stranded gas'. Introduction of gas power plants in Norway are controversial because of the CO_2 emissions. Norway has promised to stabilize and reduce its CO_2 emissions through the Kyoto agreement. Chemical conversion is a good alternative, in some cases also 'stranded gas'. Conversion increases the value of the raw material 3 - 10 times. Future energy carriers such as hydrogen and methanol can be produced by the conversion of natural gas. The political interest in gas conversion is shown in

the Research Council of Norway's programmes *Governmental R&D-Programme for Utilization of natural gas (SPUNG)* (1987 - 1992), *Chemical conversion of natural gas* (1992 - 1999) and *Natural gas* (1997 - 2002). Natural gas can be converted to many products. The main commercially routes are methanol and ammonia via synthesis gas.

In June 1997 Statoil opened a methanol plant at Tjeldbergodden. It is among the largest in the word with a capacity of 830 000 metric tons per year, which equals 1/4 of Europe's capacity (Statoil 2000*b*). It is the first example of industrial scale natural gas conversion in Norway.

1.1.2 Methanol

Methanol is a primary liquid petrochemical. It is used as fuel, as solvent and as a building block to produce chemical intermediates.

36 per cent of today's methanol demand is used to produce formaldehyde. Products like urethane foam, spandex fibres and adhesives in laminated wood are made from formaldehyde. Production of acetic acid accounts for 8 per cent of the methanol demand. Telepthalic acid (PTA), vinyl acetate monomer (VAM) and solvent esters are derivatives of acetic acid. PTA is used to produce polyester fibres and polyethylene telephtalate (PET) for recyclable beverage bottles. VAM is used in water-based paints and coatings. 29 per cent of the methanol demand goes to methyl tertiary butyl ether (MTBE). MTBE is used as a source of oxygen and as an octane enhancer in gasoline, and can replace lead and aromatics. The market for MTBE in the United States is uncertain. MTBE will be prohibited in California from 2002 because the ground water in California is contaminates by MTBE from leaking underground gasoline tanks. The marked for MTBE in the European Union is promising because new regulations about cleaner burning gasoline become effective in 2005. Methanol is also used as fuel in Indy race cars, and blends of gasoline and methanol are used as fuel in flexible fuel vehicles. Other uses of methanol are production of silicone and acrylic polymers. The information on current methanol use is taken from Methanex (2000*b*).

Methanol is the most promising fuel for fuel cells (Methanex 2000*a*, Statoil 2000*a*). A fuel cell converts chemical energy directly into electrical energy. Hydrogen is the 'dream' fuel for fuel cells because the only reaction product is water. The Direct Hydrogen Fuel Cell (DHFC) technology is well developed. However, there are many unsolved problems with production, storage, transportation and

safety of hydrogen gas. There are two alternatives for the use of methanol in fuel cells; Reformed Methanol Fuel Cell System (RMFCS), where methanol is steam reformed to provide hydrogen to a fuel cell engine, and Direct Methanol Fuel Cell (DMFC) where methanol is used as the reducing agent in the fuel cell engine. Reforming of methanol is considered to be the easiest way to supply hydrogen from a liquid fuel. The RMFCS is technologically mature and is expected to reach the market in five years. The emissions of CO_2 on a life cycle basis from fuel cell vehicles will be reduced by 42 per cent compared to today's gasoline vehicles. Several producers have developed methanol driven fuel cell vehicles with this technology. Methanex and Statoil have started a pilot programme on the supply, distribution and marketing of methanol for fuel cell vehicles (Statoil 2000*a*). Pilot programmes on domestic and industrial use of methanol driven fuel cells are also started by the two companies and Northwest Power Systems (Statoil 2000*c*). The DMFC eliminates the need for a methanol reformer, which reduces the cost and weight of the fuel cell engine. This technology is 3 - 4 years behind hydrogen fuel cells.

1.1.3 Dynamic optimization

Steady state simulations and optimization are everyday use in all parts of the process industry. The increased competition and stricter environmental regulations have led to a need for better design and operation of the processes, and further improvements demand considerations of the dynamic aspects of the process. Dynamic simulation with first principles nonlinear process models are used increasingly in all phases of a project's life, from conceptual design to operation and control, see e.g. Naess *et al.* (1993). It is natural to look for model-based applications that can exploit the resources invested in development of dynamic models.

> *In fact, many of the oft quoted applications of dynamic simulation technology are more properly formulated as dynamic optimization problems; i.e., systematic improvements of a dynamic system's performance using optimization techniques as opposed to ad hoc improvements using simulation based 'what if' studies.* Barton (1998)

Dynamic optimization is used to improve both design and operations of processes. There has been an increase in method development, tool development and industrial use of dynamic optimization the last decade. The investment cost needed to improve operation is generally low, leading to short pay back times. The major obstacle for the use of model-based tools is the lack of detailed knowledge of the process. Dynamic optimization is mainly used in industries with hight volumes and well understood processes, like the oil/gas and petrochemical industry. The added value from raw materials and utilities to products are small per unit, making even a small decrease in production cost per unit valuable. Dynamic optimization has a large potential in:

- Start-up and shut-down
- Moving from one steady state to another
- Optimization of batch processes
- Optimization of constrained processes
- Design optimization of distributed parameter systems

Dynamic optimization can be used both off-line and on-line. The off-line is use for example to find optimal trajectories for batch runs. The on-line use is usually termed *model predictive control* (MPC), and is used to control the process in an economically optimal manner. Model predictive control is only one of many optimization levels in an advanced production facility, see Table 1.1. MPC in industry is dominated by linear step response models. The reason for the industrial success of linear MPC is its simple structure and its ability to directly incorporate constrains (Strand 1991). Further improvements can be obtained by allowing for first principles nonlinear process models, constrains and objective function in the optimizations (Vassiliadis 1993, Strand 1991, Bequette 1991). This approach is taken in this thesis. Nonlinear dynamic optimization problems are difficult and time-consuming to solve.

Table 1.1
Optimization and control levels in a refinery

Level	Model	Optimization	Update intervals
Site	Static, linear	LP	Weekly
Section	Static, linear	NLP	Hours
Unit/Section	Dynamic, nonlinear	MPC	Minutes
Unit	None	Basic control	Seconds

1.2 Aims

The overall theme for this thesis is to find the optimal operation of methanol synthesis undergoing catalyst deactivation. The aims of the work are:

- Demonstrate methods of modelling, dynamic optimization and model estimation on a realistic large-scale industrial case.
- Develop a framework for dynamic optimization that can be implemented in the operation of a methanol synthesis plant with feedback from the process.
- Estimate a catalyst deactivation model from process data.
- Contribute to better understanding of the methanol synthesis:
  - The long-term dynamic effects
  - Optimal time-varying operation
  - Catalyst deactivation

1.3 Outline

The thesis is written in the form of a book, with common references, appendix and notation list. Parts of Chapters 4, 5 and 6 have previously been published (Løvik *et al.* 1998, Løvik *et al.* 1999, Løvik *et al.* 2000, Løvik *et al.* 2001). Implementing details, detailed process design and process measurements have been avoided in the thesis. The first reason for this is to focus on the methods and results, and the second is that some details are confidential information to Statoil.

Chapter 2 gives a literature survey of the methanol process with special focus on deactivation of the $Cu/Zn/Al_2O_3$ catalyst.

Chapter 3 presents the development of a rigorous model of the methanol synthesis loop with deactivation. The model is used throughout the remainder of the thesis.

Chapter 4 studies dynamic optimization of the methanol synthesis undergoing catalyst deactivation. The operating policy must change with time to counteract the adverse effect of catalyst deactivation on the process yield.

Chapter 5 analyses the sensitivity of the dynamic optimization in Chapter 4 with respect to the deactivation model.

Chapter 6 deals with the development of a deactivation model for the methanol synthesis catalyst based on historical process data from a methanol plant.

Chapter 7 gives an overall conclusion of the thesis and directions for future work.

Chapter 2

Literature Survey of the Methanol Process

This chapter gives an overview of the methanol process with special focus on catalyst deactivation of the $Cu/Zn/Al_2O_3$ catalyst.

2.1 Process description

The methanol process consists of three parts; synthesis gas preparation, the methanol synthesis and methanol distillation. The following introduction is based on Lange (2001) and Skrzypek *et al.* (1994). The first technology, the high-pressure synthesis, was commercialized in 1923. It operated above 300 bar and used a Cr-based catalyst. The low-pressure methanol synthesis replaced the high-pressure methanol synthesis in the 60s. The low-pressure process resulted from the formulation of a new and more active Cu-based catalyst, and the ability to produce a sulphur-free synthesis gas. The low-pressure synthesis operates between 50 and 100 bar. Two low-pressure methanol processes dominate the market; the ICI process uses multi-bed synthesis reactors with feed-gas quench cooling and the Lurgi process uses multitubular synthesis reactors with internal cooling. The synthesis gas is a mixture of CO, CO_2 and H_2 that can be produced form different feed stocks: natural gas, higher hydrocarbons and coal. The conventional process for synthesis gas production is steam reforming, but partial oxidation, CO_2 reforming, autothermal reforming or combinations are also used.

The case studied in this work is Statoil's methanol plant at Tjeldbergodden in Norway, with focus on the methanol synthesis loop. The technology at Tjeldbergodden is Lurgi's Low Pressure Methanol Process with combined reforming of oil associated natural gas (Lurgi 1995, *Methanol* 1997). The essential process steps are shown in Figure 2.1.

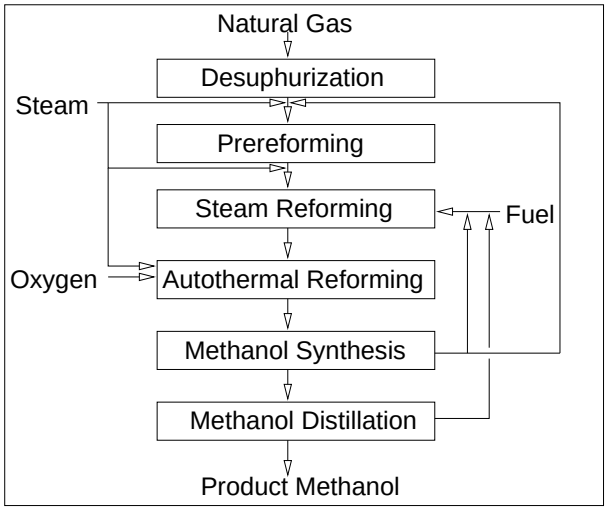

Figure 2.1. Essential process steps in Lurgi's low-pressure methanol process

The natural gas is first desulphurized and saturated with process steam, then reformed in three steps; prereforming, steam reforming, and autothermal reforming. A Ni-based catalyst is used in all reformer steps. The following overall reactions occur in the synthesis gas preparation:

$$C_nH_m + nH_2O \rightarrow nCO + (n + \frac{m}{2})H_2 \tag{2.1}$$

$$CH_4 + H_2O \rightleftharpoons CO + 3H_2 \qquad -\Delta H_{rx,298K} = -206\ kJ/mol \tag{2.2}$$

$$CH_4 + \frac{1}{2}O_2 \rightleftharpoons CO + 2H_2 \qquad -\Delta H_{rx,298K} = 35\ kJ/mol \tag{2.3}$$

Steam reforming of higher hydrocarbons (Equation 2.1) is irreversible and endothermic. Steam reforming of methane (Equation 2.2) is endothermic and partial oxidation of methane (Equation 2.3) is slightly exothermic. The water-gas shift reaction (Equation 2.4), occurs in all the reformer steps:

$$CO + H_2O \rightleftharpoons CO_2 + H_2 \qquad -\Delta H_{rx,298K} = 40\ kJ/mol \tag{2.4}$$

In the prereformer, higher hydrocarbons are converted to methane by steam reforming and methanation (reverse of Equation 2.2) in an adiabatic reactor. In the steam reformer, parts of the methane are converted to synthesis gas by the highly endothermic steam reforming reaction. The reaction energy is supplied from the burning of natural gas outside the catalyst tubes in a multitubular reactor. The remaining methane is converted to synthesis gas in the autothermal reformer. The autothermal reformer has a burner in the top where oxygen is mixed with partly converted synthesis gas. Gas phase combustion of hydrogen and carbon monoxide raises the heat to 1000 - 1200 ^oC. Hydrogen and carbon monoxide are oxidized to water and carbon dioxide, which take part in steam reforming and dry reforming of methane ($CH_4 + CO_2 = 2CO + 2H_2$) in the lower catalyst zone of the reactor. The heated gas supply reaction heat for the endothermic reforming in the catalyst zone. The conditions at the reactor exit are 35 bar and 960 ^oC. The total reaction in the autothermal reformer can be expressed as partial oxidation of methane. The oxygen is supplied from an air separation unit. The composition of synthesis gas is characterized by the stoichiometric number for the methanol synthesis:

$$SN = \frac{H_2 - CO_2}{CO + CO_2} \tag{2.5}$$

An SN-number of 2 means that the reactants are present in stoichiometric equivalent amounts, see Equation 2.6 and Equation 2.4. The optimal SN-number is 2.05, i.e. a small surplus of hydrogen. The SN-number is adjusted by the oxygen/steam ratio to the autothermal reformer. The synthesis gas is cooled and compressed to 80 bar before the methanol synthesis.

In the methanol synthesis, synthesis gas is converted to methanol over a $Cu/Zn/Al_2O_3$ catalyst. The following strongly exothermic reaction occurs together with the water-gas shift reaction (Equation 2.4):

$$CO_2 + 3H_2 \rightleftharpoons CH_3OH + H_2O \qquad -\Delta H_{rx,298K} = 50\ kJ/mol \tag{2.6}$$

A flow sheet of the methanol synthesis loop is given in Figure 2.2. In the Lurgi reactor, the catalyst is packed in vertical tubes surrounded by boiling water. The reaction heat is transferred to the boiling water and steam is produced. Efficient heat transfer gives small temperature gradients along the reactor. Typical operating conditions are 523 K and 80 bar. The reactor temperature is controlled by the pressure of the boiling water. Because of

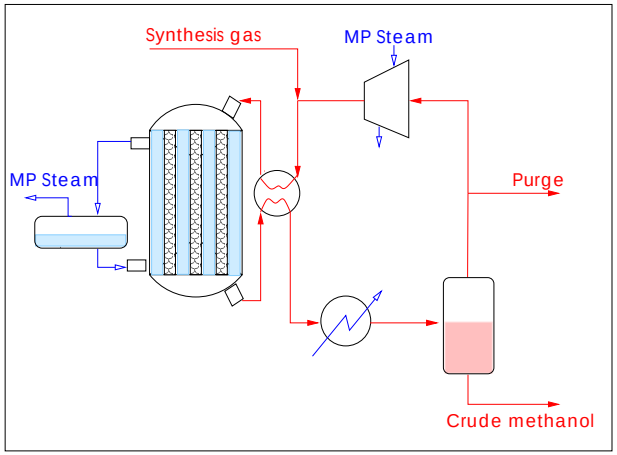

Figure 2.2. Flow sheet of Lurgi's methanol synthesis loop

the quasi-isothermal reaction conditions and high catalyst selectivity, only small amounts of by-products are formed. Methanol conversion is limited by equilibrium. Unreacted synthesis gas is separated from crude methanol, then compressed and recycled. A portion of recycle gas is purged to remove inerts. The H_2-rich purge stream is partly used as fuel in the steam reformer, and partly recycled to the synthesis gas section, see Figure 2.1. The methanol synthesis loop consists of two parallel reactors with a common steam drum, a feed/effluent interchanger, a cooler, a methanol separator and a recycle compressor. Part of the MP steam produced in the steam drum is utilized in the recycle compressor.

The crude methanol is purified by distillation. Only small amounts of by-products are present. Ethanol is the most difficult component to remove. Dissolved gases are first removed by flashing at low pressure. Low- and high- boiling by-products are removed in a energy-integrated three column distillation sequence. In the stabilizer column, low-boiling by-products are removed from the top. The second and third columns separate pure methanol from water and low-boiling by-products. Ethanol is removed in a side-stream in the third column. The second column operates at elevated pressure and the third operates at ambient pressure. The condenser in the high-pressure column is integrated with the reboiler in the low-pressure column.

2.2 Kinetics

Three overall reactions are possible in the methanol synthesis - hydrogenation of carbon monoxide, hydrogenation of carbon dioxide and the reverse water-gas shift reaction:

$$CO + 2H_2 \rightleftharpoons CH_3OH \tag{2.7}$$
$$CO_2 + 3H_2 \rightleftharpoons CH_3OH + H_2O \tag{2.6}$$
$$CO_2 + H_2 \rightleftharpoons CO + H_2O \tag{2.4'}$$

Hydrogenation of carbon monoxide used to be viewed as the principal reaction. The present view is that methanol is formed from CO_2 over copper containing catalyst. This is confirmed by C^{14} labelling (Chinchen *et al.* 1987) and *in-situ* measurements (Muhler *et al.* 1994). Only two of these reactions are linearly independent and define the equilibrium composition. The first kinetic equation was proposed by Natta (1955) for the $Zn0/Cr_2O_3$ catalyst used in the high-pressure process:

$$r = \frac{f_{co} f_{H_2}^2 - f_{CH_3OH}/K_{eq}^1}{A + B f_{CO} + C f_{H_2} + D f_{CH_3OH}} \tag{2.8}$$

The following kinetic models from recent literature have been evaluated:

Graaf *et al.* (1988)

- Based on all three Reactions 2.7, 2.6 and 2.4′ (labelled 1, 2 and 3).
- Dual-site Langmuir - Hinshelwood mechanism where CO and CO_2 absorb on site s_1 and H_2 and H_2O absorb on site s_2. Formation of methanol occurs through successive hydrogenation and the water gas shift reaction by a formate mechanism.
- Rate determining steps:

$$H_2COs1 + Hs2 \rightleftharpoons H_3COs1 + s1 \tag{2.9}$$
$$HCO_2s1 + Hs2 \rightleftharpoons COs1 + H_2Os2 \tag{2.10}$$
$$H_2CO_2s1 + Hs2 \rightleftharpoons H_3COs1 + s2 \tag{2.11}$$

- Experimental conditions: T = 200 - 244 ^{o}C, P = 15 - 50 bar, $Cu/ZnO/Al_2O_3$ catalyst MK101 from Haldor Topsøe A/S.

$$r_1 = \frac{k_1 K_{CO}(f_{CO} f_{H_2}^{3/2} - f_{CH_3OH}/(f_{H_2}^{1/2} K_{eq}^1))}{(1 + K_{CO} f_{CO} + K_{CO_2} f_{CO_2})(f_{H_2}^{1/2} + (K_{H_2O}/K_{H_2}^{1/2} f_{H_2O}))} \tag{2.12}$$

$$r_2 = \frac{k_2 K_{CO_2}(f_{CO_2} f_{H_2}^{3/2} - (f_{CH_3OH} f_{H_2O})/(f_{H_2}^{3/2} K_{eq}^2))}{(1 + K_{CO} f_{CO} + K_{CO_2} f_{CO_2})(f_{H_2}^{1/2} + (K_{H_2O}/K_{H_2}^{1/2} f_{H_2O}))} \tag{2.13}$$

$$r_3 = \frac{k_3 K_{CO_2}(f_{CO_2} f_{H_2} - f_{H_2O} f_{CO}/K_{eq}^3)}{(1 + K_{CO} f_{CO} + K_{CO_2} f_{CO_2})(f_{H_2}^{1/2} + (K_{H_2O}/K_{H_2}^{1/2} f_{H_2O}))} \tag{2.14}$$

Skrzypek *et al.* (1991)

- Based on Reactions 2.6 and 2.4′ (labelled 1 and 2). Demonstrates experimentally that methanol not can be formed from hydrogen and carbon monoxide without the present of water.
- Langmuir - Hinshelwood mechanism where CO_2 and H_2 react on the surface with few intermediate steps.
- Rate determining step:

$$CO_2 * + H_2 * \rightleftharpoons H_2CO_2 * \tag{2.15}$$

  * denote adsorbed species

- Experimental conditions: T = 187 - 277 ^{o}C, P = 30 - 90 bar, Polish commercial $Cu/ZnO/Al_2O_3$ catalyst that has been used for one year.

$$r_1 = \frac{k_1 K_{H_2}^2 K_{CO_2}(p_{H_2}^2 p_{CO_2} - (1/K_{eq}^1)(p_{MeOH} p_{H_2O}/p_{H_2}))}{den^3} \tag{2.16}$$

$$r_2 = \frac{k_2 K_{H_2} K_{CO_2}(p_{H_2} p_{CO_2} - (1/K_{eq}^2)(p_{CO} * p_{H_2O}))}{den^3} \tag{2.17}$$

$$den = 1 + K_{H_2} p_{H_2} + K_{CO_2} p_{CO_2} + K_{MeOH} p_{MeOH} + K_{H_2O} p_{H_2O} + K_{CO} p_{CO}$$

Vanden Bussche and Froment (1996)

- Based on Reactions 2.6 and 2.4′ (labelled 1 and 2).
- Langmuir - Hinshelwood Hougen-Watson mechanism. Methanol is formed by successive hydrogenation via formate, and the reverse water gas shift reaction occurs by a red-ox mechanism. The mechanism is based on surface species measurements and of a review of proposed mechanism.
- Rate determining steps:

$$CO_2(g) + * \rightleftharpoons O* + CO(g) \tag{2.18}$$

$$HCO_2 2* + H* \rightleftharpoons H_2CO_2 2* + * \tag{2.19}$$

- Experimental conditions: T = 180 - 280 ^{o}C, P up to 51 bar, commercial ICI 51-2 $Cu/ZnO/Al_2O_3$ catalyst

$$r_1 = \frac{K'_{5a} K'_2 K_3 K_4 K_{H_2} p_{CO_2} p_{H_2} [1 - (p_{H_2O} p_{CH_3OH})/(p^3_{H_2} p_{CO_2} K^1_{eq})]}{den^3} \tag{2.20}$$

$$r_2 = \frac{K'_1 p_{CO_2} [1 - (p_{H_2O} p_{CO})/(p_{CO_2} p_{H_2} K^2_{eq})]}{den} \tag{2.21}$$

$$den = 1 + (K_{H_20}/K_8 K_9 K_{H_2})(p_{H_2O}/p_{H_2}) + (K_{H_2} p_{H_2})^{1/2} + K_{H_2O} p_{H_2O}$$

Aksgaard *et al.* (1995)

- Based on Reactions 2.6 and 2.4′ (labelled 1 and 2).
- Mechanism determined from surface studies of single crystals. The reverse water gas reaction occurs by a red-ox-mechanism and formation of methanol by successive hydrogenation.
- Rate determining step:

$$H_2CO_2 * + H* \rightleftharpoons H_3CO* + O* \tag{2.22}$$

- The model parameters are estimated from gas phase thermodynamic and surface properties. The calculations needed to find the parameters are very elaborate.
- Experimental conditions: T = 220 - 300 ^{o}C, P = 50 - 100 bar

$$r_1 = k_{-11} K_{11} K_{10} \frac{\theta_{HCOO*} \theta^2_{H*}}{\theta_*} - k_{-11} \theta_{H_3CO*} \theta_{O*} \tag{2.23}$$

$$r_2 = k_{-11} K_{11} K_{10} \frac{\theta_{HCOO*} \theta^2_{H*}}{\theta_*} - k_{-11} \theta_{H_3CO*} \theta_{O*} - k_7 \theta_{CO*} \theta_{O*} + \frac{k_7}{K_7} \theta_{CO_2} \theta_{O*} \tag{2.24}$$

The kinetic model by Graaf *et al.* simultaneously predicts two different concentrations of intermediate species. Some intermediate species feature in two different overall reactions, and this has not been accounted for. Skrzypek's model is based on measurements on a deactivated catalyst, and the effect of deactivation is not accounted for. Hence, the reaction rates are probably too slow. The mechanism proposed by Vanden Bussche and Froment, and Aksgaard *et al.* are the most detailed and convincing. To some extent, the mechanism in these models also agrees. According to the authors, Aksgaard's model does not give an accurate prediction of the methanol reaction rate at industrial conditions. Also, lengthy calculations are needed to find the model parameters. Vanden Bussche and Froment's model accurately predicts the kinetic behaviour reported from other authors outside the experimental window. The model is also able to predict a maximum in the conversion rate at 2 per cent CO_2 that had earlier been explained by a deactivation effect. On this basis, the model by Vanden Bussche and Froment was selected.

2.3 Catalyst deactivation

Deactivation of $Cu/Zn/Al_2O_3$ catalyst is caused by *chemical poisoning* and *thermal sintering*. Sulphur compounds, chlorine and heavy metals act as poisons to the catalyst. Sintering is a solid state transformation which occurs at high temperatures and is promoted by water. Under normal operation only sintering occurs, because the catalyst poisons are removed from the synthesis gas earlier in the process. The literature on sintering is mainly qualitative. The purpose of this section is to review the literature on catalyst deactivation to understand the mechanisms of sintering of the $Cu/Zn/Al_2O_3$ catalyst and find a good mathematical model of this process.

2.3.1 Mechanism of sintering

Effect of temperature

Copper is the active phase in the catalyst. Zinc oxide plays an important role in stabilizing the copper crystals (Skrzypek *et al.* 1994). Sintering of copper occurs slowly at temperatures typical for methanol synthesis, and sintering of zinc oxide may also occur. Sintering occurs by migration of atoms or crystals to larger agglomerates. This leads to increased crystal size and decreased active surface. Sintering increases exponentially by increasing temperature (Satterfield 1980, Holmen 1996). Under normal operation the catalyst deactivates slowly and has a lifetime of several years (Supp 1981, Skrzypek *et al.* 1994, Kung 1992). An initial, fast deactivation is observed. A fresh, reduced catalyst deactivates by as much as 60 per cent in the first 20 hours (Kung 1992). Researchers disagree on the details of how the catalyst behaves at different temperatures.

Skrzypek *et al.* (1994) describes sintering by the *Tamman temperature*, defined as the temperature where the crystal lattices become mobile. Crystal growth occurs by migration of atoms under the Tamman temperature and by migration of crystals over the Tamman temperature. The Tamman temperature is calculated by Baker's formula:

$$T^i_{Tamman}\ [K] \approx 0.5 \cdot T^i_{melting}\ [K] \tag{2.25}$$

Where $T^i_{melting}$ is the melting point of the pure component. The Tamman temperature is 397 ^{o}C for copper and 887 ^{o}C for zinc oxide, indicating that only sintering of copper occurs in the methanol synthesis catalyst.

The same definition of the Tamman temperature is used in the textbook by Satterfield (1980). The Hutting temperature is also used, defined as the temperature when the surface atoms become mobile:

$$T^i_{Hutting}\ [K] \approx 0.3 \cdot T^i_{melting}\ [K] \tag{2.26}$$

The Hutting temperature for copper is 129 ^{o}C, and 423 ^{o}C for zinc oxide. According to the theory, sintering only occurs in the copper phase. Sintering is expected to increase at $T^{Cu}_{Tamman} = 397$ ^{o}C.

Several experimental studies of sintering of the $Cu/Zn/Al_2O_3$ catalyst are performed. Supp (1981) reports in a paper from Lurgi that copper recrystallizes at temperatures above 270 ^{o}C, causing severe deactivation and decreased selectivity.

Roberts *et al.* (1993) have measured an increase in copper crystal size from 75 Å to 100 Å at 250 ^{o}C. Growth of zinc oxide was not observed. A correlation was found between copper crystal size and the BET-surface.

In a review by Kung (1992), sintering of zinc oxide is also reported. X-ray measurements showed sintering of copper at temperatures above 227 ^{o}C. Sintering of zinc oxide was measured above 300 ^{o}C. The growth of zinc oxide crystals contributed to the sintering of copper.

Ladebeck (1993) supports that sintering of both copper and zinc oxide occurs. According to his article, sintering leads to destruction of both the pore system and the matrix material, in addition to the loss of active surface. By matrix material the author is referring to the spacer structure; where particles of alumina and zinc oxide act as spacers between copper particles. By reducing the distance between the particles, sintering is reduced. Ladebeck (1993) defines the the Tamman temperature as the temperature where *metallic clusters* start to migrate, and state that the Tamman temperature for copper is 190 - 200 ^{o}C. This is much lower than the value given by Baker's formula.

To sum up the experimental results, a measurable sintering of copper in the catalyst starts at 190 - 227 ^{o}C. At higher temperatures, 270 - 300 ^{o}C, the sintering becomes more severe and sintering of zinc may also occurs.

Effect of reaction gas composition

Synthesis gas contains CO, CO_2, H_2 and H_2O. Additional H_2O is formed in the methanol synthesis. CO and H_2 are reducing and CO_2 and H_2O oxidizing species.

It is known that the catalyst activity is at a maximum and the deactivation rate is low at low CO_2 concentration (2 - 5 Vol %) in the synthesis gas (Skrzypek *et al.* 1994, Ladebeck 1993, Kung 1992). This is usually explained by copper being at an optimal oxidation state (Cu^+/Cu^-) caused by reversible red-ox reactions:

$$Cu + CO_{2(g)} \rightleftharpoons Cu^+ + O^- + CO_{(g)} \tag{2.27}$$

$$Cu + H_2O_{(g)} \rightleftharpoons Cu^+ + OH^- + 1/2H_2 \tag{2.28}$$

In a recent surface science study (Ovesen *et al.* 1997) a positive correlation between the surface area and reduction potential, defined as $(P_{CO}P_{H2})/(P_{CO_2}PH_2O)$ was found. The change in the surface area is related to a change in the number of oxygen vacancies at the $Zn-O-Cu$ interface caused by the reversible red-ox reactions:

$$CO(g) + Zn - O - Cu \rightleftharpoons C_2O(g) + Zn - [] - Cu \quad (2.29)$$
$$H_2(g) + Zn - O - Cu \rightleftharpoons H_2O(g) + Zn - [] - Cu \quad (2.30)$$

The oxygen vacancies are denoted by []. A dynamic kinetic model where the surface area changes was developed from these results. Reversible changes related to reaction gas composition should be considered in connection with reaction kinetic, as it is by (Ovesen *et al.* 1997). Only irreversible changes should be considered as true deactivation.

Formation of brass (Cu_nZn) on the catalyst can occur in a gas with very high reduction potential and high temperature. Large copper crystals can also be formed at a very high reduction potential. This makes the catalyst pink. Both processes are irreversible and lead to dramatic deactivation, but are prevented if a small amount of CO_2 is present (Skrzypek *et al.* 1994, Kung 1992).

CO_2 - rich synthesis gas leads to higher deactivation rate. Several explanations are presented. According to Skrzypek *et al.* (1994) higher CO_2 concentration in the synthesis gas leads to over-oxidation of copper, either by CO_2 or H_2O. Rahimpour *et al.* (1998) postulate a deactivation mechanism where CO_2 occupies active sites. Ladebeck (1993) reports that the deactivation rate was increased by one order of magnitude when the CO_2 content in the synthesis gas was increased from 3 per cent to 12 per cent. The deactivation is not caused by CO_2, but by H_2O produced from CO_2 in the methanol synthesis or the reverse shift reaction. This is experimentally demonstrated by exposing the catalyst to pure CO_2 and pure H_2O. H_2O destroys the matrix material and decreases the copper surface tension, leading to sintering. Sahibzada *et al.* (1997) support this view. They have showed that H_2O promotes activity below 4 per cent and inhibits activity above 4 per cent. No deactivation effect of CO_2 was found. Kung (1992) also reports that high partial pressure of H_2O leads to sintering.

2.3.2 Deactivation models

Simple Rate Models

Sintering can generally be modelled as a power law expression (PLE):

$$\frac{da}{dt} = -K_d(T)a^n \quad (2.31)$$

were the deactivation order, n, varies from 1 to 16 (Skrzypek *et al.* 1994). If migration of atoms is the dominant mechanism n should be between 2 and 16, according to the theoretical Flynn and Wanke model. The deactivation rate constant, K_d, varies with temperature according to the Arrhenius equation:

$$K_d(T) = K_d \exp\left(\frac{E_d}{R_g T}\right) \quad (2.32)$$

The deactivation models for the methanol synthesis catalyst found in the literature are of the PLE form.

Several authors (Bartholomew 1993, Forzatti and Lietti 1999) have proposed a generalized power law expression (GPLE) to better describe sintering:

$$\frac{da}{dt} = -K_d(T)\,(a - a^{eq})^n \quad (2.33)$$

Deactivation curves for sintering are steep in the beginning and level out after some time. The $-a^{eq}$ term accounts for the asymptotic approach. First or second deactivation order is always found in GPLE. High deactivation orders are necessary to describe deactivation curves with PLE. The extrapolation error is larger in the PLE expression. No generalized power law expression is published for the methanol synthesis catalyst.

The following models were evaluated in a simulation study:

1. Sahibzada *et al.* (1997)

   - Experimental conditions: $T = 250$ ^oC, $P = 5$ MPa, crushed industrial catalyst in gas-phase Berty reactor, representative feed composition and gas velocity.

- First order deactivation after an initial phase of 10 hours. n $\approx$ 10 in the initial phase. The rate constant is not presented in the paper, but calculated from the graph.

$$\frac{da}{dt} = -K_{d,1}a \qquad K_{d,1} = 4 \cdot 10^{-4} h^{-1} \tag{2.34}$$

2. Kuechen and Hoffmann (1993)

- Experimental conditions: $T = 240$ ^{o}C, $P = 5$ MPa, 5 x 5 mm catalyst pellets in gas phase Berty reactor, representative feed composition and gas velocity.
- Second order deactivation. The rate constant is not presented in the paper, but calculated from the graph.
- Reduction potential is introduced in the model, but m is not found.

$$\frac{da}{dt} = K_d' \left(\frac{f_{CO}}{f_{CO_2}} \right)^m a^2 = -K_{d,2}a^2 \qquad k_{d,2} = 1.5 \cdot 10^{-2} h^{-1} \tag{2.35}$$

3. Cybulski (1994)

- Review article
- Experimental conditions: Liquid phase pilot plant. $T = 250$ ^{o}C.
- First order deactivation. Rate constant and activation energy are found.

$$\frac{da}{dt} = -K_{d,3}a \quad K_{d,3} = 2.1 \cdot 10^{-4} h^{-1} \quad E_d = 91270[J/mol] \tag{2.36}$$

4. Skrzypek *et al.* (1994)

- Data from Bart and Sneeden (1987). No information about where in the reactor the temperature and activity are measured.
- Experimental conditions: Fixed bed reactor, $T = 240$ ^{o}C, $P = 70$ MPa, $H_2/CO/CO_2/in = 82/14/3.5/10.5$ Vol %.
- Fifth order deactivation and rate constant are found.

$$\frac{da}{dt} = -K_{d,4}a^5 \quad K_{d,4} = 8.78 \cdot 10^{-3} h^{-1} \tag{2.37}$$

5. Skrzypek *et al.* (1994)

- Data from Roberts *et al.* (1993)
- Experimental conditions: Slurry auto clave reactor. $T = 250$ ^{o}C, $P = 5.27$ MPa, $H_2/CO/CO_2 = 35/51/13$ Vol %.
- Fifth order deactivation and rate constant are found.

$$\frac{da}{dt} = -K_{d,5}a^5 \quad K_{d,5} = 2.4 \cdot 10^{-3} h^{-1} \tag{2.38}$$

6. Skrzypek *et al.* (1994)

- Data from Roberts *et al.* (1993)
- Experimental conditions: Liquid phase pilot bubble column. $T = 250$ ^oC, $P = 5.27$ MPa, $H_2/CO/CO_2 = 35/51/13$ Vol %.
- n = 1.5 and rate constant are found.

$$\frac{da}{dt} = -K_{d,6}a^{1.5} \quad K_{d,6} = 2.7 \cdot 10^{-4} h^{-1} \tag{2.39}$$

7. Roberts *et al.* (1993)

- Experimental conditions: Liquid phase pilot bubble column. $T = 250$ ^{o}C, $P = 5.27$ MPa, $H_2/CO/CO_2 = 35/51/13$ Vol %.
- First order deactivation and rate constant found. The difference from no. 6 is the definition of initial activity. The first points are not included here.

$$\frac{da}{dt} = -K_{d,7}a \quad K_{d,7} = 2.1 \cdot 10^{-4} h^{-1} \tag{2.40}$$

The deactivation models were compared by simulation for a period of 4 years. Activation energy from Cybulski (1994) was used in all models. The activity versus time from the different models are shown in Figure 2.3. Only models number four and five can be used. The other models resulted in zero activity after short time.

In a paper by Islam and Earl (1990), deactivating behaviour of the ICI-51-Z catalyst in an ICI quench reactor is studied. One deactivation model for each catalyst bed is found from operational data. This model can only be used for this specific process, because other effects than deactivation are lumped together in the model. Deactivation rates rage from 0.07 to 0.5 per year at temperatures from 440 K to 540 K.

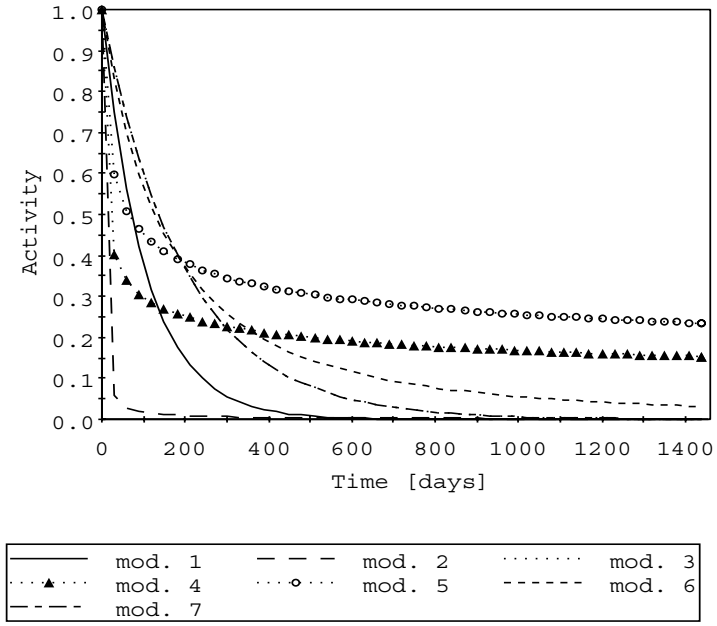

Figure 2.3. Comparison of activity profiles over four years from models 1 to 7.

Mechanistic Models

The only mechanistic deactivation model in the literature is published by Rahimpour *et al.* (1998). A deactivation mechanism where CO_2 and CO occupies active sites is postulated. Hydrogenation of CO_2 and CO occurs on two different types of active sites. Deactivation occurs when CO_2 occupies a CO-site and vice versa. This deactivation mechanism is not in agreement with the literature on the subject, see Section 2.3.1. A detailed LHHW-type model describing both reaction kinetic and deactivation kinetic is developed:

$$r_1 = a_1 \frac{k_{f1} K_{CO} K_H^2 K_{CH} p_{CO} p_{H_2}^2}{1 + K_{CO} p_{CO} + K_{CO} K_H^{3/2} K_{CH} p_{CO} p_{H_2}^{3/2}} \tag{2.41}$$

$$r_2 = a_2 \frac{k_{f2} K_{CO_2} K_H K_{HCO_2} p_{CO_2} p_{H_2}}{1 + K_{CO_2} p_{CO_2} + K_{CO_2} K_H^{1/2} K_{HCO_2} p_{CO_2} p_{H_2}^{1/2}} \tag{2.42}$$

$$\frac{da_1}{dt} = -a_1^{d1} \frac{k_{d1} p_{CO_2}^2}{1 + K_{CO} p_{CO} + K_{CO} K_H^{3/2} K_{CH} p_{CH} p_{H_2}^{3/2}} \tag{2.43}$$

$$\frac{da_2}{dt} = -a_2^{d2} \frac{k_{d2} p_{CO_2}^2}{1 + K_{CO_2} p_{CO_2} + K_{CO_2} K_H^{1/2} K_{HCO_2} p_{CO_2} p_{H_2}^{1/2}} \tag{2.44}$$

The authors used data from Kuechen and Hoffmann (1993) to fit the model parameters. The deactivation model was simulated for 3 months with the pseudo-homogeneous methanol reactor model presented in Section 3.2.1 as a test. Figure 2.4 shows the two activities in the middle of the reactor as a function of time. After only 3 months the activity a2 is low and a1 is close to zero. Figure 2.5 shows the methanol formation rate versus time and reactor position. The methanol formation rate drops too fast. The catalyst lifetime is expected to be 3 - 4 years, so it is clear that Rahimpour's model with the published parameters not can be used in simulation of industrial scale reactors.

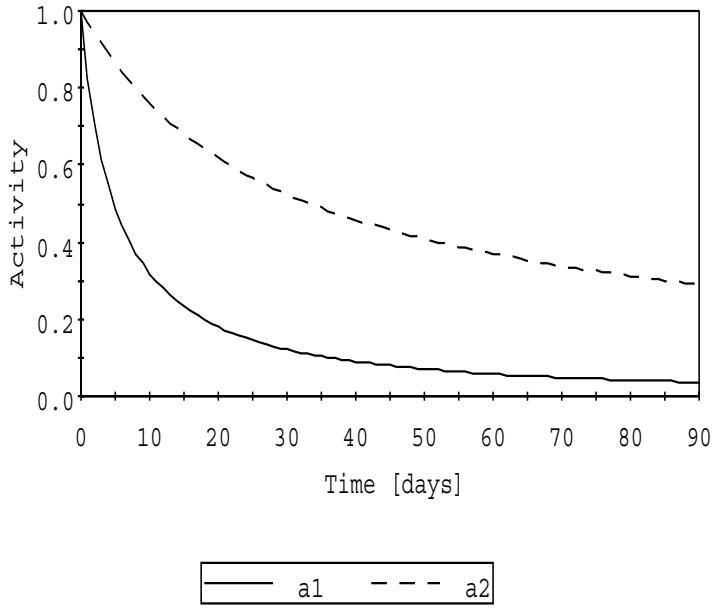

Figure 2.4. Catalyst activity from Rahimpour's model.

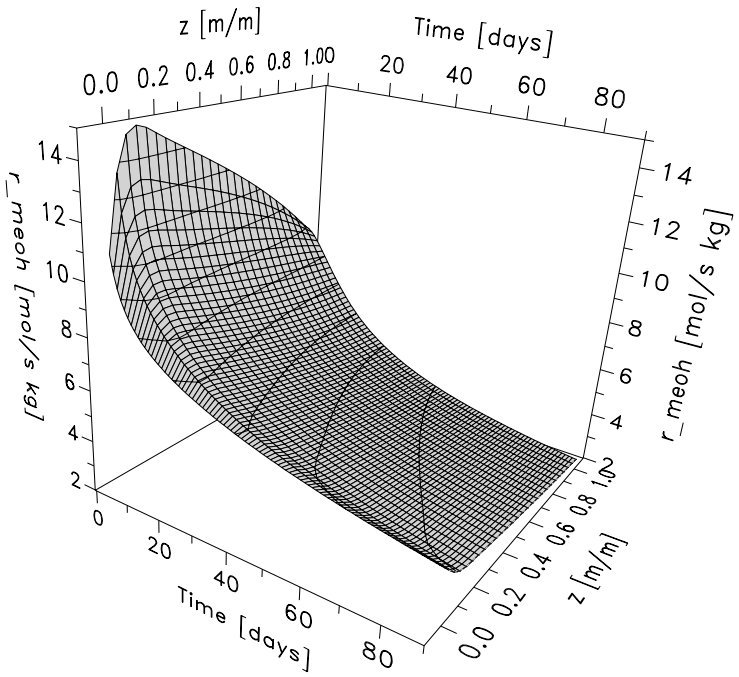

Figure 2.5. Rate of methanol formation from Rahimpour's model.

Model development

A deactivation model is developed by adjusting model 4. The simulation study showed that only models 4 and 5 can be used to simulate deactivation over several years. Model 4 was chosen because it is taken from a gas phase fixed bed reactor. Even if this model gives slow deactivation compared to the others in the simulation study, it gives faster deactivation than expected from the literature on operation of methanol reactors, see Section 2.3.1. To fit the deactivation described in the literature, these adjustments were done:

- An initial activity a_0 of 0.4 was assumed. The simulation starts after the initial fast deactivation. A relative activity $\tilde{a}$, scaled to start at 1, is used to find the reaction rate.
- The deactivation rate constant K_d was halved.

The adjusted deactivation model is show below:

$$\begin{aligned} \frac{da}{dt} &= -K_d \exp\left(\frac{-E_d}{R_g}(\frac{1}{T}-\frac{1}{T_0})\right) a(t)^5 \\ a_{t=0} &= a_0 \\ \tilde{a} &= 1 - \frac{a_0 - a}{a_0} \\ K_d &= 4.39 \cdot 10^{-3} h^{-1} \quad E_d = 91270[J/mol] \end{aligned} \tag{2.45}$$

The adjusted model gives a reasonable deactivation with 2 years of half-life. Reactor temperature profiles with fresh catalyst, after some deactivation and after 3 - 4 years of deactivation and increased cooling temperature are shown in an article by Supp (1981). Simulation with the adjusted deactivation model (Equation 2.45) and the pseudohomogeneous reactor model in Section 3.2.1 were performed. The cooling temperature was kept constant at 523 K for 3 years and then increased to 528 K in the 4th year. The temperature profiles from simulation are compared with Supp's profiles i Figure 2.6. The simulation shows similar behaviour. The temperature top at the start of the reactor drops in the same way. Supp's profiles in cases II and III have a flat top in the middle of the reactor, which is something that the simulation profiles do not have. This indicates that the catalyst in the start of the reactor is more deactivated, giving a lengthened reaction zone. This can be caused by reaction gas composition or poisoning. The predicted methanol content in the reactor effluent from the simulation agree with Supp's information.

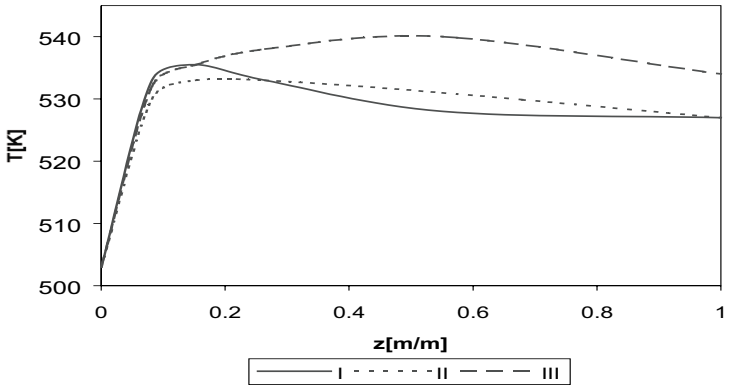

(a)

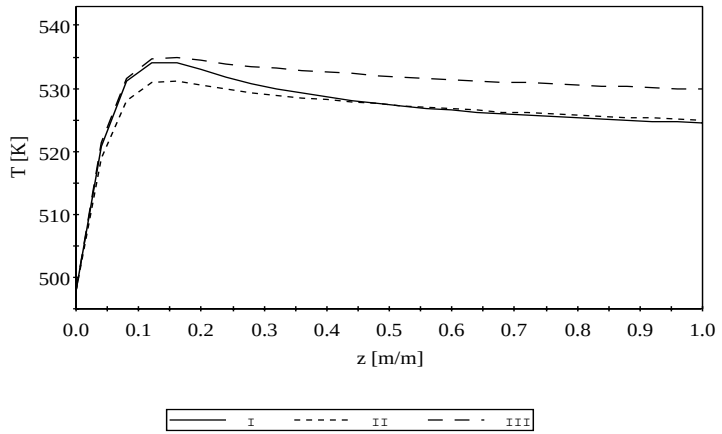

(b)

Figure 2.6. Reactor temperature profiles from Supp(1981)(a) and from simulation with adjusted deactivation model(b). I: fresh catalyst II: after 1 year deactivation III: after 4 years deactivation and increased cooling temperature.

Chapter 3

Modelling of the Methanol Synthesis Loop

This chapter describes the development of the model that is used throughout the thesis. The model was developed specifically for long-term dynamic optimization, with emphasis on the reaction and deactivation effects.

The pseudo-steady state model of the total methanol synthesis loop consists of a rigorous reactor model and lumped models of the remaining units. Two reactor models with different levels of complexity were developed. The choice of complexity level is a trade-off between accuracy and calculation time. The model was verified against a design flow sheet and to some extent, validated against process measurements. Overall, good agreement was found. The deactivation model and the thermodynamic calculation in the separator are the weak areas of the model. The separator model can be improved by estimating the binary interaction parameters from process data. A deactivation model is estimated from historical process data in Chapter 6.

3.1 Introduction

A simplified flow sheet of the methanol synthesis loop is shown in Figure 3.1. Methanol is separated from unreacted synthesis gas in two steps: a high pressure separator followed by a low pressure separator. Only the high pressure separator is included in the flow sheet. Figure 3.2 illustrates how the process was split into unit models.

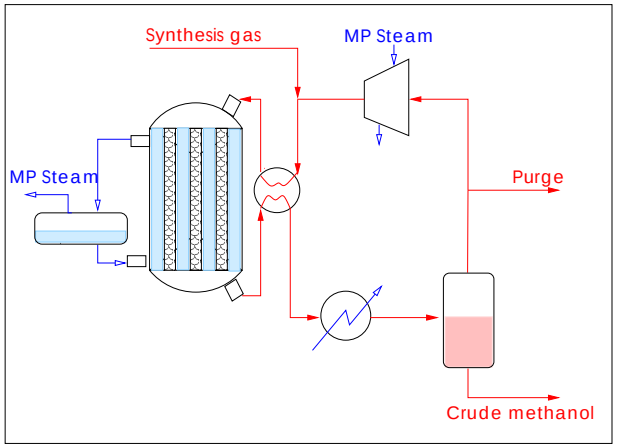

Figure 3.1. Flow sheet of the methanol synthesis loop.

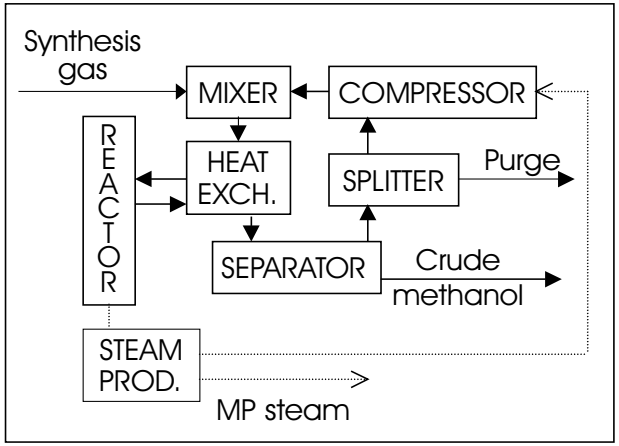

Figure 3.2. Unit model representation of the methanol synthesis loop.

The following simplifications of the flow sheet were make:

- Cooling before the separator was included in the separator
- The low-pressure separator was omitted

The first simplification has no overall effect. The second simplification

has a small effect on the purity of the crude methanol, but no effect on the recycle stream in the methanol synthesis loop. The gas separated in the low pressure separator is recycled back to the reformer section as shown in Figure 2.1. Only 5 per cent of the separation occurs in the low-pressure separator.

Two rigorous reactor models with different level of complexity were developed. The remaining units were represented by lumped models. The unit models were connected trough the stream variables F, T, P, y_i *og* H. Ideal gas correlation for enthalpy (Equation 3.27) were used in all streams. The following species were included: carbon dioxide, carbon monoxide, hydrogen, water, methanol and methane. Methane is an inert component. Nitrogen and byproducts are present in small amounts, and are neglected in the model. Implementation and solution of the model are considered in Section 4.4.2.

3.2 Reactor models

3.2.1 Pseudo-homogeneous model

This is the simplest of the two reactor models. It can be classified as a pseudo-steady-state two-dimensional pseudo-homogeneous reactor model. The model was originally developed by Hillestad (1995), and has been extended to include catalyst deactivation. The reaction kinetic has also been improved. The following assumptions were made:

- Pseudo-steady-state: The catalyst deactivation is the only dynamic effect included in the model, and steady-state is assumed for composition, temperature and pressure along the reactor.
- Dispersion of mass in axial and radial directions is negligible.
- Dispersion of heat in axial direction is negligible.
- Radial temperature gradients can be approximated by a second order polynomial.
- Temperature gradients between gas and solid are negligible.
- The effectiveness factor η is constant throughout the reactor.

The pseudo-steady-state assumption is reasonable because the dynamics in composition, temperature and pressure are much faster than the deactivation dynamics. The fast dynamics are not interesting when the total catalyst lifetime

of 3 to 4 years is considered. The next four assumptions are reasonable, and have been controlled by simulations. The effectiveness constant is known to vary along the reactor, and was assumed to be constant to simplify the solution of the model. This assumption was relaxed in the heterogeneous reactor model. Simulation studies have shown that the model gives a fairly good description of the process.

Model equations

Component mass balance, energy balance, and Ergun's pressure drop equation with boundary conditions:

$$\frac{dy_i}{dz} = L_r \cdot \frac{\rho_s}{\epsilon C u_g}\left(\sum_{j=1}^{n_r}\nu_{ij}\tilde{r}_j - y_i\sum_{i=1}^{n_c}\sum_{j=1}^{n_r}\nu_{ij}\tilde{r}_j\right) \tag{3.1}$$

$$\frac{dP}{dz} = -L_r \cdot 10^{-5} \cdot \left(1.75 + 150\,\frac{1-\epsilon}{Re}\right) \cdot \frac{1-\epsilon}{\epsilon^3} \cdot \frac{u_g^2 \rho_g}{D_p} \tag{3.2}$$

$$\frac{d\overline{T}}{dz} = L_r \cdot \frac{1}{M' C_{p_g}} \cdot \left(\frac{2\,U_{eff}}{R_r}(T_c - \overline{T}) + \rho_s \sum_{i=1}^{n_r}(-\Delta H_{rx}^j \tilde{r}_j)\right) \tag{3.3}$$

$$y_i\big|_{z=0} = y_{i,inlet} \tag{3.4}$$

$$P\big|_{z=0} = P_{inlet} \tag{3.5}$$

$$\overline{T}\big|_{z=0} = T_{inlet} \tag{3.6}$$

Where z is a dimensionless axial coordinate. Derivation of Equations 3.1 to 3.6 are given in Section 11.5.1. in Froment and Birchoff (1990). Because the component balance is on mole fraction basis, it is necessary to correct for the change in number of moles in the methanol synthesis reaction. U_{eff} in the energy balance is an overall effective heat transfer coefficient from the mean radial position to the cooling water.

Radial temperature profile:

$$T(r) = d_0 + d_2 r^2 \tag{3.7}$$

$$d_0 = \frac{\left(1 + (2k_{r,g})/(U_{w,g}R_r)\right)\overline{T} - \frac{1}{4}T_c}{\frac{3}{4} + 2k_{r,g}/U_{w,g}R_r}$$

$$d_2 = \frac{T_c - \overline{T}}{\left(\frac{3}{4} + (2k_{r,g})/(U_{w,g}R_r)\right)R_r^2}$$

The radial temperature profile was derived from the two-dimensional energy equation with boundary conditions from Section 11.7.2 in Froment and Birchoff (1990):

$$0 = k_{r,g}\left(\frac{\partial^2 T}{\partial r^2} + \frac{1}{r}\frac{\partial T}{\partial r}\right) - \rho_g u_g \epsilon C_{p_g}\frac{\partial T}{\partial r} + \rho_s \sum_{i=j}^{n_r}(-\Delta H_{rx}^j \tilde{r}_j)$$

$$T\big|_{z=0} = T_{inlet}$$

$$\left.\frac{\partial T}{\partial r}\right|_{r=0} = 0$$

$$\left.\frac{\partial T}{\partial r}\right|_{r=R_r} = \frac{-U_{w,g}}{k_{r,g}}\left(T(R_r) - T_c\right)$$

Several authors, such as Khanna and Seinfeld (1987), verify that a second order polynomial estimates the radial temperature variations well. The boundary conditions and the expression for $\overline{T} = T(R_r/2)$ were applied to a second order polynomial: $T(r) = d_0 + d_1 r + d_2 r^2$. Three equations which define d_0, d_1 and d_2 appear:

$$d_1 = 0$$
$$T_c = d_0 + (R_r^2 + 2R_r k_{r,g})d_2$$
$$\overline{T} = d_0 + \frac{1}{4}R_r^2 d_2$$

The actual reaction rate in the gas phase:

$$\tilde{r}_j = \tilde{a}\eta\, r_j \tag{3.8}$$

The kinetic model is given by Vanden Bussche and Froment (1996). Reaction 1 is hydrogenation of carbon dioxide (Equation 2.6) and Reaction 2 is the reverse water-gas shift reaction (Equation 2.4′). The kinetic parameters are given in Table 3.1. The arguments for selecting this model are given in Section 2.2.

$$r_1 = \frac{k_d p_{CO_2} p_{H_2}(1 - (1/K_1^{eq})(p_{H_2O}p_{CH_3OH}/p_{H_2}^3 p_{CO_2}))}{\left(1 + k_c p_{H_2O}/p_{H_2} + k_a\sqrt{p_{H_2}} + k_b p_{H_2O}\right)^3} \tag{3.9}$$

$$r_2 = \frac{k_e p_{CO_2}(1 - K_2^{eq}(p_{H_2O}p_{CO}/p_{CO_2}p_{H_2}))}{1 + k_c p_{H_2O}/p_{H_2} + k_a\sqrt{p_{H_2}} + k_b p_{H_2O}} \tag{3.10}$$

A deactivation model based on Skrzypek *et al.* (1994) and Cybulski (1994) was selected. The activity was scaled to fit a temperature profile from an industrial reactor given by Supp (1981). The selection and scaling of the deactivation model are described in Section 2.3.2. The deactivation parameters are given in Table 3.2.

Table 3.1
Parameter values in the kinetic model.

$k = A \cdot exp(B/R_g T)$	A	B
$k_a[bar^{-1/2}]$	0.499	17 197
$k_b[bar^{-1}]$	6.62e-11	12 4119
k_c	3 453.38	
$k_d[mol/kg\ s\ bar^2]$	1.07	3 669
$k_e[mol/kg\ s\ bar]$	1.22e10	-9 4765
$K^{eq} = 10^{(A/T-B)}$	A	B
$K_1^{eq}[bar^{-2}]$	3066	10.592
K_2^{eq}	2073	2.029

$$\frac{da}{dt} = -K_d \exp\left(\frac{-E_d}{R_g}\left(\frac{1}{\overline{T}} - \frac{1}{T_0}\right)\right) a(t)^5$$
$$a_{t=0} = a_0$$
$$\tilde{a} = 1 - \frac{a_0 - a}{a_0} \tag{2.45}$$

The cooling requirements, molar flow and mass flux are calculated to connect the reactor model with the other unit models:

$$Q_{c,reactor} = H_{in} * F_{in} - H_{out} * F_{out} \tag{3.11}$$

$$F_{in} = \frac{1000 \cdot M}{\sum_{i=1}^{n_c}(y_{i,in} M w^i)} \tag{3.12}$$

$$F_{out} = \frac{1000 \cdot M}{\sum_{i=1}^{n_c}(y_{i,out} M w^i)} \tag{3.13}$$

$$M' = \frac{M}{n_t \pi R_r^2} \tag{3.14}$$

Conversion and the approach to equilibrium temperature describe the reaction yield:

$$X_{MeOH} = \frac{F_{out} \cdot y_{MeOH,out} - F_{in} \cdot y_{MeOH,in}}{F_{in} \cdot (y_{CO,in} + y_{CO_2,in})} \tag{3.15}$$

$$K_1^{eq}\left(T_{eq}^1\right) = \frac{p_{H_2O,out} p_{MeOH,out}}{p_{H_2,out}^3 p_{CO_2,out}} \tag{3.16}$$

$$K_2^{eq}\left(T_{eq}^2\right) = \frac{p_{CO,out} p_{H_2,out}}{p_{H_2O,out} p_{CO,out}} \tag{3.17}$$

$$\Delta T_{eq}^j = T_{eq}^j - \overline{T}_{out} \tag{3.18}$$

Table 3.2
Parameter values in the deactivation model.

$K_d[day^{-1}]$	$E_d[J/mol]$	$T_0[K]$	a_0
4.39e-3	91270	513	0.4

Model parameters

Total concentration and density are found from the ideal gas law:

$$C = \frac{P10^2}{R_g \overline{T}} \tag{3.19}$$

$$\rho_g = C \sum_{i=1}^{n_c}(y_i * M w^i) \tag{3.20}$$

Linear gas velocity:

$$u_g = \frac{M'}{\rho_g \epsilon} \tag{3.21}$$

The heat of reactions are found from correlations:

$$-\Delta H_{rx}^1 = 57980 + 35(\overline{T} - 498.15) \tag{3.22}$$
$$-\Delta H_{rx}^2 = -39892 + 8(\overline{T} - 498.15) \tag{3.23}$$

Viscosity, conductivity, heat capacity and molar enthalpy are found from correlations. The Reynolds and Prandtl numbers are found from their definitions:

$$\mu = 67.2 \cdot 10^{-7} + 0.21875 \cdot 10^{-7} \cdot \overline{T} \tag{3.24}$$
$$k_g = 0.01234 \cdot 10^{-3} + 1.84375 \cdot 10^{-7} \cdot \overline{T} \tag{3.25}$$

$$C_{p_g} = \frac{\sum_{i=1}^{n_c} y_i \cdot (A_i + B_i \cdot T + C_i \cdot T^2 + D_i \cdot T^3)}{\sum_{i=1}^{n_c}(M w^i \cdot y_i)} \tag{3.26}$$

$$H = \sum_{i=1}^{n_c} y_i \cdot (H_{ref}^i + A_i \cdot (T - T_{ref}) + B_i \cdot (T - T_{ref})^2 + C_i \cdot (T - T_{ref})^3 + D_i \cdot (T - T_{ref})^4) \tag{3.27}$$

$$Re = M' \cdot R_p \cdot \frac{2}{\mu} \tag{3.28}$$

$$Pr = \mu \cdot \frac{Cp_g}{k_g} \tag{3.29}$$

The effective heat transfer coefficient from $\overline{r}$ to the cooling water, $Ueff$, is found by combining the contributions in series:

$$U_{w,g} = \left(\frac{1}{h_{i,g}} + \frac{R_r/R_{r,y}}{h_{o,c}} + \frac{R_r \ln(R_r/R_{r,y})}{2k_w}\right)^{-1}$$

$$U_{w,s} = \left(\frac{1}{h_{i,s}} + \frac{R_r/R_{r,y}}{h_{o,c}} + \frac{R_r \ln(R_{r,y}/R_r)}{2k_w}\right)^{-1}$$

$$U_{eff} = \left(\frac{1}{U_{w,g}} + \frac{3R_r}{8k_{r,g}}\right)^{-1} + \left(\frac{1}{U_{w,s}} + \frac{3R_r}{8k_{r,s}}\right)^{-1} \tag{3.30}$$

The radial conductivity in the both phases and the individual heat transfer coefficients are found from correlations:

$$k_{stat} = k_g \cdot \left[\left(0.5 + 0.493 \cdot \frac{k_s/k_g - 1}{22 + k_s/k_g}\right) \cdot \left(\frac{k_s/k_g}{k_s/k_g \cdot \epsilon + (1-\epsilon)}\right) + 1 - \left(0.5 + 0.493 \cdot \frac{k_s/k_g - 1}{22 + k_s/k_g}\right) \cdot \left(\epsilon + (1-\epsilon) \cdot \frac{k_s}{k_g}\right)\right]$$

$$k_{dyn} = k_g \cdot \frac{RePr}{(7 + 135.8 \cdot R_p/R_r)^2}$$

$$k_{r,g} = k_{stat} + k_{dyn}$$

$$k_{r,s} = k_{stat}$$

$$h_{i,g} = \frac{1.23 \cdot Re \cdot 0.53 \cdot k_g}{2R_p}$$

$$h_{i,s} = \frac{0.48 + 0.192 \cdot (R_r/R_p - 1)^2 k_{r,s}}{R_p}$$

$$h_{o,c} = \frac{0.020 \cdot Re_c^{0.8} Pr_c^{1.0/3.0} (R_{r,y}/R_r)^{0.53} \cdot k_w}{2R_{r,y}}$$

Parameters for the reactor model are given in Table 3.3. In addition, system specific parameters like reactor dimensions are needed.

Table 3.3
Parameters in the reactor model.

	Mw^i	A_i	B_i	C_i	D_i	H^i_{ref}
	$[kg/mol]$	$[J/molK]$	$[J/molK^2]$	$[J/molK^3]$	$[J/molK^4]$	$[J/mol]$
CO	28.010	30.87	-1.285e-2	2.789e-5	-1.272e-8	-110530
CO_2	44.010	19.80	7.344e-2	-5.602e-5	1.715e-8	-393510
H_2	2.016	27.14	9.274e-3	-1.381e-5	7.645e-9	0
H_2O	18.016	32.24	1.924e-3	1.055e-5	3.596e-9	-241826
$MeOH$	32.042	21.15	7.092e-2	2.587e-5	-2.852e-8	-201000
CH_4	16.042	19.25	5.213e-2	1.197e-5	-1.132e-8	-74600

n_c	n_r	η	T_{ref}	k_w	k_s	Re_c	Pr_c
			$[K]$	$[kW/ms]$	$[kW/ms]$		
6	2	0.7	298	20.0e-3	4.18e-3	1923	0.843

3.2.2 Heterogeneous model

In this more complex model, balance equations over the catalyst pellet were included. It can be classified as a pseudo-steady-state two-dimensional heterogeneous reactor model. The model development is based on the textbook by Froment and Birchoff (1990) and a model developed by Hillestad (1995). The following assumptions were made:

- Viscous flow in catalyst pellets is negligible
- Isotherm catalyst pellet

Viscous flow is negligible when pressure drop and pore size are small (Froment and Birchoff 1990). Simulation have confirmed that the pressure drop is small, and the pore size is small in this case. The neglection of the viscous flow is a considerable simplification of the model compared to the model developed by Hillestad (1995). The assumption of isotherm catalyst pellet is reasonable,

and has been controlled by simulation. The model gives a better description of the process than the pseudo-homogeneous model. The temperature profiles in the reactor are in better agreement with the observed profiles. In addition, the composition profiles inside the catalyst are known.

Model equations

The following equations are added to the set of equations given in Section 3.2.1. Component mass balance over the catalyst pellet with boundary conditions:

$$\frac{D_e^i}{10^5 R_g T_s R_p^2}\left(\frac{d^2 p_s^i}{dx^2}+\frac{2}{x}\frac{dp_s^i}{dx}\right)+\rho_c\sum_{j=1}^{n_r}\nu_{ij}r_j^s\tilde{a}=0 \qquad i=1\ldots n_c-1 \tag{3.31}$$

$$\left.\frac{dp_s^i}{dx}\right|_{x=0}=0 \qquad i=1\ldots n_c-1 \tag{3.32}$$

$$-D_e^i\left.\frac{dp_s^i}{dx}\right|_{x=1}=k_g^i(p_{s,s}^i-p^i) \qquad i=1\ldots n_c-1 \tag{3.33}$$

$$p_s^{n_c}=p^{n_c} \tag{3.34}$$

$$P_s=\sum_{i=1}^{n_c}p_s^i \tag{3.35}$$

Where $x=\frac{r}{R_p}$ is dimensionless radial coordinate and component n_c is inert. Derivation of Equations 3.31 to 3.35 are given in Chapter 11.9.1 in Froment and Birchoff (1990).

The pellet equations and the reactor equations are connected by the actual reaction rate in the gas phase, $\tilde{r}_j$:

$$\tilde{r}_j=\frac{r_j^{obs,global}}{\rho_s}=\int_0^1 3x^2 r_j^s\tilde{a}dx \qquad j=1\ldots n_r \tag{3.36}$$

Equation 3.36 replaces Equation 3.8.

Model parameters

Effective diffusion coefficient in the pellet are found from the Bosanquet equation (Froment and Birchoff 1990):

$$D_e^i=\frac{\epsilon_s}{\tau}\left(\frac{1}{D_m^i}+\frac{1}{D_k^i}\right)^{-1} \qquad i=1\ldots n_c \tag{3.37}$$

Knudsen diffusion coefficient, D_k^i, is calculated from Froment and Birchoff (1990):

$$D_k^i=R_{pore}\frac{4}{3}\left(\frac{2}{\pi}\frac{R_gT}{Mw^i}\right)^{1/2} \qquad i=1\ldots n_c \tag{3.38}$$

The multi-component molecular diffusion coefficient, D_m^i, is found from the Wilke equation (Reid *et al.* 1988):

$$D_m^i=\sum_{j=i}^{n_c,j\neq i}\frac{y_s^j}{D_b^{i,j}} \qquad i=1\ldots n_c \tag{3.39}$$

With binary diffusion coefficients from Reid *et al.* (1988):

$$D_b^{i,j}=\frac{0.143T^{1.75}}{P_sW_m^{0.5}(V_i^{1/3}+V_j^{1/3})^2} \qquad i,j=1\ldots n_c \tag{3.40}$$

$$W_m=\frac{2}{1/Mw^i+1/Mw^j} \qquad i,j=1\ldots n_c$$

V_i is the diffusion volume for component i, and is given in Table 3.4.

The correlation for mass transfer coefficients is taken from Table 9.3.2 in Cussler (1984):

$$k_g^i=1.17Re^{-0.42}Sc^{i\,-0.67}u_g\cdot 10^3 \qquad i=1\ldots n_c \tag{3.41}$$

$$Sc^i=\frac{\mu}{\rho_g D_m^i\cdot 10^{-4}} \qquad i=1\ldots n_c$$

$$Re=\frac{2R_pu_g}{\mu}$$

System specific parameters like the catalyst dimension and properties must be known to calculate the model parameters.

Table 3.4
Diffusion volumes.

	CO	CO_2	H_2	H_2O	$MeOH$	CH_4
$V_i[m^3]$	18.0e-4	26.9e-4	6.12e-4	13.1e-4	31.25e-4	25.14e-4

3.3 Separator

The model is derived in Biegler *et al.* (1997). Pressure and temperature are specified (PT-flash).

Component balance, sum of molar fraction and phase equilibrium:

$$F \cdot z_i - V \cdot y_i - L \cdot x_i = 0 \qquad i = 1 \ldots n_c \tag{3.42}$$

$$\sum x_i = 0 \tag{3.43}$$

$$\sum y_i = 0 \tag{3.44}$$

$$y_i \cdot \Phi^i_{vap} = x_i \cdot \Phi^i_{liq} \qquad i = 1 \ldots n_c \tag{3.45}$$

The Soave-Redlich-Kwong equation of state (SRK) is used to find fugacity coefficients for both phases and enthalpy in the liquid phase (Reid *et al.* 1988). The SRK equations are not shown here because of space limitations. The SRK parameters used are shown in Table 3.5. The binary interaction parameters were found from the database in Aspen PLUS (Asp 2000) and critical properties and the acentric factor were found from Graaf *et al.* (1986). The enthalpy in gas phase is calculated from the ideal gas correlation (Equation 3.27) to achieve consistency with the enthalpy in the rest of the loop.

3.4 Compressor

The compressor was modelled as a polytropic compressor. Polyropic compression is defined as partial adiabatic compression along the true compression line in the enthalpy - entropy plane. Polytropic efficiency = 0.78 and mechanic efficiency = 0.98 were assumed. The model and typical values for efficiency are taken from Øverli (1992). The outlet pressure is specified and the compressor duty, Q_{comp}, is calculated.

Table 3.5
SRK parameter values.

	CO	CO_2	H_2	H_2O	$MeOH$	CH_4
$P_c[bar]$	35.0	73.8	20.5	221.2	80.4	46.0
$T_c[K]$	132.9	304.1	43.6	647.3	512.6	190.4
ω	0.066	0.239	0	0.344	0.556	0.011
$k_{i,j}$	CO	CO_2	H_2	H_2O	$MeOH$	CH_4
CO	0	0	0.0804	0	0	0.0322
CO_2	0	0	-0.3462	0.0737	0.0148	0.0933
H_2	0.0804	-0.3462	0	0	0	-0.0222
H_2O	0	0.0737	0	0	-0.0789	0
$MeOH$	0	0.0148	0	-0.0789	0	0
CH_4	0.0322	0.0933	-0.0222	0	0	0

Adiabatic factor:

$$\gamma = \frac{Cp_g}{Cp_g - R_g} \tag{3.46}$$

Compressor duty and temperature change:

$$Q_{comp} = F \cdot \frac{\gamma}{(\gamma - 1)\eta_m} R_g T_{in} \left[\left(\frac{P_{out}}{P_{in}} \right)^{\left(\frac{\gamma-1}{\gamma \cdot \eta_p}\right)} - 1 \right] \tag{3.47}$$

$$T_{out} = T_{in} \cdot \left(\frac{P_{out}}{P_{in}} \right)^{\left(\frac{\gamma-1}{\gamma \cdot \eta_p}\right)} \tag{3.48}$$

3.5 Heat exchanger

The model is developed in Biegler *et al.* (1997). The model was first used for design: Inlet streams were specified and the lumped parameter UA adjusted to achieve the wanted reactor inlet temperature. During simulation UA and inlet streams are specified. Stream number 1 is the hot stream.

Logarithmic mean temperature difference and energy balance:

$$\Delta T_{mean} = \frac{(T^1_{in} - T^2_{out}) - (T^1_{out} - T^2_{in})}{\log \frac{|T^1_{in} - T^2_{out}|}{|T^1_{out} - T_{in}|}} \tag{3.49}$$

$$Q = UA\Delta T_{mean} \tag{3.50}$$

$$Q = F^1(H^1_{in} - H^1_{out}) \tag{3.51}$$

$$Q = F^2(H^2_{out} - H^2_{in})$$

The following inequality prevents crossover temperature:

$$0 \leq (T^1_{in} - T^2_{out}) \cdot (T^1_{out} - T^2_{in}) \tag{3.52}$$

3.6 Steam production

MP steam is produced in the methanol reactor, and the recycle compressor is powered by MP steam expanding to LP stream. Steam production and consumption are proportional with energy production and consumption. The proportionality coefficients were found from Hysys simulations (Hyp 2000).

Net steam production:

$$F_{steam,MP} = 1.281 \cdot 10^{-3} \cdot Q_{c,reactor} - 9.873 \cdot 10^{-3} Q_{comp} \tag{3.53}$$

$$F_{steam,LP} = 9.873 \cdot 10^{-3} \cdot Q_{comp} \tag{3.54}$$

3.7 Mixer

The model was taken from Biegler *et al.* (1997).

Mass, component and enthalpy balance:

$$F_{out}x^i_{out} = \sum_{k=1}^{n_{is}} (F^k_{in} \cdot x^i_{in}, k) \qquad i = 1 \ldots n_c \tag{3.55}$$

$$F_{out} = \sum_{k=1}^{n_{is}} (F^k_{in}) \tag{3.56}$$

$$F_{out}H_{out} = \sum_{k=1}^{n_{is}} (F^k_{in} \cdot H^k_{in}) \tag{3.57}$$

The outlet pressure was assumed to be the mean of the inlet pressures:

$$P_{out} = \frac{\sum_{k=1}^{n_{is}} (P^k_{in})}{n_{is}} \tag{3.58}$$

3.8 Splitter

The model was taken from Biegler *et al.* (1997). F_{out} in $n_{os} - 1$ output streams must be specified.

Mass, component and energy balance:

$$F_{in} = \sum (F_{out}) \tag{3.59}$$

$$P_{in} = P^k_{out} \qquad k = 1 \ldots n_{os} \tag{3.60}$$

$$x^i_{in} = x^{i,k}_{out} \qquad k = 1 \ldots n_{os} \tag{3.61}$$

$$H_{in} = H^k_{out} \qquad k = 1 \ldots n_{os} \tag{3.62}$$

$$T_{in} = T^k_{out} \qquad k = 1 \ldots n_{os} \tag{3.63}$$

3.9 Model verification

The model was verified against a design flow sheet and to some extent, validated against process measurements. Overall, good agreement is found. The temperature profile in the reactor and the half-life of the catalyst activity have been compared to process data with satisfactory results. The heterogeneous reactor model fits the observed temperature profile better than the pseudo-homogeneous model, as expected. When compositions, temperature, pressures and flows in all streams were compared with the design flow sheet, a small deviation in the streams from the high pressure separator was found. The rigorous SRK thermodynamic model does not predict the phase equilibrium accurately enough. The behaviour of this specific mixture is hard to predict. For instance, the solubility of carbon dioxide in water causes special problems.

A more thorough validation and estimation against process data is recommended. The separator model can be easily improved by estimating the binary interaction parameters from process data. The catalyst deactivation model is believed to be uncertain, even if the half-life is well predicted. A deactivation model is estimated from historical operation data in Chapter 6. The estimated

model is not used for simulation and optimization because the parameters are not valid for the total catalyst lifetime, and in addition, they are confidential. The separator model can easily be improved by estimating the binary interaction parameters from the process data.

Chapter 4

Optimization of the Methanol Synthesis with Catalyst Deactivation

Parts of the work were presented at the Escape 8 conference, Brugge, 1998 and the Escape 9 conference, Budapest, 1999.

The scope of the work presented in this chapter is to find an optimal operating policy for a fixed bed reactor system with catalyst deactivation. The operating policy must change with time to counteract the adverse effect of catalyst deactivation on the process yield. Catalyst deactivation occurs in practically all fixed bed reactors. The process studied is Lurgi's methanol synthesis, but the method also applies to other fixed bed reactor systems. The catalyst lifetime is considered to be known. An economic objective is maximized with respect to coolant temperature and recycle ratio by control vector parameterization and a sequential optimization method.

Both the reactor by itself, and the reactor system with recycle (i.e. the loop) are studied, and it is shown that it is necessary to consider the loop to find the optimal operating policy. It is also shown that a heterogeneous reactor model gives different optimal policy and more correct results than a pseudo-homogeneous reactor model. Optimization of the loop leads to USD 3 165 000 , or 0.75 per cent, increased profit over four years compared to a selected reference case with constant operation policy. The optimal operation strategy is compared with the operating procedure recommended for the Tjeldbergodden

methanol plant. The optimal operation strategy gives a little higher profit: USD 752 700 over four years compared to the operation procedure. However, there are two important advantages from optimization: The ability to find the optimal operation if some of the variables in the optimization problem change, and the ability to track changes in the process by model updating and repeated optimization. It is not recommended to implement the calculated optimal control strategies directly. The work presented can serve as a framework for implementing dynamic optimization in the control system of a methanol synthesis plant with feedback, as discussed in Section 7.3.

4.1 Introduction

4.1.1 Previous work

Extensive research has been done on the optimal operation of fixed bed reactors undergoing catalyst deactivation, with focus on simplified theoretical cases. Assumptions like first order reaction, ideal reactor models and constant model parameters are commonly used.

In their much cited paper, Ognue and Ray (1971) considered optimal control of both single bed and multi-ple bed tubular reactors experiencing catalyst decay. Optimal control of adiabatic and isothermal reactors, optimal catalyst distribution along the reactor and feed distribution between multi-ple reactor beds were studied. A general objective function representing the profit over a catalyst operating cycle were optimized. An optimization method called *control vector iteration* was derived from Pontryagin's weak maximum principle. In this method the state equations are integrated forwards in time and space, then the adjoint equations are integrated backwards in time and space to calculate the gradients in the control vector. Symbolic derivation of the system equations are necessary to find the adjoint equations. Several authors have used the *control vector iteration* method and Ogunye and Rays framework. Elnashaie and Abdel-Hakim (1988) used a heterogeneous model to calculate the optimal feed temperature to an adiabatic reactor. Asrar and Moharir (1991) optimized the feed temperature to an adiabatic reactor as an inner optimization problem, and the catalyst lifetime as an outer optimization problem. Dixit and Grant (1996) studied optimal coolant temperature in a non-isothermal reactor. The butadiene polymerization process was considered as an industrial case. A pseudo-homogeneous plug flow model with constant parameters was used. Bozga (1999) reconsidered one of the problems from Ogunye and Ray: optimal control

of feed temperature to multi-stage adiabatic reactors with direct or indirect cooling. A reversible exothermic reaction is used, and the topic of equilibrium limitations discussed.

Buzzi-Ferraris *et al.* (1984) used the *control vector parameterization* method on some of the optimization problems from Ogunye and Ray's paper, and reported better results. Computation times are reduced, and more general problems can be solved. The method does not involve symbolic derivatives, which is an advantage for realistic problems with large process models. *Control vector parameterization* is the most common method for large-scale dynamic optimization problems in chemical engineering. It is described in detail in Section 4.3. The same method is also used by Gonzales-Velasco et al. on several industrial cases with realistic reaction and deactivation models (Gonzalez-Velasco *et al.* 1985, Gonzalez-Velasco *et al.* 1987, Gonzalez-Velasco *et al.* 1990, Gonzalez-Velasco *et al.* 1991, Gonzalez-Velasco *et al.* 1992). The reactor models used are simple with constant parameters, and path constraints on the state variables are not considered.

In this work a more realistic approach is taken. A rigorous model of the total reactor system with recycle is used, with varying model parameters and thermodynamic properties. A thorough analysis of the process is enployed to formulate the optimization problem. Path constrains on the reactor temperature are considered, and the actual time varying control variables in the reactor system, the recycle rate and coolant temperature, are optimized. The control vector parameterization method is used in this work.

4.1.2 Problem analysis

The $Cu/Zn/Al_2O_3$ catalyst can deactivate becasue of chemical poisoning or thermal sintering (see Section 2.3). Catalyst poisons are not likely to occur in the process gas. Sulphur is removed early in the process (see Figure 2.1). Heavy metals in the natural gas are likely to be absorbed on the catalyst in the reformer section. Under normal operating conditions, sintering is the deactivation mechanism. The catalyst deactivates slowly, and must be replaced after 3 to 4 years. The sintering mechanism changes at higher temperatures; copper crystals migrate together, causing severe sintering and deactivation. Catalyst selectivity is also affected. Different temperatures when this severe sintering occurs are reported, and range from 543 K to 670 K. The lowest temperature is chosen as a conservative constraint in the optimization. At normal operational conditions, extremely small amounts of byproducts are formed. Byproduct formation also

increases if the temperature exceeds 543 K (Supp 1981). It is important to limit the byproduct formation since the separation cost depends strongly on the amount of byproducts.

A common operation policy is to increase the temperature at the end of the catalyst lifetime to compensate for decreased activity (Supp 1981). A raised temperature gives higher reaction rates, but also higher deactivation rates. Because the reaction is limited by equilibrium, the conversion is also affected by temperature. Increased temperature increases conversion up to a certain temperature and decreases conversion above. The temperature corresponding to maximum conversion increases as the catalyst deactivates. This makes the coolant temperature an interesting optimization variable. The recycle rate is also a possible optimization variable. Increased recycle lowers the conversion per pass in the reactor because the inert content in the loop increases, but this increases the overall conversion of the reactor loop because the loss of unreacted synthesis gas in the purge stream is reduced. Typical operation conditions ($T_c = 523.15$ K and $R = 3.86$) were selected as a reference case.

A shut down of a part of the plant is necessary to change catalyst. The maintenance plan and the catalyst activity in all reactors at the plant determine when to replace the catalyst. This is why the catalyst lifetime is not considered as a variable in this optimization problem. In general, mathematical optimization of processes often confirms that the plant is operated close to optimal by the operators who rely on experience. This question is addressed by comparing the optimal operation policy with an operation procedure recommended for use at Tjeldbergodden methanol plant in Section 4.6). A situation in which dynamic optimization is specially valuable is considered in case 6. What if the catalyst lifetime changes unexpectedly? In unexpected situations it is less likely that the operators make the optimal decisions. Another advantage of mathematical optimization is the ability to track changes in the process (e.g. catalyst activity, fouling) by updating and repeated optimization. Updating and repeated optimization are addressed in Section 7.3.

4.2 Problem formulation

The task of finding an optimal operation policy is formulated mathematically as a dynamic optimization problem. Different formulations arise if the reactor or the loop are considered.

4.2.1 Reactor

$$\begin{aligned}
\max_{T_c(t)} P &= \int_{t_0}^{t_l} \left(F_{MeOH}(t)\right) dt \\
\text{subject to} & \\
\dot{x}(t) &= f\left(x(t), y(t), T_C(t)\right) \\
0 &= g\left(x(t), y(t), T_C(t)\right) \\
x(0) &= x_0 \\
T_{r,max}(t) &\leq 543\ K \\
513\ K \leq T_c(t) &\leq 533\ K
\end{aligned} \tag{4.1}$$

The problem can be classified as a fixed terminal time nonlinear dynamic optimization problem. The objective function, P, is the total production of methanol over the catalyst lifetime. The process model (f, g and x_0) serves as equality constrains. Two inequality constrains are included: The boiling water temperature is bounded between 513 K and 533 K, and the reactor temperature must be below 543 K at all points in the reactor at all times to prevent severe deactivation. The constraint on the reactor temperature is a path constraint (a constraint on a state variable over the total time horizon).

4.2.2 Loop

$$\begin{aligned}
\max_{T_c(t),R(t)} P &= \int_{t_0}^{t_l} \left(F_{MeOH}(t) p_{MeOH} + F_{Steam}(t) p_{Steam}\right) dt \\
\text{subject to} & \\
\dot{x} &= f\left(x(t), y(t), T_C(t), R(t)\right) \\
0 &= g\left(x(t), y(t), T_C, R\right) \\
x(0) &= x_0 \\
T_{r,max}(t) &\leq 543\ K \\
Q_{comp}(t) &\leq 1.1 \cdot Q_{comp}^{ref} \\
513\ K \leq T_c(t) &\leq 533\ K \\
2 \leq R(t) &\leq 5
\end{aligned} \tag{4.2}$$

The problem can be classified as a fixed terminal time nonlinear dynamic optimization problem. The objective function, P, represents the net profit over the catalyst lifetime. It consists of the value of the production of methanol and

net production of steam over the catalyst lifetime. The value of the synthesis gas consumed is not included in the objective function because this amount is constant. The prices of methanol (Methanex 1998) and steam (Edgar and Himmelblau 1989) are USD 115 /metric ton and USD 11/metric ton, respectively. The process model (f, g and x_0) serve as equality constrains. The coolant temperature is bounded between 513 K and 533 K and the recycle rate is bounded between 2 and 5. There are two path constrains; the temperature in the reactor must be below 543 K to prevent severe deactivation, and the recycle compressor has a capacity limit. It was assumed that the compressor duty can be increased by 10 per cent. In case 5 this limit is increased to 20 per cent.

4.3 Solution approach

4.3.1 Optimization

Dynamic optimization problems are infinite dimensional. In general, these problems can be solved by continuous methods based on Pontryagin's maximum principle or by discretization methods. The discretization methods can be classified as simultaneous (Biegler 1984) or sequential (Vassiliadis *et al.* 1994*b*, Vassiliadis *et al.* 1994*a*) methods. All variables are discretized with respect to time in the first method, resulting in a large nonlinear programming (NLP) system with algebraic constrains. In the latter method only the optimization variable is discretized and the problem is reduced to a finite dimension NLP with differential algebraic equations (DAE) as constrains. The optimization and integration are carried out in sequence, with the integration in an inner loop. One advantage of the sequential method is that the time step in the integration and the optimization can be of different length. The sequential method is also called control vector parameterization.

The optimization problem was solved by control vector parameterization. The optimization variables, $T_c(t)$ and $R(t)$, were discretized as piecewise constant profiles, which are easy to implement in real operation. A sequential quadratic programming (SQP) method is used to solve the NLP problem. The path constraints in this problem are hard constraint, meaning that even small violations are unacceptable. The path constraints were handled by converting the path constraints to endpoint constraints, and using interior point constraints in addition to to improve convergence (Vassiliadis 1993). Interior point constrains only hold at interior points, i.e. the steps used to discretized the optimization variables, and can be violated in between. The path constraints were converted to endpoint constraints by integrating the constraint violation over the time horizon, and re-

quiring the integral to be less than or equal to zero. An example of temperature constraint violation is shown in Figure 4.1. The pseudo-homogeneous reactor model was simulated with $T_c = 533$ K. The maximum reactor temperature is above the temperature constraint at the start. The integral of the constraint violation is the volume between the temperature surface and the constraint plane.

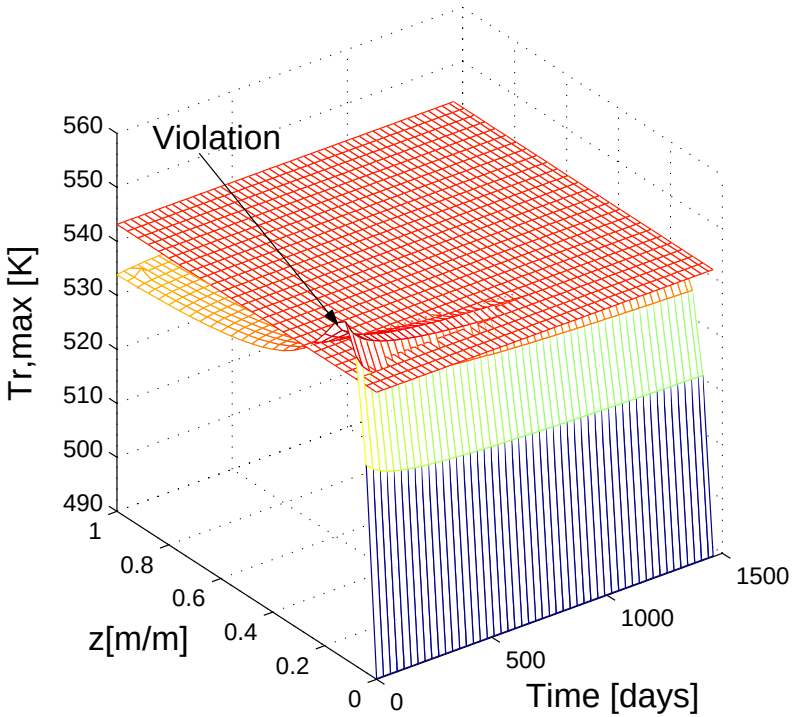

Figure 4.1. Maximum reactor temperature surface and constraint plane from simulation with $T_c = 533$ K

4.3.2 Simulation

The process model described in Chapter 3 can be classified as an integral partial differential algebraic equation (IPDAE) system. There are three spatial dimensions, axial and radial in the reactor and radial in the pellet. The model contains

partial derivatives with regards to the axial dimension in the reactor and the radial dimension in the pellet, in addition to the time dimension. Integration over the reactor length is used to calculate the path constraint violation, and integration over pellet radius is used to calculate the actual reaction rate in the gas phase. The process model was solved by the method of lines (Schiesser 1991). The reactor and the pellets were discretized by second order backward finite differences and first order collocation respectively, converting the IPDAE system to a DAE system. The finite difference method in the opposite direction of the flow is recommended for purely convective problems like the reactor equations. The pellet equations are a purely dispersive with a possibility for flow reversal, in which case orthogonal collocation with low order is recommended (PSE 1998, Schiesser 1991)

4.4 Numerical implementation

The optimization problem was implemented in the general purpose modelling environment *gPROMS* (Pantelides and Barton 1993, Oh and Pantelides 1996, PSE 2000*b*, PSE 2000*a*). This system was selected because of: 1) The flexible modelling language that separates the modelling issues from the numerical ones. 2) The state-of-the-art simulator engine. 3) The distributed systems feature and the dynamic optimization and estimation tools *gOPT* and *gEST*. The simulation approach is equation oriented and all models are solved simultaneously. A combination of symbolic, structural and numerical solution methods is used.

4.4.1 Optimization

The optimization variables were discretized in piecewise constant profile using 8 intervals. The computation time for optimization of the loop was between 5 and 10 hours on a 2 processor, 200 MHz SUN Ultra. It was also tried to increase the number of intervals, and to use a piecewise linear profile. This resulted in much larger computational time but an identical solution. Different starting points were used to make sure that the global optimum was found. The objective function was scaled to vary between 1 and 10. The optimization accuracy is shown in Table 4.1.

4.4.2 Simulation

The discretization grids in the reactor and pellet were increased to the point where a further increase did not alter the solution. The number of discretization points used and the simulation accuracy are shown in Table 4.1. Block decomposition was used.

Table 4.1
Solution parameters

Accuracy		Discretization points	
Simulation(absolute)	1e-7	Reactor	25
Simulation (relative)	1e-5	Pellet	3
Optimization	1e-3		

Initialization

Initialization of the model was challenging. The initialization of DAE systems in general is a difficult numerical problem (Kroner *et al.* 1997, Majer *et al.* 1995). Problems can arise in consistent specification of initial conditions, and in solution of the consistency equations. Convergence problems occurred in solution of the consistency equations.

The DAE system in the current problem is semi-explicit of index-1:

$$\begin{aligned} \dot{x} &= f(x,y) \\ 0 &= g(x,y) \end{aligned} \tag{4.3}$$

The specification $x(0) = x_0$ defines consistent initial conditions for this class of DAEs, and converts Equation 4.3 to a set of nonlinear algebraic equation known as the consistency equations. *gPROMS* uses a damped Newton's method to solve this large set of nonlinear equations, given initial guesses for y_0. Ordinary Newton's methods are not globally convergent; sufficient close initial guesses are needed to converge. A damped Newton's method improves convergence:

$$y_0^{n+1} = y_0^n + \alpha\delta, \quad g_z\delta = -g(y_0^n) \tag{4.4}$$

Where g_z is the Jacobian matrix. The step length α is varied between zero and one to ensure improvement in each step. The step length is small in the beginning, and increases gradually near the solution. In practice, this method is not sufficient for tough problems. Sometimes in makes no sense to step

in the Newton direction for any step length, either because the first order approximation is too coarse, or because the initial guess is too far away from the solution. The current DAE system arises from the discretization of the IPDAE system with a constant grid. This method provides no control of the local error, as opposed to integration methods with variable step size and order. A large local discretization error can lead to an ill-conditioned DAE system, and cause convergence problems in the solution of the consistency equations. The steep reaction and temperature profiles in the reactor and the pellet are a source of local discretization error, as well as strong nonlinearity in the consistency equations. The local discretization error can be controlled by the use of adaptive grid methods, but this option is not available in *gPROMS*.

Initialization of the total synthesis loop was only possible by gradual increase of one process model or sub-model at a time, supplied with the solution of the previous model. The reactor model was complicated to initialize even in the pseudo-homogeneous version. In order to obtain a solution, a strategy proposed by Ph.D. student Jens Erik Hansen (Hansen 1998) was applied. The reactor model is first solved with no reaction at all. Then, during integration, the reaction rate is slowly increased to the values given by the rate equations. The strategy is implemented by pre-multiplication of the rate expression by a variable which is initially zero and then increases to 1 as a second order response. The strategy can be viewed as a continuation method; the reactor equations with and without reaction belongs to the same family of problems, and the solution is found by integration from the easy problem to the given problem along a homotopy path. Continuation can be used to study intermediate solutions along the homotopy path, but here it is only used to find the final solution. Majer *et al.* (1995) have used continuation methods for reinitialization of DAEs, and showed that they are globally convergent for index-one DAEs. This strategy with gradual introduction of nonlinearity is analogous to a gradual increase in step length in the damped Newton's method. A similar approach was used by Kroner *et al.* (1997) to initialize simulation of a step response, by approximating the step response by a smooth input function of second order.

Integration

A fully implicit Runge-Kutta method based on the Radau IIA collocation method called SRADAU was used to integrate the DAE system. The integration was stable and fast in most cases. All variables are bounded between upper and lower limits during simulation in *gPROMS*. To make the integration robust enough for optimization, it was necessary to expand the bounds on the variables. No

problems occurred with reinitialization after step changes in the optimization variables.

4.5 Results

4.5.1 Reactor

At first, only the reactor was considered. Constant feed rate and feed composition were assumed. In practical operation, constant feed composition is hard to achieve as the catalyst deactivates. Operation with constant coolant temperature at 513.15 K was used as a reference.

Case 1: Pseudo-homogeneous reactor model

The optimal coolant temperature profile is shown in Figure 4.2. The temperature increases gradually as expected to compensate for deactivation. The temperature is above the reference temperature most of the time and in the last interval the temperature is at the upper limit at 533.15 K. The methanol production rate with optimal and reference operation is shown in Figure 4.3. The optimal production rate is lower in the first interval where the optimal coolant temperature is lower. In the remaining intervals the production rate is higher, and decreases slower than the in reference case. The total methanol production was increased by 2.56 per cent. The relative activity distribution with optimal operation and the relative activity in the middle of the reactor with optimal and reference operation is shown in Figure 4.4. The relative activity in the optimal case is higher than in the reference case the first 1.5 years, and after that lower than in the reference case. As can be seen from Figure 4.5, the maximum reactor temperature (i.e. in the centre of the tubes) is below the constraint at all times. The constraint is active at several points in the last year.

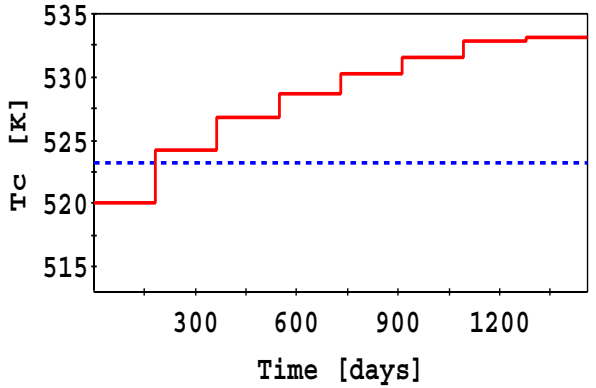

Figure 4.2. Optimal coolant temperature profile, case 1. (optimal - reference · · ·)

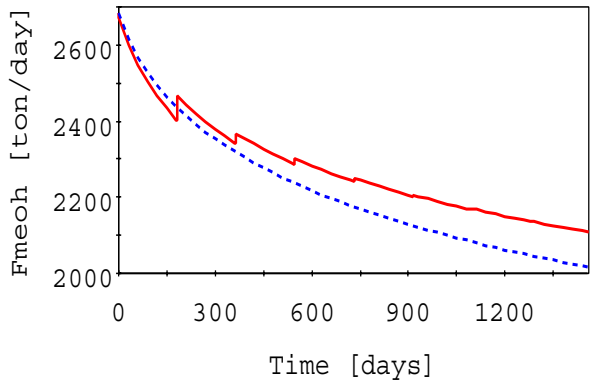

Figure 4.3. Methanol production rate, case 1. (optimal - reference · · ·)

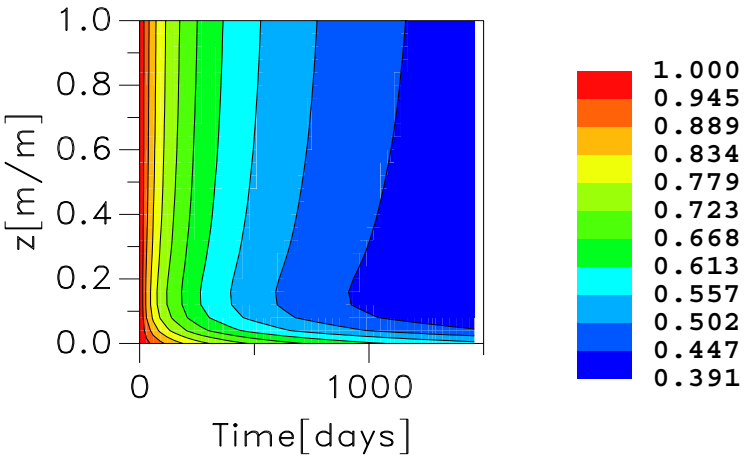

(a)

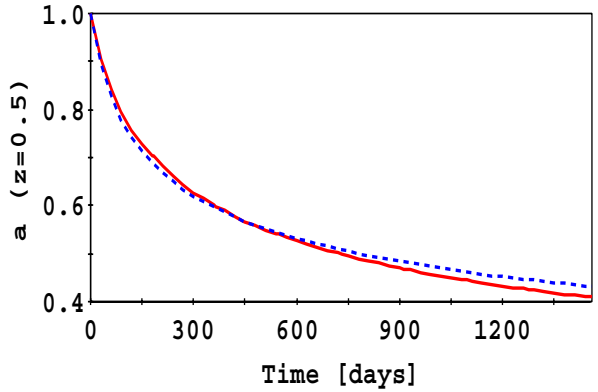

(b)

Figure 4.4. (a) Relative activity, case 1. (b) Comparison of relative activity at z = 0.5. (optimal - reference · · ·)

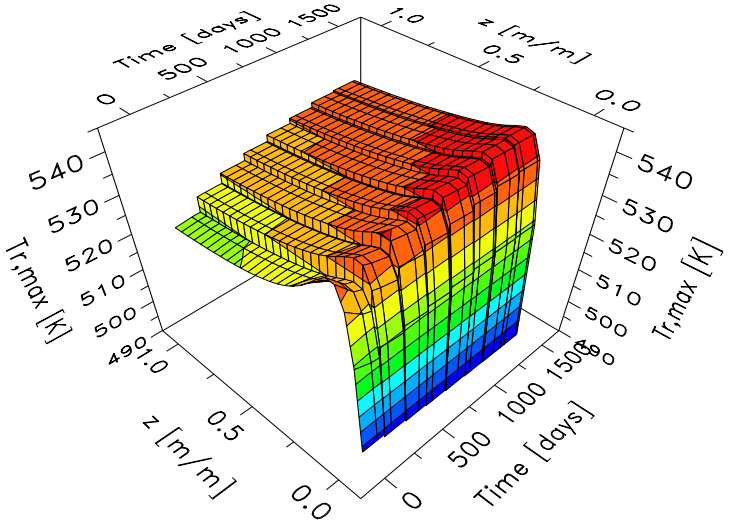

Figure 4.5. Maximum reactor temperature, case 1.

Case 2: Heterogeneous reactor model

The optimal coolant temperature profile is shown in Figure 4.6, together with the optimal coolant temperature from case 1. The temperature is above the reference temperature most of the time but never reaches the upper limit. The optimal temperature profile is lower than in case 1, especially at the end. The methanol production rate with optimal and reference operation are shown in Figure 4.7. The total methanol production was increased by 1.11 per cent. The relative activity with optimal and reference operation is shown in Figure 4.8. The relative activity in the optimal case is higher in the first 2 years, and lower the last 2 years. As can be seen from Figure 4.9, the maximum reactor temperature is well below the constraint at all times.

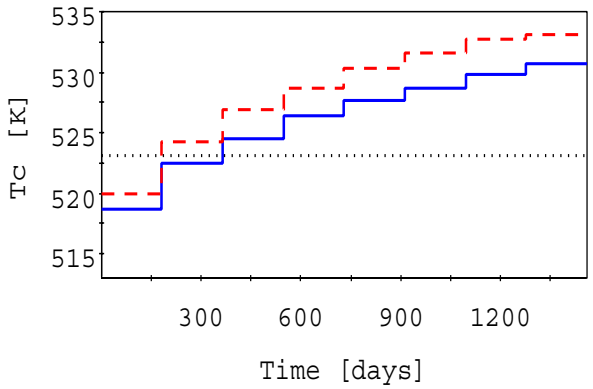

Figure 4.6. Optimal coolant temperature profile, case 2. (case 1 - - case 2 - reference · · ·)

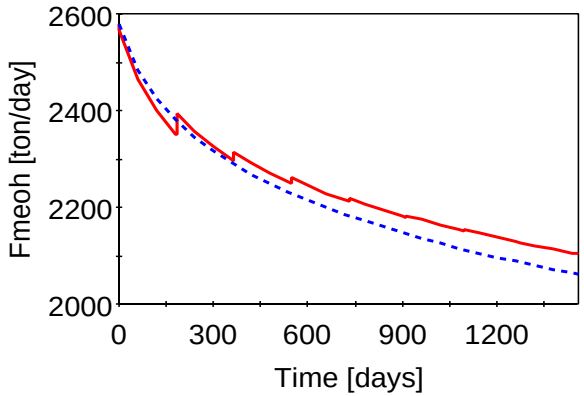

Figure 4.7. Methanol production rate, case 2. (optimal - reference · · · .)

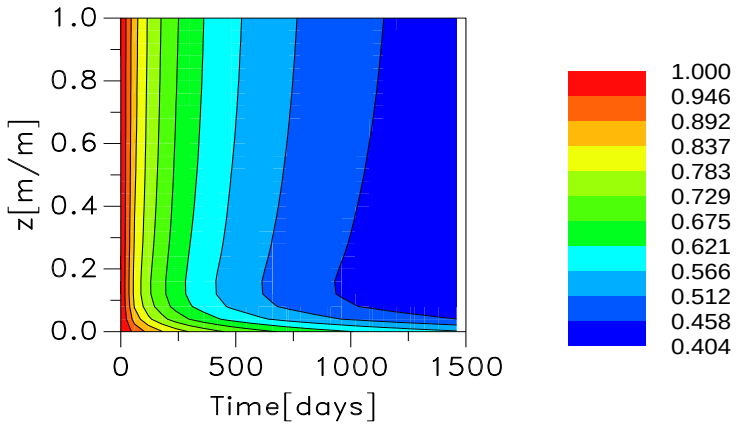

(a)

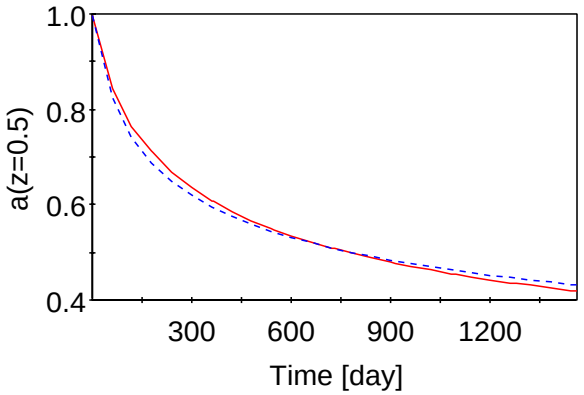

(b)

Figure 4.8. (a) Relative activity, case 2. (b) Comparison of relative activity at z = 0.5. (optimal - reference $\cdots$).

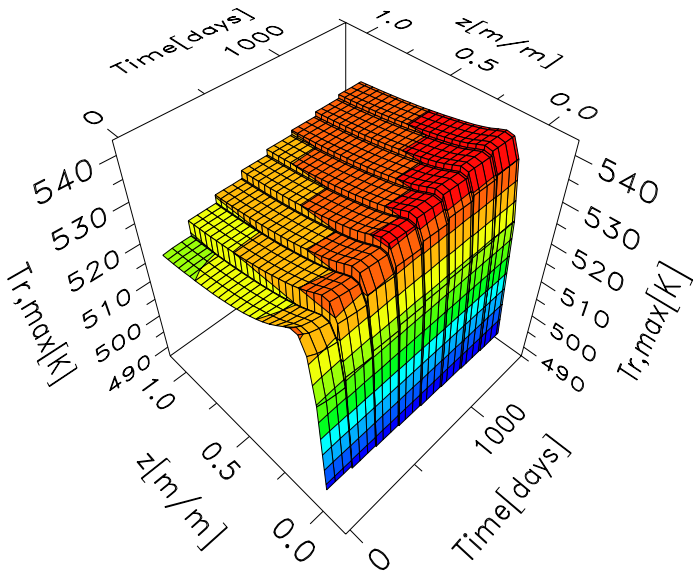

Figure 4.9. Maximum reactor temperature, case 2.

The pseudo-homogeneous model and the heterogeneous model predict different reaction rate profiles and temperature profiles, see Figure 4.10 and Figure 4.11, which leads to different optimal policies. The heterogeneous model is more correct than the pseudo-homogeneous model as discussed in Section 3.9. It is also harder to solve. The major difference in the optimal policy and predicted performance in cases 1 and 2 justifies the extra computational effort involved in the heterogeneous model.

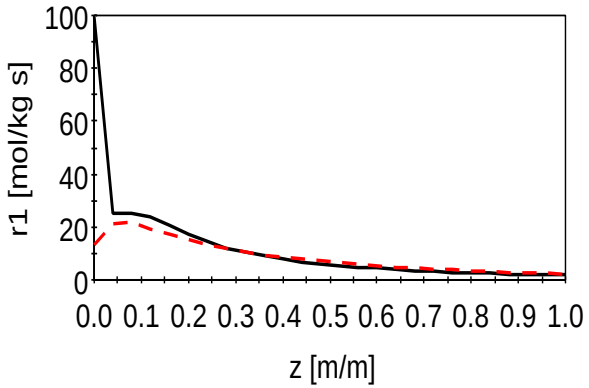

Figure 4.10. Comparison of initial reaction rate profile, reference case. (heterogeneous model - pseudo-homogeneous model - -)

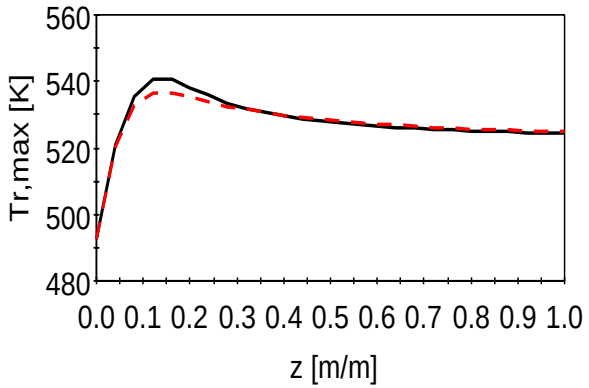

Figure 4.11. Comparison of initial maximum temperature profile, reference case. heterogeneous model - pseudo-homogeneous model - -

4.5.2 Loop

Next, optimization of the total reactor loop was considered. Constant operation with $T_c = 523.15$ K and $R = 3.86$ was used as reference case. The heterogeneous rector model was used in all cases.

Case 3: Base loop case

The optimal coolant temperature profile is shown in Figure 4.12 together with the coolant temperature profile from case 2. The same trend is seen, but the optimal temperature profile for the loop is higher than the optimal temperature profile for the reactor. The recycle rate is at a constant value corresponding to maximum compressor duty, see Figure 4.13. The methanol production rate with optimal and reference operation is shown in Figure 4.14. The optimal production rate is higher initially because the recycle rate is higher, and decreases slower due to slower catalyst deactivation caused by the gradual temperature increase. The total methanol production was increased by 1.08 per cent. The net steam production rate with optimal and reference operation is shown in Figure 4.15. The net steam production rate with optimal operation is lower because more steam is consumed in the compressor with higher recycle rate. The relative activity with optimal and reference operation is shown in Figure 4.16. The relative activity in the optimal case is higher in the first 2 years, and lower the last 2 years. The maximum reactor temperature is well below the constraint at all times, as can be seen from Figure 4.17. The total profit was increased by 0.75 per cent.

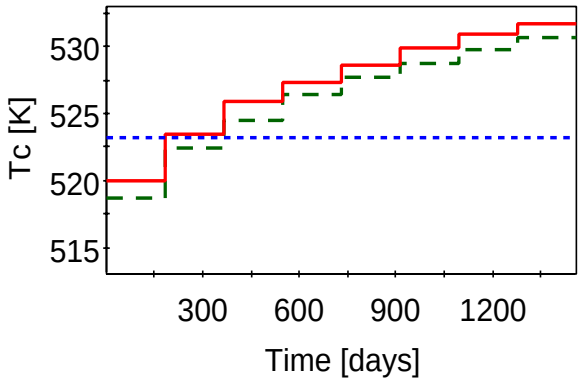

Figure 4.12. Optimal coolant temperature profile, case 3. (case 2 - - case 3 - reference · · ·)

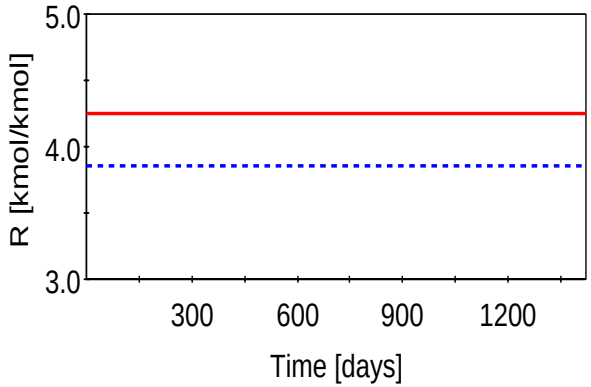

Figure 4.13. Optimal recycle rate profile, case 3. (optimal - reference · · ·)

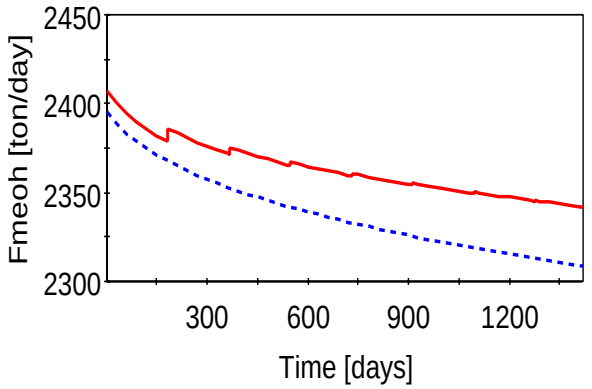

Figure 4.14. Methanol production rate, case 3. (optimal - reference · · ·)

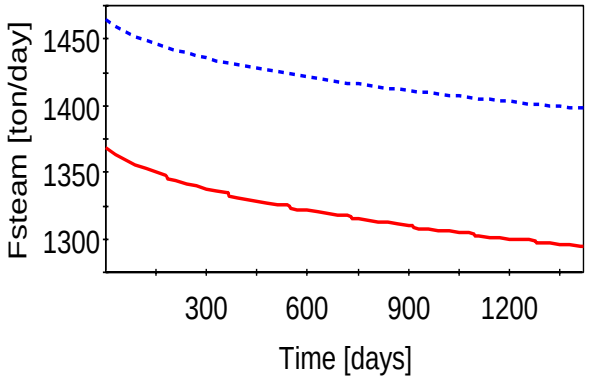

Figure 4.15. Steam production rate, case 3. (optimal - reference · · ·)

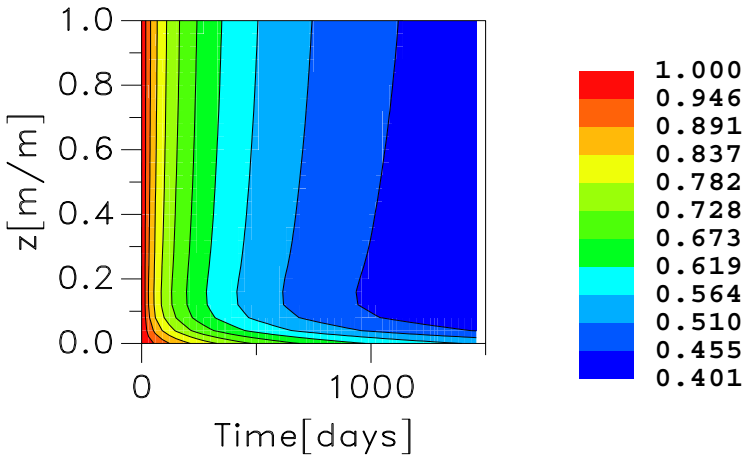

(a)

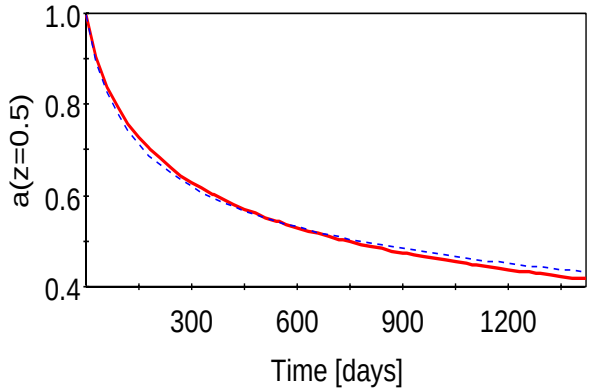

(b)

Figure 4.16. (a) Relative activity, case 3. (b) Comparison of relative activity at z = 0.5. (optimal - reference $\cdots$)

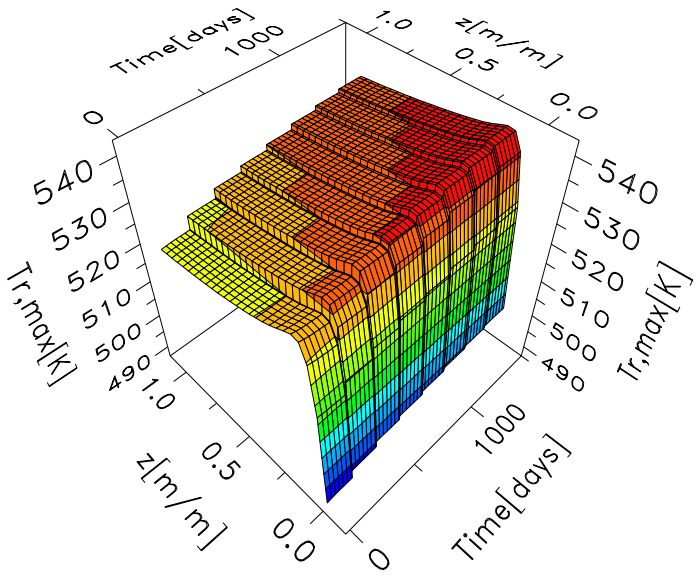

Figure 4.17. Maximum reactor temperature, case 3.

To explain the difference between cases 2 and 3: conversion, approach to equilibrium temperature, mole fraction hydrogen in the reactor feed and production rate from the reactor are compared in Figures 4.18 to 4.21. The conversion is lower in case 3 because the high recycle rate causes high concentration of inert componets, but the production rate is higher because the high recycle rate gives high throughput. The production rate also declines less in case 3, as a result of the changes in the recycle stream. As the conversion decreases, the hydrogen content in the recycle increases. Hence, the hydrogen content in reactor feed increases, which has a counteractive effect on conversion. The approach to equilibrium temperature is a little lower in case 3, indicating that the reaction mixture is closer to equilibrium.

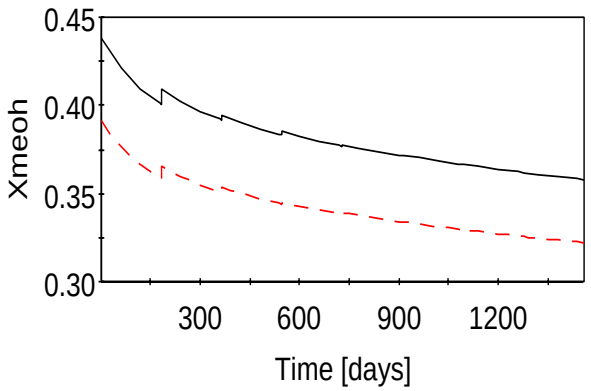

Figure 4.18. Comparison of conversion. (case 2 - case 3 - -)

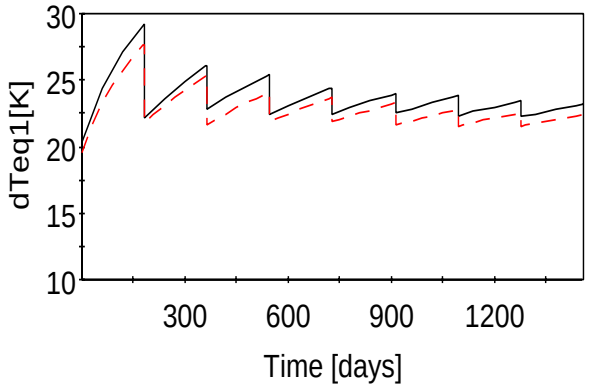

Figure 4.19. Comparison of approach to equilibrium temperature. (case 2 - case 3 - -).

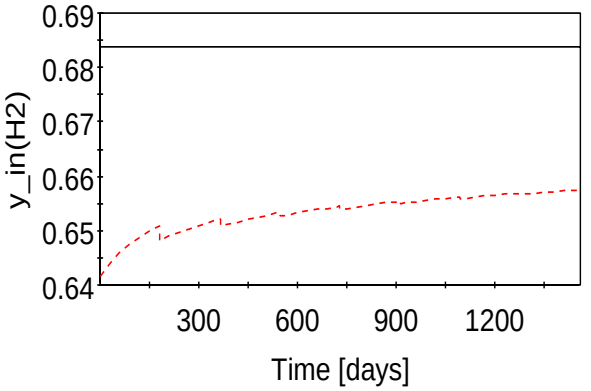

Figure 4.20. Comparison of mole fraction hydrogen in reactor feed. (case 2 - case 3 - -)

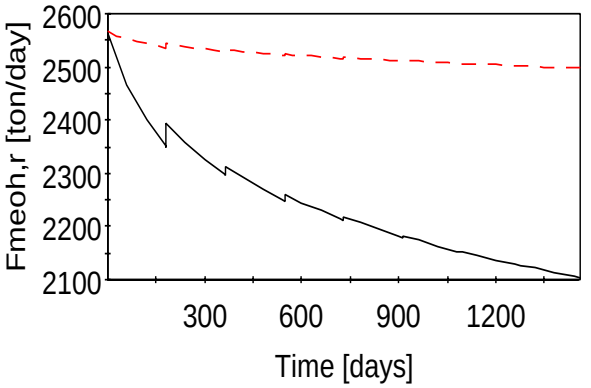

Figure 4.21. Comparison of methanol production rate from the reactor. (case 2 - case 3 - -)

Case 4: The total methanol production is maximized

The optimal coolant water temperature profile in cases 3 and 4 is almost identical as can be seen from Figure 4.22, and the optimal recycle rate is at a value corresponding to the maximum compressor duty as in case 3. The increase in profit and methanol production is almost identical (see Table 4.2 and Table 4.3). It is clear that the economic objective function is dominated by the methanol production, because the methanol price is much higher than the steam price.

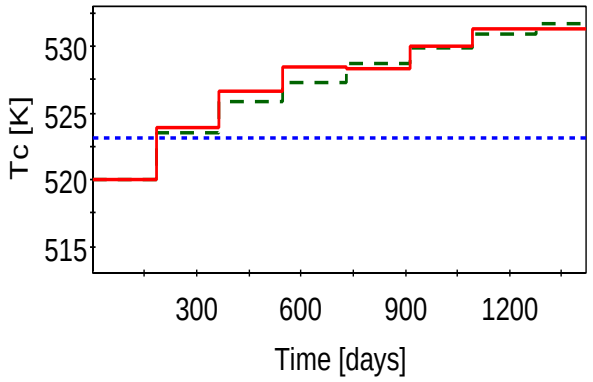

Figure 4.22. Comparison of optimal coolant temperature profiles. (case 3 - - case 4 - reference · · ·)

Case 5: 20 Percentage maximum compressor duty increase

The optimal coolant temperature profile is shown in Figure 4.23 together with the temperature profile from case 3 and the reference temperature profile. The same trend is seen as in case 3, but the temperature profile is somewhat lower. The recycle rate is at a constant value corresponding to maximum compressor duty, see Figure 4.24. The methanol production rate with optimal and reference operation is shown in Figure 4.25. The same trend is seen as in case 3, but the production rate is higher than in case 3 because the recycle rate is higher.

The total methanol production was increased by 1.67 per cent. The net steam production rate with optimal and reference operation is shown in Figure 4.26. The same trend is seen as in case 3, but the steam production rate is lower because the recycle rate is higher. The relative activity with optimal and reference operation are shown in Figure 4.27. The relative activity in the optimal case is higher in the first 2 years, and lower the last 2 years. The maximum reactor temperature is well below the constraint at all times, as can be seen from Figure 4.28. The total profit was increased by 1.03 per cent. It can be concluded that increased compressor duty limit gives greater profit.

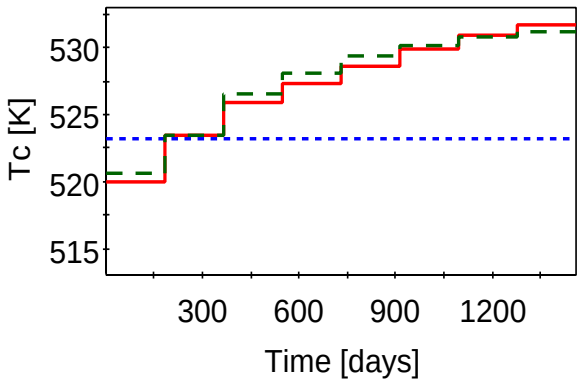

Figure 4.23. Optimal coolant temperature profile, case 5. (case 5 - case 2 - - reference · · ·)

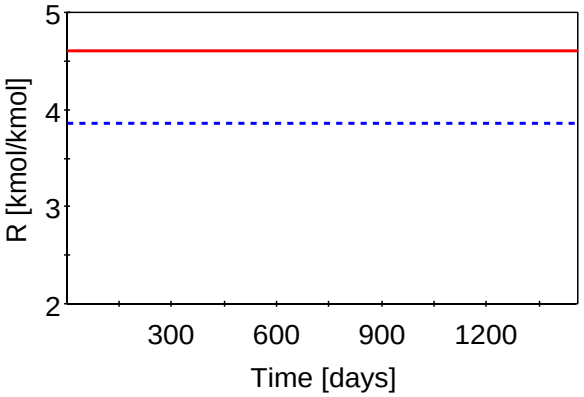

Figure 4.24. Optimal recycle rate profile, case 5. (optimal - reference · · ·)

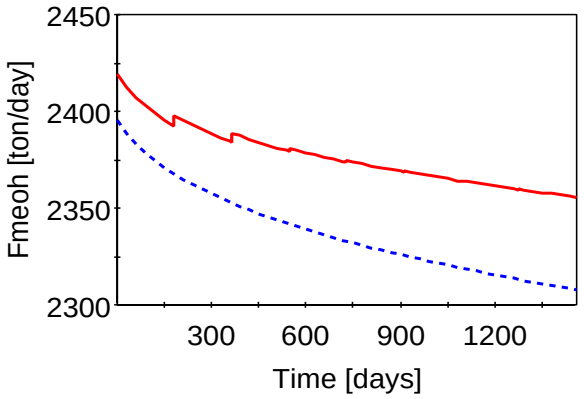

Figure 4.25. Methanol production rate, case 5. (optimal - reference · · ·)

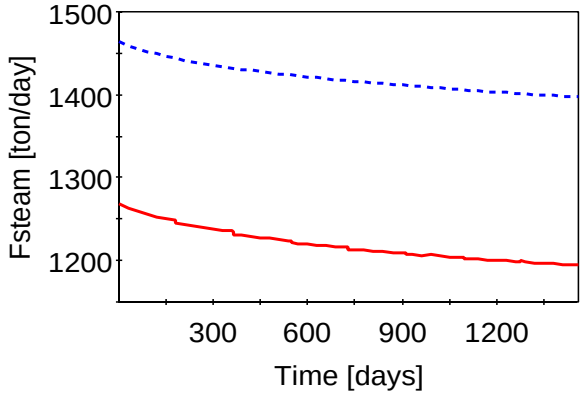

Figure 4.26. Steam production rate, case 5. (optimal - reference · · ·)

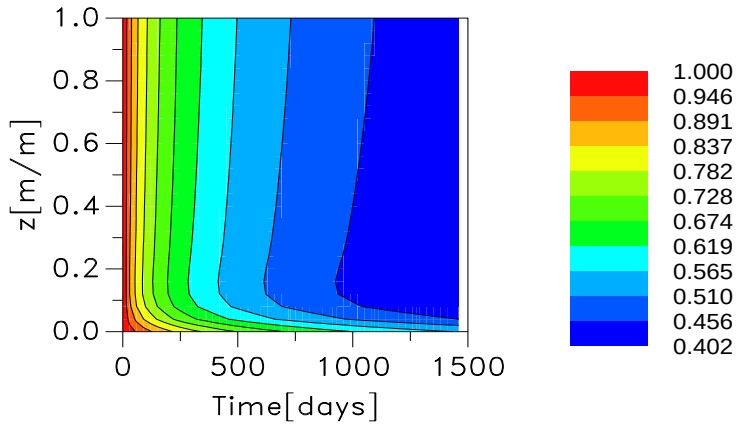

(a)

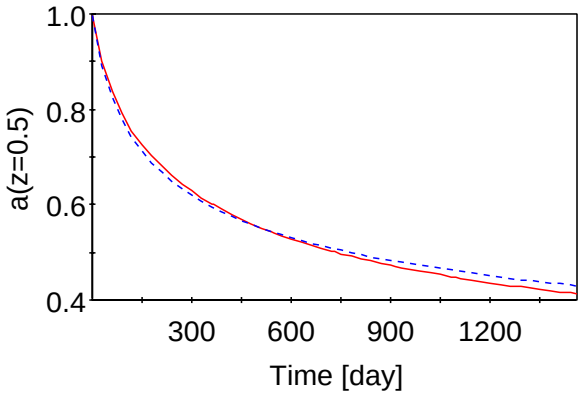

(b)

Figure 4.27. (a) Relative activity, case 5. (b) Comparison of relative activity at z = 0.5. (optimal - reference · · ·)

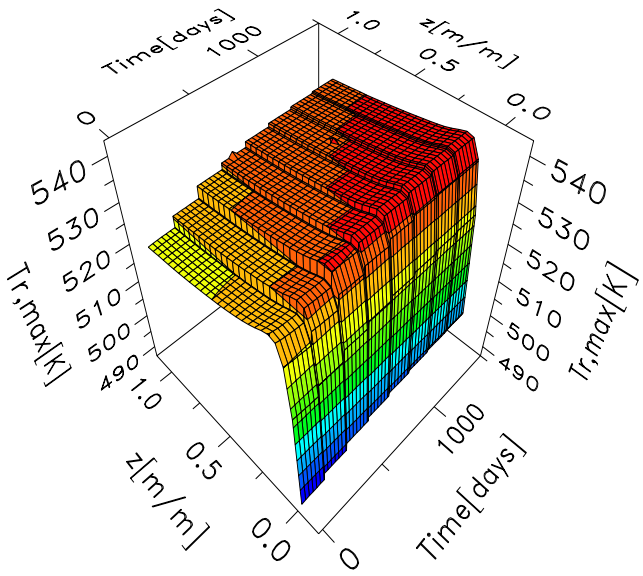

Figure 4.28. Maximum reactor temperature, case 5.

Compared to case 3, the conversion is lower and the approach to equilibrium temperature is higher in case 5, because the coolant temperature is lower (see Figure 4.29 and Figure 4.30). It seems as if it is optimal to maintain the methanol production with a high recycle rate and lower the coolant temperature somewhat in order to save the catalyst.

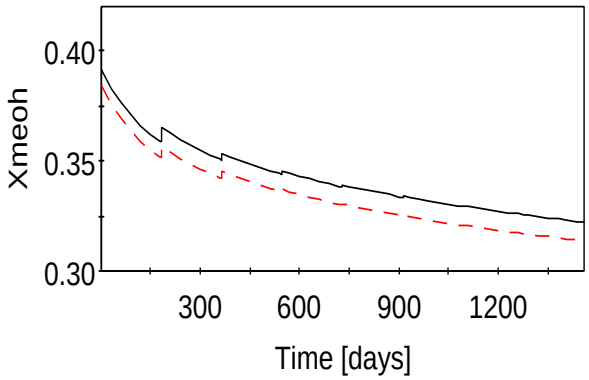

Figure 4.29. Comparison of conversion. (case 3 - case 5 –)

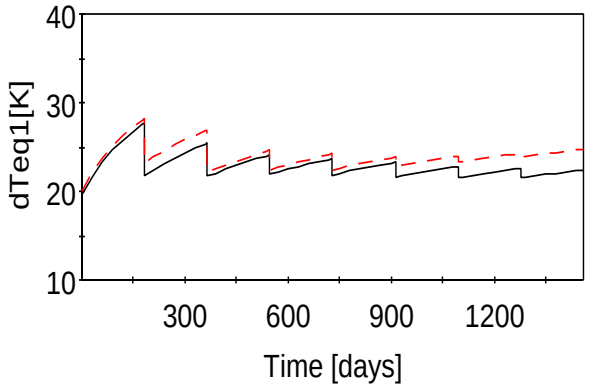

Figure 4.30. Comparison of approach to equilibrium temperature. (case 3 - case 5 –)

Case 6: Unexpected change in catalyst lifetime

After 2 years of optimal operation, it is unexpectedly decided to change the catalyst after 3 more months. Catalyst problems such as poisoning and coking in other reactors or unstable natural gas supply can lead to changes in the plant's maintenance plan. The optimal operation found in case 3 is followed for 2 years (730 days). Then the operation over the next 3 months (90 days) is optimized. T_c and R are discretized as piecewise constant profiles in 3 intervals.

The optimal coolant temperature profile is shown in Figure 4.31 together with the optimal coolant temperature profile from case 3. The coolant temperature in the last 3 months is higher than in case 3. The recycle rate is at a constant value corresponding to maximum compressor duty, as in case 3. Increased coolant temperature leads to higher methanol production rate (see Figure 4.32) caused by closer approach to equilibrium (see Figure 4.34). The total methanol production was increased by 164 metric tons over 3 months, compared to case 3. The steam production rate is lowered (see Figure 4.33), because less heat of reaction is removed when the cooling temperature is increased. The relative activities in cases 6 and 3 are compared in Figure 4.27. The relative activity is lower in case 6, as expected. The maximum reactor temperature is well below the constraint at all times, as can be seen from Figure 4.36. The total profit was increased by USD 13 997 over 3 months compared to case 3.

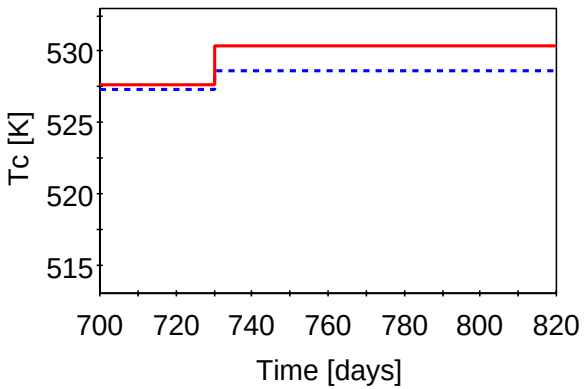

Figure 4.31. Optimal coolant temperature profile, case 6. (case 6 - case 3 $\cdots$)

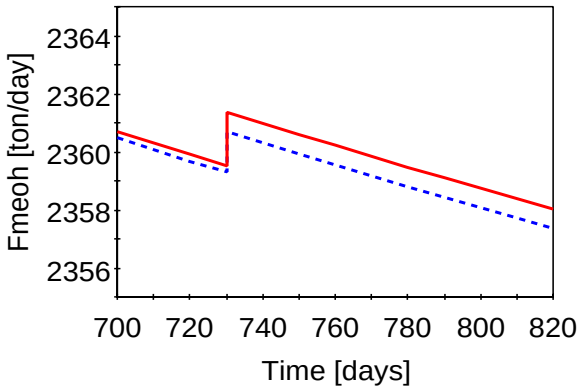

Figure 4.32. Methanol production rate, case 6. (case 6 - case 3 $\cdots$)

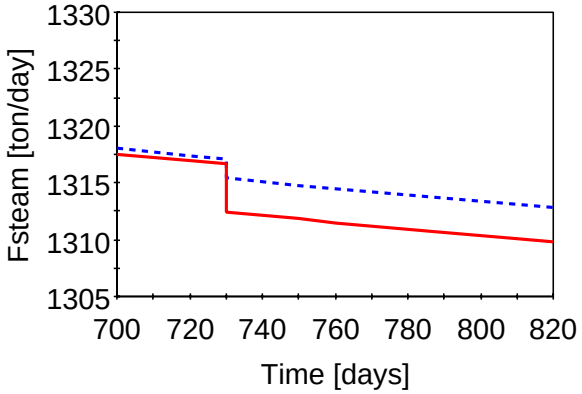

Figure 4.33. Steam production rate, case 6. (case 6 - case 3 $\cdots$)

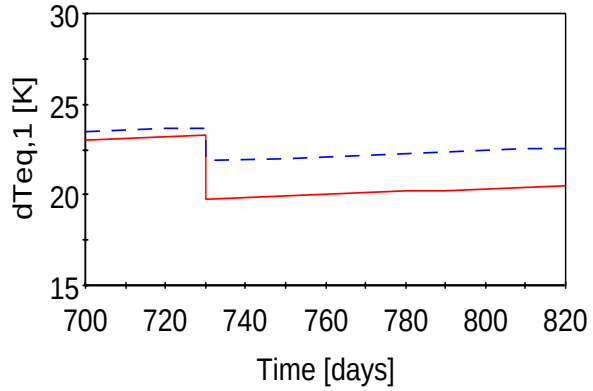

Figure 4.34. Approach to equilibrium temperature, case 6. (case 6 - case 3 $\cdots$)

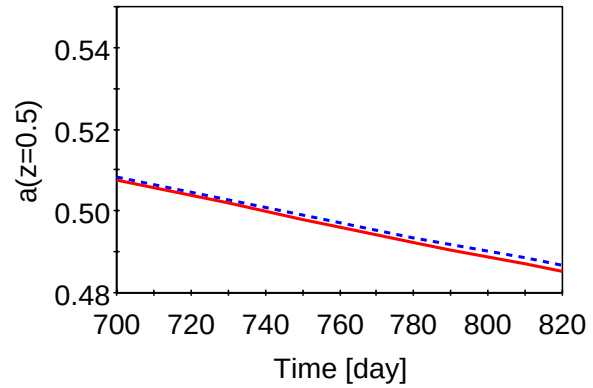

Figure 4.35. Relative activity at z = 0.5, case 6. (case 6 - case 3 $\cdots$)

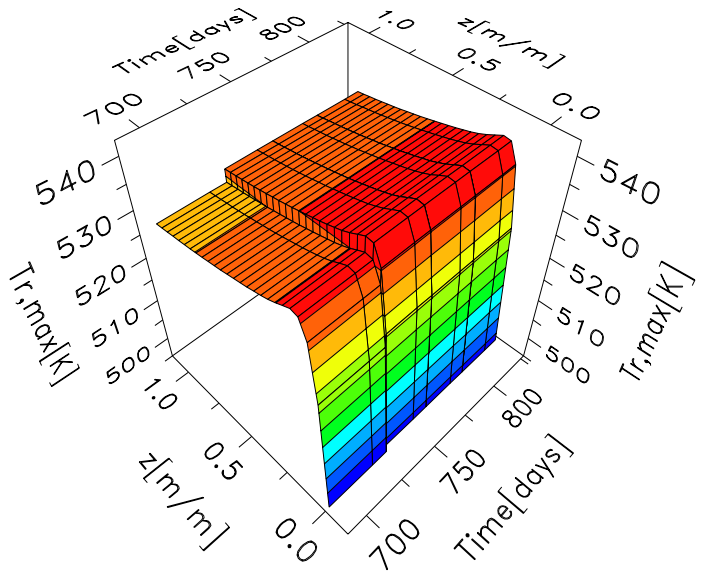

Figure 4.36. Maximum reactor temperature, case 6.

Summary of optimization results

In general, the optimal coolant temperature profile is a trade-off between being close to equilibrium conversion (low ΔT_{eq}) and limiting the catalyst deactivation. The optimal cooling temperature profiles increase gradually. The optimal recycle rate is always at a constant value corresponding to maximum compressor duty. High recycle lowers the conversion per pass, but increases the throughput. The increase in production and profit resulting from optimization in the different cases are summarized in Table 4.2 and Table 4.3. Optimization of the loop leads to an increased profit of USD 3 165 000 over four years compared to the reference case, or 0.75 per cent. If the compressor capacity can be increased, the profit can be increased by USD 4 352 000 over four years, or 1.03 per cent. When the catalyst lifetime was unexpectedly changed in case 6, the profit was increased even more in the last 3 moths.

Table 4.2
Increase in total methanol production over catalyst lifetime compared to the reference case.

Case	Δ Production [metric ton]	Value [$]	Per Cent
1	82 797	9 521 655	2.56
2	35 955	4 134 810	1.11
3	36 888	4 242 172	1.08
4	37 153	4 272 579	1.09
5	56 835	6 536 009	1.67
6†	164	18 883	

†Case 6 is compared with 2 years and 3 months of case 3. Increased production over 3 months.

Table 4.3
Increase in total profit over catalyst lifetime compared to the reference case.

Case	Δ Profit [$]	Per Cent
3	3 165 376	0.75
4	3 156 576	0.75
5	4 352 276	1.03
6†	13 997	

†Case 6 is compared with 2 years and 3 months of case 3. Increased profit over 3 months.

4.6 Comparison of optimal operation policy and operation procedure

In this section, the optimal operation policy is compared with an operation procedure recommended for use at the Tjeldbergodden methanol plant. The purpose of the operation procedure is to maintain methanol production as the catalyst deactivates. The operation procedure is described below:

Operation procedure

1. Start with T_c^{start} and R^{start}
2. If $F_{purge} > F_{purge}^{max}$: increase R by ΔR
3. If $\Delta T_{eq}^{1} > \Delta T_{eq,max}^{1}$: increase T_c by ΔT_c

The performance of the operation procedure depends strongly on the selection of the parameters T_c^{start}, R^{start}, F_{purge}^{max}, $\Delta T_{eq,max}^{1}$, ΔR and ΔT_c. Two cases with selected parameters were studied, see Table 4.4. The initial values in case 1 are typical recommendations, and the initial values in case 2 are the reference values used in Section 4.5. The maximum purge value correspond to a 5 per cent decrease in production. The remaining parameters were selected to give a reasonable good performance.

The two operation procedures are compared with optimal operation (case 3 in the previous section) in Figure 4.37 to Figure 4.40. The coolant temperature profiles show the same trend as the optimal, but are somewhat lower. It is possible to tune the operation procedure parameters to get the exact same coolant temperature profile. The recycle rate increases gradually until the compressor limit is reached after 2 - 3 years. The methanol production is lower than the

Table 4.4
Operation procedure parameters

Case	$T_c^{start}[K]$	R^{start}	$F_{purge}^{max}[mol/s]$	$\Delta T_{eq,max}[K]$	ΔR	ΔT_c
1	518.15	2.5	400	25 K	0.2	2 K
2	523.15	3.86	400	25 K	0.2	2 K

Table 4.5
Decrease in total profit over catalyst lifetime with operation procedure compared to optimal operation.

Case	Δ Profit [$]	Per Cent
1	752 700	0.18
2	1 152 700	0.27

optimal in the first 2 - 3 years as a result of the low recycle rate. Note that in procedure 1, the methanol production rate is kept almost constant for the total catalyst lifetime. This might be beneficial if there is a capacity limit in the distillation section. The steam production is higher than in the optimal case as a result of the low recycle. The total profit over the catalyst lifetime is lower than in the optimal case, see Table 4.5.

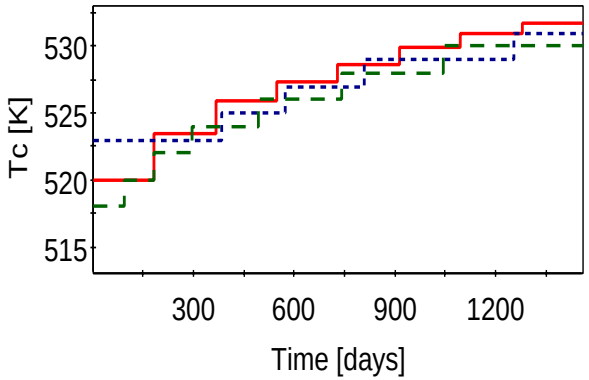

Figure 4.37. Comparison of coolant temperature profiles. (optimal - case 1 - - case 2 · · ·)

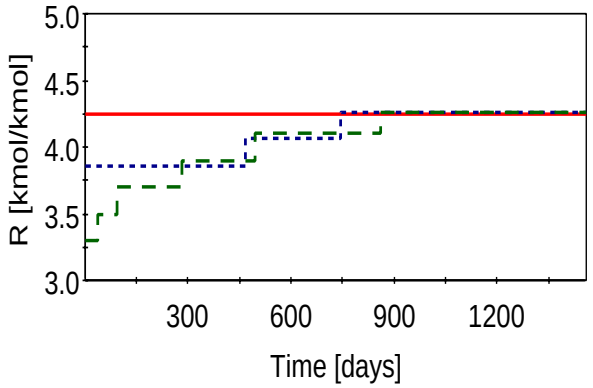

Figure 4.38. Comparison of recycle rates. (optimal - case 1 - - case 2 · · ·)

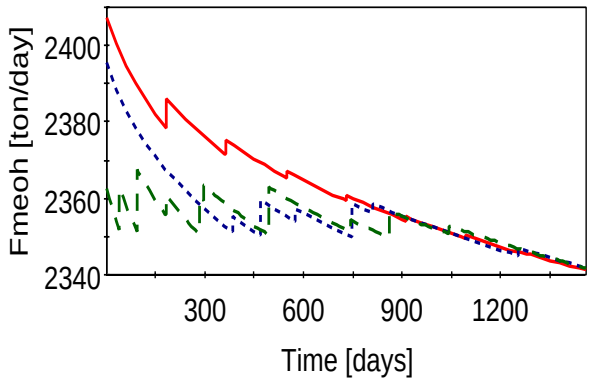

Figure 4.39. Comparison of methanol production rates. (optimal - case 1 - - case 2 · · ·)

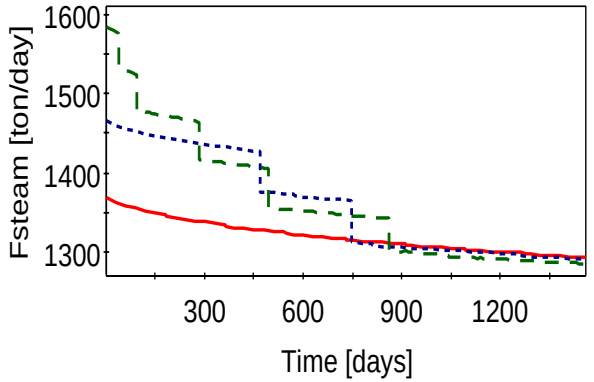

Figure 4.40. Comparison of steam production rates. (optimal - case 1 - - case 2 · · ·)

4.7 Conclusions

The methanol synthesis undergoing catalyst deactivation has been optimized with respect to coolant temperature and recycle rate.

Both the reactor alone and the loop were optimized. It is shown that a heterogeneous reactor model gives different optimal policy and more correct results than a pseudo-homogeneous reactor model. It is also shown that it is necessary to consider the loop, not only the reator. When optimizing the loop, the effect of composition variations in the recycle stream is accounted for, and an extra optimization variable, the recycle rate, is introduced. This demonstrates the importance of considering the process, and not just separate unit operations in optimization.

The optimal coolant temperature profile increases gradually, while the optimal recycle rate is at the compressor capacity limit. Optimization of the loop leads to USD 3 165 000, or 0.75 per cent, increased profit over four years compared to a selected reference case with constant operation policy. The optimal operation policy has been compared with an operating procedure recommended for the Tjeldbergodden methanol plant. The optimal operation strategy gives a little higher profit: USD 752 700 over four years compared to the operation procedure.

However, an important advantage of optimization is the ability to find the optimal operation if some of the variables in the optimization problem (e.g. catalyst lifetime or product price) change. Another advantage of mathematical optimization is the ability to track changes in the process (e.g. catalyst activity, fouling) by updating and repeated optimization. It is not recommended to implement the calculated optimal control strategies directly. The work presented can serve as a framework for implementing dynamic optimization in the control system of a methanol synthesis plant with feedback, as discussed in Section 7.3.

Chapter 5

Sensitivity in Optimization of the Methanol Synthesis with Deactivation

Parts of the work were presented at the Escape 10 conference, Florence, 2000.

The scope of the work presented in this chapter is to analyse the sensitivity in the dynamic optimization of the methanol synthesis presented in Chapter 4 with regard to the deactivation model. The sensitivity in the simulation and optimization results with regard to the deactivation model have been investigated by a first order error propagation - approach.

It was found that the uncertainties in optimal coolant temperatures with 20 per cent standard deviation in the deactivation parameters are of the same magnitude as the optimization accuracy. From these results, it can be concluded that 20 per cent standard deviation in the deactivation parameters is sufficient for optimization purposes. This can be used as a target for uncertainty in estimation of a deactivation model from experimental data or process data.

5.1 Introduction

The parameters in the catalyst deactivation model are believed to be uncertain, as discussed in Section 2.3.2 The effects of the deactivation parameters on both simulation and optimization results are found. This resulting uncertainty in simulation and optimization results has been studied by a first order error

propagation approach. The statistical methods are taken from Box *et al.* (1975).

The catalyst deactivation rate is described by the following equations:

$$\begin{aligned} \frac{da}{dt} &= -K_d \exp\left(\frac{-E_d}{R_g}(\frac{1}{T}-\frac{1}{T_0})\right) a(t)^5 \\ a_{t=0} &= a_0 \\ \tilde{a} &= 1 - \frac{a_0 - a}{a_0} \end{aligned} \tag{2.45}$$

The effect of two factors was studied, the rate constant, K_d, and the activation energy, E_d. Both deactivation parameters were varied $\pm$ 20 per cent. The experimental design is shown in Table 5.1.

Table 5.1
Experimental design.

	80 %	E_d	120 %
80 %	- -		- +
K_d		00	
120 %	+ -		+ +

5.2 Effects on simulation and optimization

5.2.1 Effects on reference simulation

Figure 5.1 shows the activity and objective function from simulations with varying deactivation parameters, coolant temperature and recycle rate at reference values (see Section 4.5.2). The centre point is close to the response plane in both graphs. The main effects and interaction effects of K_d and E_d on the activity in the middle of the reactor after four years and the scaled objective function are shown in Table 5.2. The main effects are negative as expected from Equation 2.45. The activity is more sensitive to changes in K_d than E_d. The objective function is proportional to the conversion of methanol, which depends on the catalyst activity. This explains that the effects on the objective function show the same trend as the effects on the activity. Both interaction effects are small.

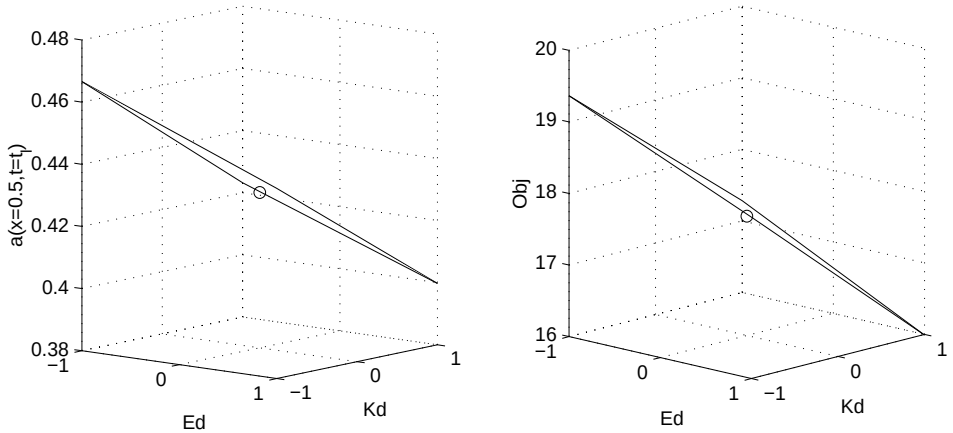

Figure 5.1. Response in activity and objective function from simulations with T_c and R at reference values. First order response plane and centre point(o).

5.2.2 Effects on simulation of the optimal case

Figure 5.2 shows the activity and objective function from simulations with optimal operation strategy (case 3 in Section 4.5.2) and varying deactivation parameters. This case illustrates what will happen if an optimal operation strategy calculated from inaccurate deactivation parameters is implemented. Both plots are nonlinear. The response surface forms two planes with a break along the $(-+)$ $(+-)$ axis. The surface is steeper in the $(++)$ direction. Changes in this direction have a larger effect than changes in the $(--)$ direction. The centre point is located above the 2^2 surface. This is expected since the operation strategy is optimized for these parameter values. The objective function at reference operation is also shown in Figure 5.2. It is interesting to note that the response plane is above this reference value most of the time. The $(++)$ corner is just below the

Table 5.2
Effects of the deactivation parameters on simulation of reference case.

Response	Mean value	Effects		
		K_d	E_d	$K_d x E_d$
$\tilde{a}^{t_l}_{z=0.5}$	0.4327	-0.0424	-0.0244	0.0010
Obj	17.7240	-2.1748	-1.2017	-0.0899

reference value. This shows that pre-calculated optimal operation strategy gives increased profit even with large, unknown variations in the deactivation parameters. The main effects and interaction effects of K_d and E_d on the activity and the object function are shown in Table 5.3. The main effects are negative as expected. The deactivation rate is directly proportional to K_d, and is independent of temperature. Higher E_d increases the deactivation rate initially, and enhances the increase in the deactivation rate when the temperature increase. This is why the E_d effects are larger compared to the effects with constant temperature. The interaction effects are of the same order of magnitude as the main effects. Both interaction effects have the same sign as the main effects. This means that the K_d effect is larger (and negative) when E_d reaches the high level.

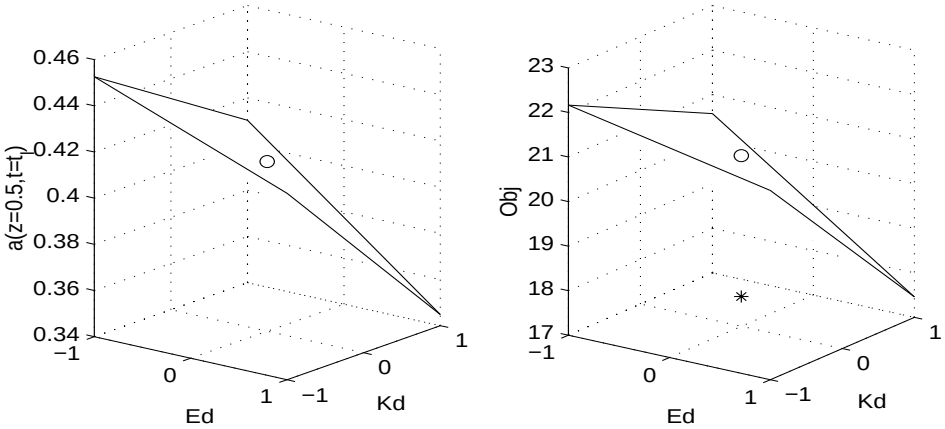

Figure 5.2. Response in activity and objective function. Simulation of pre-calculated optimal operation (case 3). First order response surface, centre point(o) and reference point(*)

5.2.3 Effects on optimization

Figure 5.3 shows the optimal discretized coolant temperatures from optimizations with varying parameters. The centre point is right below the response plane in the first three intervals and above in interval seven, but all points are within the standard deviation. This excludes nonlinear response surfaces. The standard deviation of the optimal coolant temperatures is estimated to ± 0.4 K

(see Appendix A).

The main effects of K_d and E_d on the optimal coolant temperatures are shown in Table 5.4. There are no significant interaction effects. A trade-off between reaction and deactivation determines the optimal coolant temperature profile. The K_d effects are positive. The coolant temperatures are increased to compensate for the increased deactivation rate from an increase in K_d. The E_d effects are negative and shrinking in the first three time intervals, and not significant in the rest of the intervals. Increased E_d makes the deactivation rate more sensitive to temperature. The coolant temperature is lowered to reduce the deactivation. The temperatures in the first intervals are more important because most of the deactivation takes place at the start. To sum up, an increase in K_d lifts the optimal profile and an increase in E_d changes the shape of the profile.

Table 5.3
Effects of the deactivation parameters on activity and objective function from simulations of pre-calculated optimal operation (case 3).

Response	Mean value	Effects		
		K_d	E_d	$K_d x E_d$
$\tilde{a}^{t_l}_{z=0.5}$	0.4071	-0.0591	-0.0487	-0.0168
Obj	20.3615	-2.6904	-2.0156	-1.0971

Table 5.4
Effects of deactivation parameters on optimal coolant temperatures.

Response	Mean value	Effects	
		K_d	E_d
$T_c(1)$ $[K]$	520.3 ± 0.2	0.7 ± 0.4	-1.4 ± 0.4
$T_c(2)$ $[K]$	523.9 ± 0.2	0.9 ± 0.4	-1.0 ± 0.4
$T_c(3)$ $[K]$	526.1 ± 0.2	0.9 ± 0.4	-0.7 ± 0.4
$T_c(4)$ $[K]$	527.6 ± 0.2	1.1 ± 0.4	
$T_c(5)$ $[K]$	529.0 ± 0.2	0.8 ± 0.4	
$T_c(6)$ $[K]$	530.0 ± 0.2	0.8 ± 0.4	
$T_c(7)$ $[K]$	530.9 ± 0.2	1.0 ± 0.4	
$T_c(8)$ $[K]$	531.7 ± 0.2	0.9 ± 0.4	

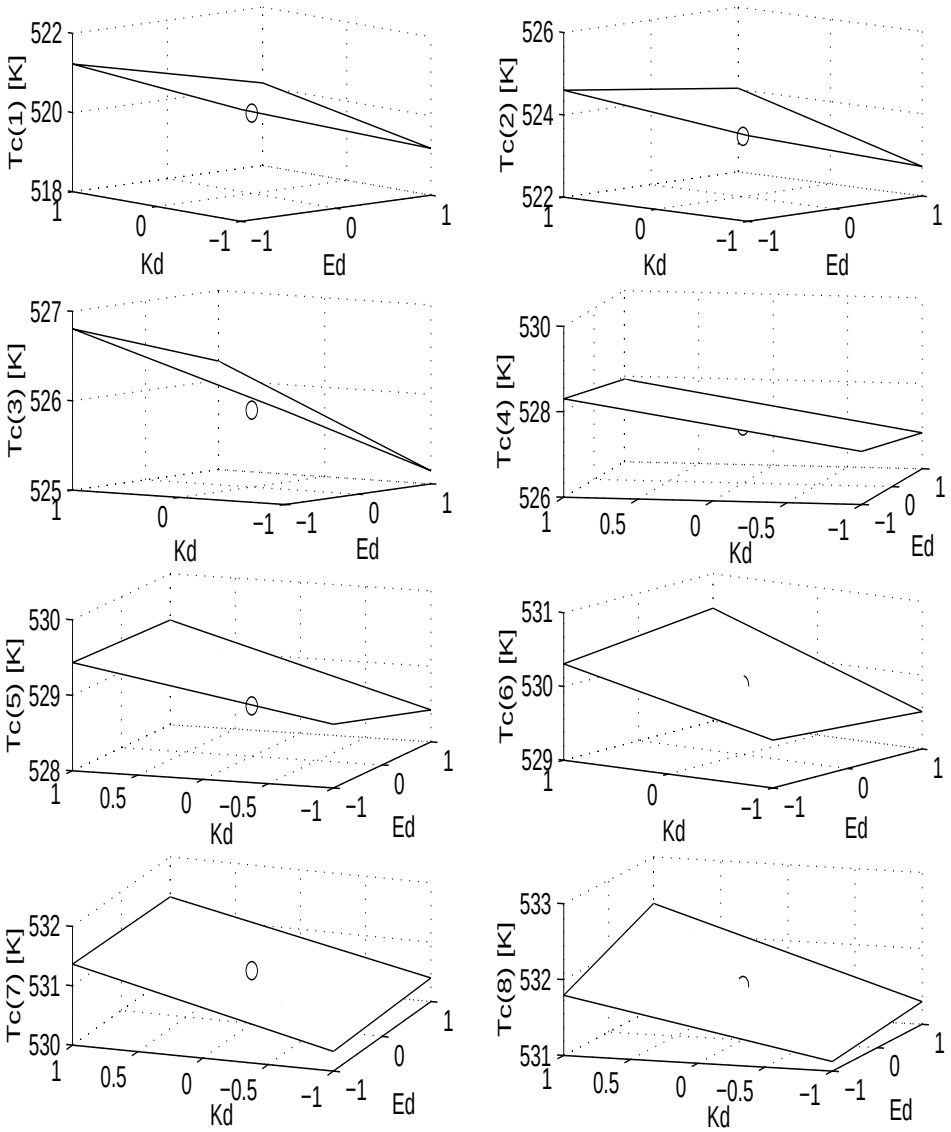

Figure 5.3. Response in optimal coolant temperatures. First order response plane and centre point(o).

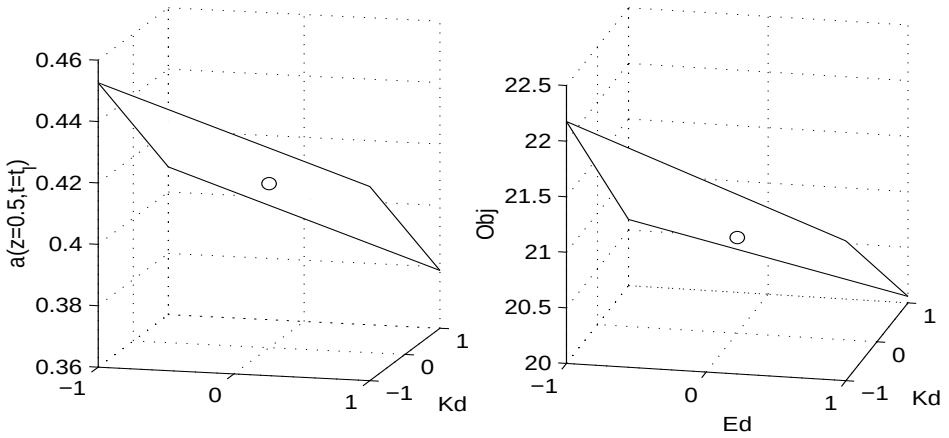

Figure 5.4. Response in optimal activity and objective function. First order response plane and centre point(o).

The activity and objective function from optimization with varying parameters are shown in Figure 5.4. The centre points are close to the response plane, excluding a curved response surface. Main effects and interaction effects of K_d and E_d on the optimal objective function and profit are shown in Table 5.5. As expected, both effects are negative. An increase in both factors leads to an increased deactivation rate. Increased deactivation leads to lower activity and objective function, even if the cooling temperatures are optimized to counteract this effect. Compared to Section 5.2.2, the effects on activity are similar but the effects on the objective function are much smaller. This is a result of the optimization. The interaction effect in the objective function has an opposite sign to the main effects, meaning that the K_d effect is larger (and negative) when E_d is at the low level. There is no significant interaction effect on the activity.

Table 5.5
Effect of deactivation parameters on optimal activity and objective function.

Response	Mean value	Effects		
		K_d	E_d	$K_d x E_d$
$\tilde{a}^{t_l}_{z=0.5}$	0.4157	-0.0444	-0.0294	
Obj	21.0220 ± 0.0005	-1.389 ± 0.001	-0.728 ± 0.001	0.190 ± 0.001

5.3 Uncertainty propagation

It is interesting to see how statistical uncertainty in the deactivation parameters propagates to the optimization and simulation results. Different cases were studied, with combinations of standard deviations and correlation factors of K_d and E_d as shown in Table 5.6 . These uncertainties are regarded as extreme cases, were case 1 represents small uncertainty and case 6 large uncertainty.

The propagated statistical uncertainties from the deactivation parameters to the simulation and optimization variables (f) were calculated from the following equation:

$$Var(f) = \left(\frac{df}{dK_d}\right)^2 Var(K_d) + \left(\frac{df}{dK_d}\right)^2 Var(K_d) + 2\frac{df}{dK_d}\frac{df}{dE_d}Cov(K_d, E_d)$$

$$Var(E_d) = \sigma^2_{E_d}$$

$$Var(K_d) = \sigma^2_{K_d}$$

$$Cov(E_d, K_d) = \rho_{E_d,K_d}\sigma_{E_d}\sigma_{K_d} \tag{5.1}$$

The derivatives $\left(\frac{df}{dK_d}\right)$ and $\left(\frac{df}{dE_d}\right)$ were estimated by dividing the effects obtained in Section 5.2.2 by the absolute changes in K_d and E_d.

The propagated uncertainties in activity and objective function from reference simulation are shown in Table 5.7 and the uncertainties from simulation of pre-calculated optimal operation are shown in Table 5.8. The uncertainties in

Table 5.6
Standard deviation in deactivation parameters.

Case	σ_{K_d}	σ_{E_d}	ρ_{E_d,K_d}
1	10 %	10 %	0.5
2	10 %	10 %	0.95
3	20 %	20 %	0.5
4	20 %	20 %	0.95
5	40 %	40 %	0.5
6	40 %	40 %	0.95

Table 5.7
Standard deviation in simulation results. Simulations of reference operation.

Response	Centre p.	Standard deviation					
		Case 1	Case 2	Case 3	Case 4	Case 5	Case 6
$\tilde{a}^{t_l}_{z=0.5}$	0.430	± 0.015	± 0.017	± 0.029	± 0.033	± 0.059	± 0.066
Obj	17.67	± 0.74	± 0.83	± 1.48	± 1.67	± 2.96	± 3.34

Table 5.8
Standard deviation in simulation results. Simulation of pre-calculated optimal operation (case 3).

Response	Centre p.	Standard deviation					
		Case 1	Case 2	Case 3	Case 4	Case 5	Case 6
$\tilde{a}^{t_l}_{z=0.5}$	0.414	± 0.023	± 0.027	± 0.047	± 0.053	± 0.094	± 0.106
Obj	20.83	± 1.02	± 1.16	± 2.05	± 2.32	± 4.09	± 4.65

simulation of pre-calculated optimal operation are large, as expected from the effects obtained in Section 5.2.2. Variations in the correlation coefficient had small influence on the uncertainties in both the simulation and optimization results.

The propagated uncertainties in the optimal coolant temperatures, the optimal activity and objective function are shown in Table 5.9. The uncertainties in the objective function are relatively large. Converted to increased profit, the uncertainties are ±0.2 per cent in case 4 and ±0.1 per cent in case 2. The uncertainties in optimal coolant temperature are relatively small. Propagated uncertainty in coolant temperatures in cases 3 and 4 are of the same order of magnitude as the optimization accuracy. This is illustrated in Figure 5.5. It can be concluded that 20 per cent standard deviation in the deactivation parameters is sufficient for optimization purposes. More accurate deactivation models will not lead to a more accurate optimal operation. This can be used as a target for uncertainty in developing new deactivation models. In addition to uncertainty in calculation of the optimal coolant temperatures, there is uncertainty in implementation of the coolant temperature. The implementation uncertainty is estimated to ± 0.5 K. This is another reason why a more accurate deactivation model and increased optimization accuracy is unnecessary.

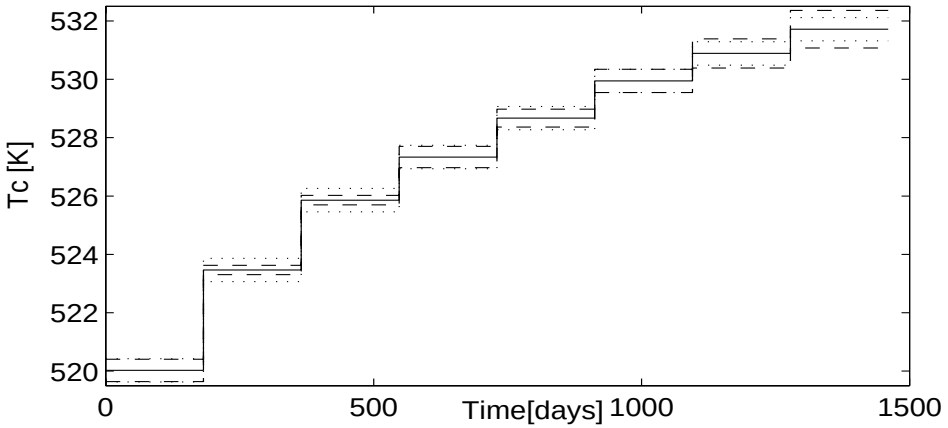

Figure 5.5. Standard deviation in optimal coolant temperature profile. Propagated error in case 4 (- -) and optimization error(· · ·)

Table 5.9
Standard deviation in optimization results.

Response	Centre p.	Standard deviation					
		Case 1	Case 2	Case 3	Case 4	Case 5	Case6
$\tilde{a}^{t_l}_{z=0.5}$	0.414	± 0.016	± 0.018	± 0.032	± 0.037	± 0.064	± 0.073
Obj	20.86	± 0.47	± 0.52	± 0.93	± 1.05	± 1.86	± 2.10
$T_c(1)$ [K]	520.03	± 0.30	± 0.19	± 0.61	± 0.38	± 1.21	± 0.77
$T_c(2)$ [K]	523.47	± 0.24	± 0.08	± 0.48	± 0.16	± 0.95	± 0.32
$T_c(3)$ [K]	525.86	± 0.21	± 0.08	± 0.41	± 0.16	± 0.82	± 0.32
$T_c(4)$ [K]	527.34	± 0.24	± 0.18	± 0.48	± 0.37	± 0.96	± 0.73
$T_c(5)$ [K]	528.67	± 0.18	± 0.15	± 0.36	± 0.31	± 0.72	± 0.61
$T_c(6)$ [K]	529.94	± 0.20	± 0.20	± 0.40	± 0.40	± 0.80	± 0.80
$T_c(7)$ [K]	530.89	± 0.25	± 0.25	± 0.50	± 0.50	± 1.00	± 1.00
$T_c(8)$ [K]	531.72	± 0.29	± 0.32	± 0.58	± 0.64	± 1.15	± 1.29

5.4 Conclusions

A sensitivity analysis of dynamic optimization of the methanol synthesis has been performed. The sensitivity in the simulation and optimization results with regard to the deactivation model has been investigated by a first order error propagation - approach.

The effects of variations in the two deactivation parameters in the simulation of reference operation and pre-calculated optimal operation were studied. Negative effects from the rate constant and activation energy on the activity and objective function were found in both cases, as expected. The response plane for the simulation of pre-calculated optimal operation is always above the reference point. This means that implementation of an optimal operation calculated from an uncertain deactivation model will lead to improvements, compared to the reference operation. Effects were also found on the optimal coolant temperature profile and objective function. Both the rate constant and the activation energy have a negative effect on the objective function. An interaction effect between the two factors was observed. A positive effect were found on the optimal coolant temperature profile from the rate constant. The activation energy had a negative effect on the first intervals of the coolant temperature profile, resulting in a steeper profile.

Uncertainty propagation from he deactivation parameters to the optimization results has been studied for different uncertainties in the deactivation parameters. The uncertainties are relative large in the scaled objective function and relative small in the optimal coolant temperatures. Uncertainties in coolant temperatures with 20 per cent standard deviation in the deactivation parameters are of the same magnitude as the optimization accuracy. From these results, it can be concluded that 20 per cent standard deviation in the deactivation parameters is sufficient for optimization purposes. More accurate deactivation parameters will not lead to a more accurate optimal operation strategy. This can be used as a target for uncertainty in the estimation of a deactivation model from process data or experimental data. In the latter case, the experimental design can be planned to achieve this standard deviation target.

Chapter 6

Estimation of a Catalyst Deactivation Model from Historical Process Data

Parts of the work will be presented at the Escape 11 conference, Kolding, 2001.

The scope of the work presented in this chapter is to develop a deactivation model for the methanol synthesis catalyst that includes the effect of temperature and water, based on historical process data from a methanol plant. There is a need for a good industrial-scale deactivation model for the methanol synthesis.

A model on the generalized power law form was successfully fitted to process data from a limited period of time. The estimated model is of second order. No measurable effect of water was found, probably because the variations in the feed compositions were too small. The model parameters found in this work are not open information. The model parameters are not valid throughout the total catalyst life-time because the deactivation process is fast in the beginning and slower after some time. To obtain a model that is valid over the total catalyst life-time, it is essential that data from a larger period of time are available. It has been demonstrated that the historical process data used contains enough information to estimate a catalyst deactivation model that describes the effect of temperature, but too little information to estimate the effect of the reaction mixture composition.

6.1 Introduction

The methanol synthesis catalyst deactivates with time, and lasts for 3 to 4 years under normal operating conditions. Sintering is the main deactivation mechanism. The catalyst deactivates asymptotically, fast in the beginning and slower after some time. A good deactivation model is necessary to predict the methanol production and optimize the operation of the reactor system. No satisfactory industrial-scale model have been published before. The development of a deactivation model for an industrial scale reactor involves several problems: Because of the asymptotic behaviour, data are needed for long periods, preferably over many years. Such time-consuming experiments are unlikely to be performed in the laboratory. Accelerated experiments in the laboratory require very clean gases to avoid catalyst poisoning, and extrapolation of the results to industrial conditions is not trivial. Planned experiments in process plants with large variations in input variables are expensive and can cause operational problems. Passive data from process plants contain less information, so it may not be possible to identify a model. Estimation of activity from process data at a given time is a problem that also occurs in state surveillance and model-based control and optimization. The challenge in this work has been to decide if the historical process data contains enough information, and if so, to estimate a mechanistic deactivation model.

6.2 Deactivation model form

Mechanisms and models of catalyst deactivation are reviewed in Section 2.3. Few deactivation models are published, and they predict quite different deactivation rates. Most of the models are developed on laboratory scale and therefore predict too fast deactivation. There is agreement in the literature that sintering increases with raised temperature and a greater fraction of water in the reacting gas. Even so, most models do not account for composition. A power law expression (PLE) with high order is normally used to model deactivation by sintering. A generalized power law expression (GPLE) describes the typical asymptotically deactivation better than a power law expression (Bartholomew 1993). The following deactivation model on the GPLE form is hereby proposed:

$$\frac{da}{dt} = -K\left(a - a_{eq}\right)^m, \qquad a_{t=0} = a_0$$
$$K = K_d\left(1 + {p_{H_2O}}^n\right)\exp\left[\frac{-E_d}{R_g}\left(\frac{1}{T} - \frac{1}{T_0}\right)\right] \tag{6.1}$$

A limiting activity, a_{eq}, is approached at infinite time. The term accounting for the effect of water is a first approach: if n is estimated to be different from zero, water has an effect, and the term can be refined. Reactor temperature, partial pressure of water and activity are all functions of reactor position z and time, indexing is omitted for simplicity.

6.3 Process data

Historical process data from a limited period of about a year were used. This period is at the end of the catalyst lifetime, where the catalyst deactivation slows down. Data for a longer period were not available, because a complete variable set had not been recorded in the earlier years. The following variables were used for estimation:

- Input: Pressure, temperature, composition and flow in the reactor feed.
- Control: Cooling water temperature.
- Output: Flow and water content of raw methanol, temperature profile in the reactor (six axial measuring points), and temperature at the reactor exit.

Mean day values of all variables except water content were available. The water content was measured every week, and day values were obtained by linear interpolation. Several temperature measurements were taken at each axial point in the reactors, and the reactor temperature profile and reactor exit temperature were measured in the two parallel reactors. Mean values and variance at each axial point and at the reactor exit were calculated from the temperature measurements. The standard deviation in the raw methanol flow was estimated to be 1 per cent.

Cooling water temperature was calculated from measured pressure in the steam drum by linear interpolation of steam tables over the temperature range in question.

The data were smoothed by omitting unlikely data points and trip days. Some of the temperature measurements in the reactor obviously were wrong, as they gave temperature profiles with several minimum and maximum points.

Excel was used as a database for the process data, and manipulations of the data such as interpolation, averaging, and smoothing were performed in Excel.

6.4 Modelling

The heterogeneous reactor model described in Section 3.2.2 was used. It is unnecessary to use the total loop model, as the reactor model provides the measured output variables from the measured input variables. Because all components were not measured, two assumptions were made:

- Other components than methanol and water in the raw methanol were neglected.
- Methanol in the feed stream was neglected.

The neglected components are present in very small concentrations, and the two assumptions have opposite effects on the estimated methanol conversion. The reactors were operated without cooling in the lower section. This causes an after-reaction that raises the reactor exit temperature compared to the temperature measured in the reactor. To capture this effect in the model, cooling was omitted in the lower section of the reactor. The reactor model is discretized by backwards finite differences in the axial direction (see Section 4.4.2). The discretization points are not located exactly at the measuring points. Linear interpolation between these discretization points was used to calculate the temperature at the measuring points.

6.5 Estimation

The simulation and estimation tools *gEST/gPROMS* were used in combination with Excel. A link between *gPROMS* and Excel for simulation was created that allows *gPROMS* to run simulation with the exact input data from the Excel file, and return the results, making an immediate comparison between measurements and simulation possible. The input data to *gPROMS* for estimation were given in a long text file to save computation time. The estimation results with statistical analysis were automatically exported to Excel.

The model parameters were estimated my minimizing the maximum likelihood objective function of the measurements (Box *et al.* 1975):

$$\Phi = \frac{nm}{2} ln(2\pi) + \frac{1}{2} \min_{\theta} \left[\sum_{i=1}^{ne} \sum_{j=1}^{nv_i} \sum_{k=1}^{nm_{ij}} \left(ln(\sigma_{ijk}^2) + \frac{(\tilde{z}_{ijk} - z_{ijk})^2}{\sigma_{ijk}^2} \right) \right] \qquad (6.2)$$

The variance in the measurements was assumed to be independent of the magnitude of the measurements. The estimation of the initial condition used the calculated variance of the averaged measurement of each output variable. In the estimation of the model parameters, the mean variance of the averaged measurements of each output variable was used. Constant variance reduces Equation 6.2 to a least squares objective function. The solution methods and simulation accuracy described in Section 4.4.2 were used, and the estimation accuracy was 10^{-3}. Because the reaction order m is an integer, and *gEST* does not handle mixed integer optimization problems, the optimal value was found by comparing optimizations with m fixed at different integer values.

The estimation problem consists of two parts: estimation of the initial activity profile, $a_0(z)$, and estimation of the five model parameters in Equation 6.1. It was more difficult to get a good estimation in the first part, because a continuous activity profile was estimated from only six temperature measurements. To simplify the initial estimation problem, the initial activity profile was described by two parameters a^1_{init} and a^2_{init}:

$$\begin{aligned} a_0 &= a^1_{init} && for\ z = 0 \cdots z_1 \\ a_0 &= a^1_{init} + \frac{(a^2_{init} - a^1_{init})(z - z_1)}{z_2 - z_1} && for\ z = z_1 \cdots z_2 \\ a_0 &= a^2_{init} && for\ z = z_2 \cdots 1 \end{aligned} \qquad (6.3)$$

6.6 Results

6.6.1 Initial condition

The two parameters in Equation 6.3 were successfully estimated with 10 per cent standard deviation[1], and gave a good fit of the temperature profile, see Figure 6.1. A large deviation in the first measuring point is observed. The temperature profile is steep around this point, so a small deviation in the location of the measuring point will cause a large deviation in the measured temperature. The standard deviation in this measurement is also large, which means that the contribution to the objective function from this measurement is small. Another explanation is that the chemical reduction of the catalyst performed to activate the catalyst at the start reduced the catalyst volume. If the catalyst tubes are empty at the top, the reaction and temperature rise will start further down in the tubes. Note

[1] Values are confidential

that the deviation in the reactor exit temperature is small. The predicted initial production rate is 99.9 per cent of the measured initial production rate.

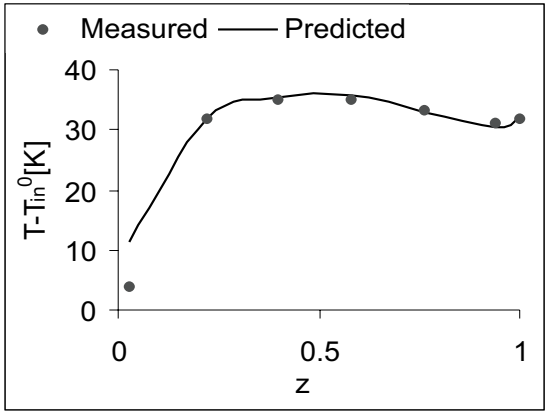

Figure 6.1. Estimated and measured relative initial temperature profile.

6.6.2 Model parameters

Case 1: Estimation with all measurements

Estimation with all measurements was first attempted. The reactor exit temperature, T_{out}, caused problems in estimation of the deactivation model parameters. A poor fit of the production rate and reactor temperatures is seen in Figure 6.3 and Figure 6.4. A large and systematic deviation in T_{out} that increased over time is seen in Figure 6.2. The large deviation in T_{out} dominates the objective function and gives a poor fit for the other measurements. No systematic deviation in the reactor temperatures was seen, except the deviation in the first measurement previously discussed. This suggests that there is an unknown effect on T_{out} that is not described by the model. Measurement error could be the cause of this effect. It was decided to exclude T_{out} from the estimation for these reasons.

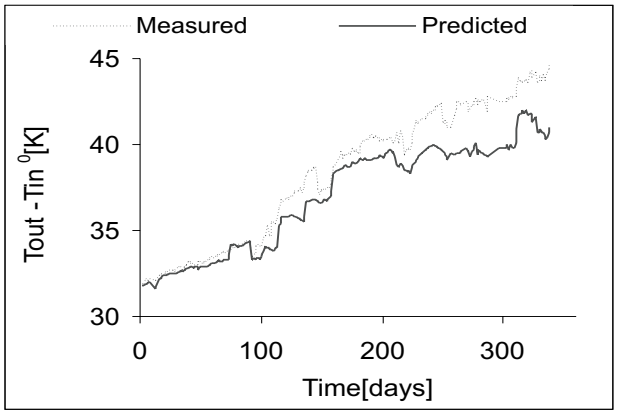

Figure 6.2. Estimated and measured reactor exit temperature, case 1.

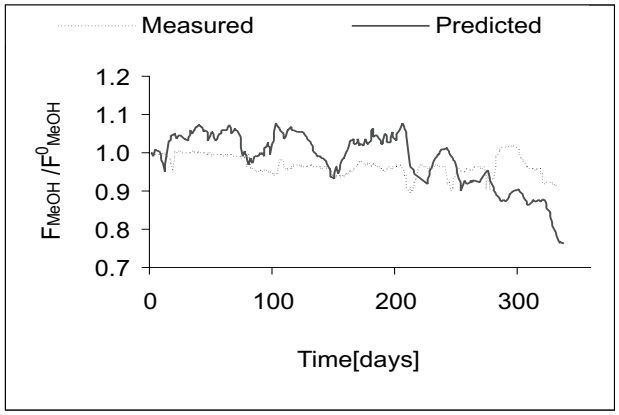

Figure 6.3. Estimated and measured relative methanol production rate, case 1.

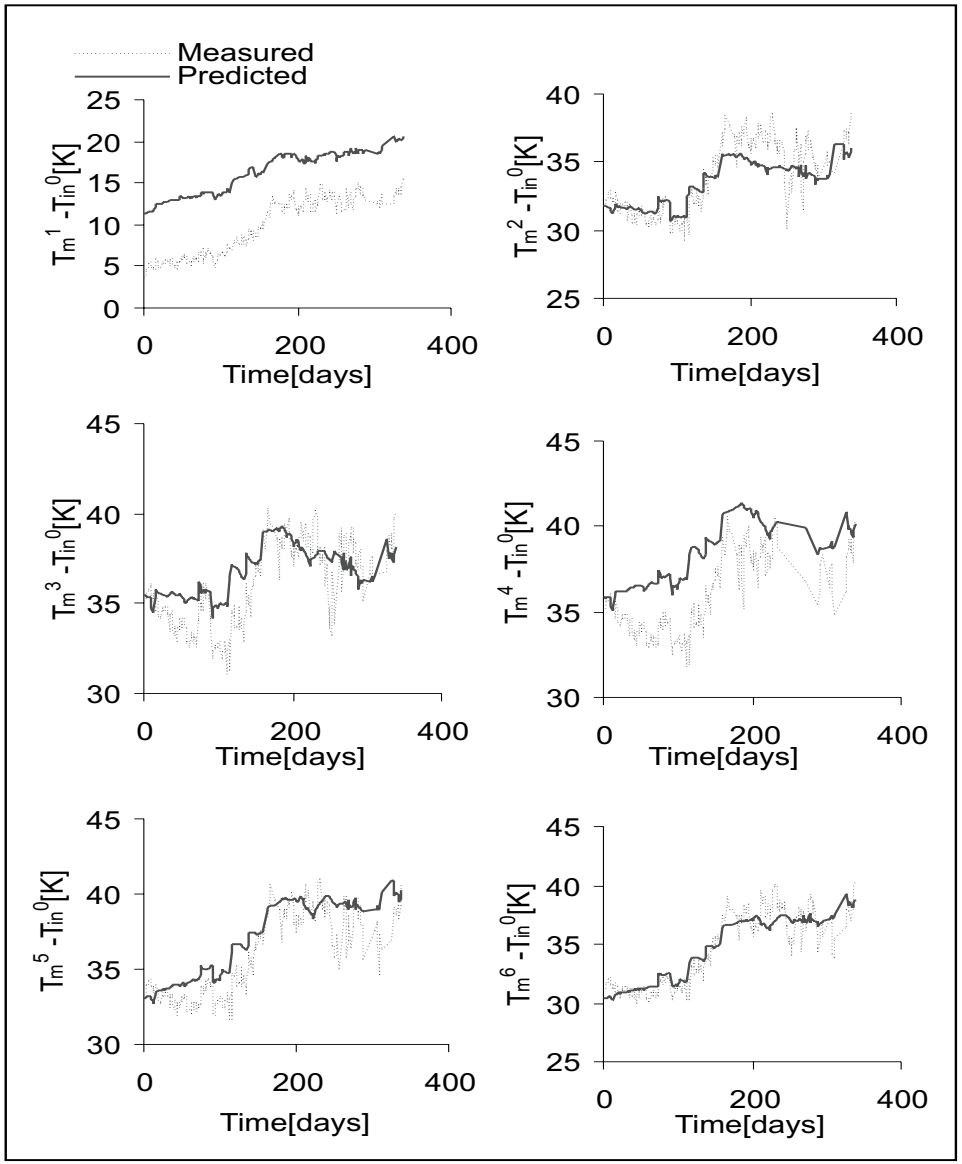

Figure 6.4. Estimated and measured relative reactor temperature at the 6 measuring points, case 1.

Case 2: Estimation without reactor exit temperature.

Estimation without T_{out} gave a good fit for the production rate, as can be seen in Figure 6.5. The deviation in methanol production is reduced by 75 per cent compared to case 1. The estimated reactor temperatures in Figure 6.6 fit the measurements well, except at the first point. The deviation at the first point is discussed previously. Some of the estimated model parameters are shown in Table 6.1. The model parameters K_d and E_d were estimated with 5 per cent standard deviation[2]. The deviation between estimated parameters and literature parameters in Equation. 2.45 is within one order of magnitude. This is acceptable, taking into account that the parameters are strongly correlated. Surprisingly, no measurable effect of water was found. The variations in feed compositions were probably not large enough to estimate the deactivation effect of water. Second order deactivation and a limiting activity a_{eq} that is different from zero is consistent with the literature on GPLE models (Bartholomew 1993).

Table 6.1
Estimated model parameters in case 2.

Parameter	m	n	a_{eq}
Value	2	0	a^1_{init}

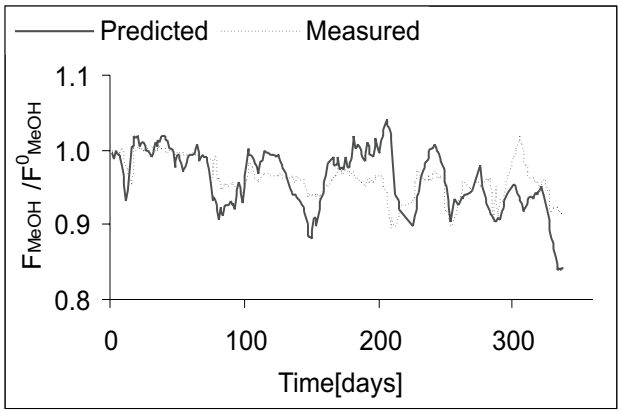

Figure 6.5. Estimated and measured relative methanol production rate, case 2.

[2]Values are confidential

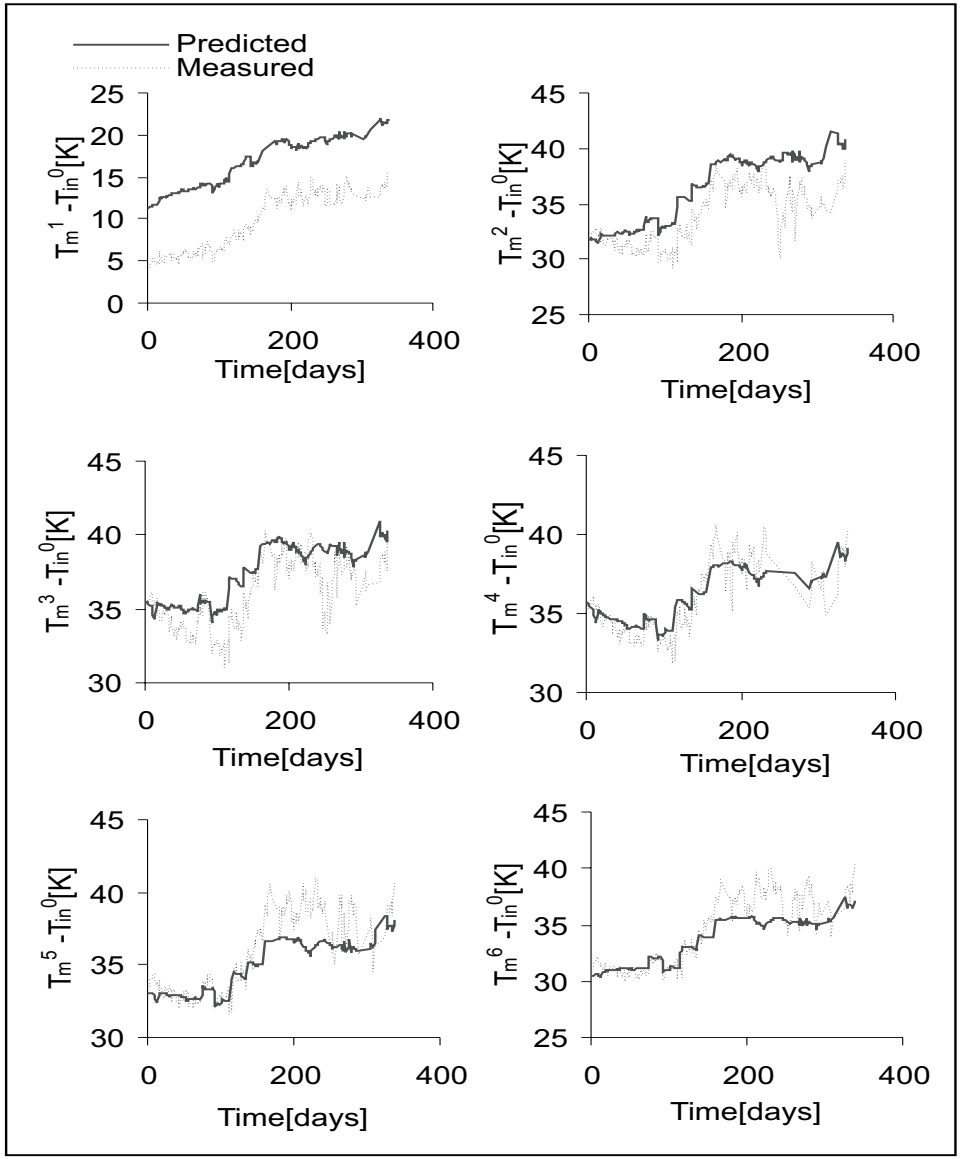

Figure 6.6. Estimated and measured relative reactor temperature at the 6 measuring points, case 2.

6.7 Conclusions

A deactivation model on the GPLE form was successfully fitted to historical process data from a limited period of time. The quality of parts of the process data were questioned. The reactor exit temperature was excluded from the estimation because of an unknown effect or a systematic measurement error. Several explanations of a deviation in the temperature measurements in the top of the reactor were proposed.

The estimation problem consists of two parts: estimation of the initial activity profile, $a_0(z)$, and estimation of the five model parameters in Equation 6.1. It was challenging to find the initial activity, because a continuous activity profile had to be estimated from only six measurements. Simplifications were used to achieve statistically significant estimates. Estimation of activity from process data at a given time is a problem that also occurs in state surveillance and model-based control and optimization. This problem needs to be given more attention.

The estimated model is a second order one. No measurable effect of water was found, probably because the variations in the feed compositions were too small. Standard deviation of the estimated parameters is between 5 and 10 per cent, well within the 20 per cent limit for optimization purposes found in Chapter 4.

The model parameters are not valid for the total catalyst lifetime because the deactivation process is fast in the beginning and slower after some time. Data from a longer period of time are needed to estimate a model that is valid over the total catalyst lifetime. It has been demonstrated that the historical process data contains enough information to estimate a catalyst deactivation model that includes the effect of time and temperature, but too little information to estimate the effect of the composition of the reaction mixture.

Chapter 7

Concluding Remarks

7.1 Conclusions

This section presents an overall discussion and concludes the thesis. A detailed discussion of the results are given in each chapter.

A rigorous pseudo-steady state model of the total methanol synthesis loop has been developed. The model has been verified against a design flow sheet and to some extent, validated against process data. Overall, a good agreement was found. The deactivation model and the phase separation are the weak areas of the model.

The methanol synthesis undergoing catalyst deactivation has been optimized with respect to coolant temperature and recycle rate over the catalyst lifetime. It is shown that it is necessary to consider the loop, not only the reactor, in the optimization. Important advantages of optimization compared to traditional operation are the ability to find the optimal operation if some of the variables in the optimization problem change, and second, the ability to track changes in the process by model updating and repeated optimization.

During modelling and optimization, it became evident that a good industrial-scale deactivation model for the methanol synthesis is needed. A sensitivity analysis of the dynamic optimization with regard to the deactivation model has been performed. It is shown that 20 per cent standard deviation in the deactivation parameters is sufficient for optimization purposes.

A deactivation model for the methanol synthesis catalyst is estimated from historical process data from a methanol plant from a limited period of time. No measurable effect of water was found, probably because the variations in the feed compositions were too small. The estimated model parameters are confidential. The model parameters are not valid for the total catalyst lifetime because the deactivation process is fast in the beginning and slower after some time. In order to obtain a model that is valid over the total catalyst lifetime, it is essential to use data from a longer period of time.

The main contribution of this thesis is a realistic, large-scale case study on modelling, estimation and dynamic optimization. Several researchers have studied optimal operation of fixed bed reactors experiencing catalyst deactivation. This work adopts a more realistic approach. A rigorous model is used of the total reactor system with recycle, with varying model parameters and thermodynamic properties. A thorough analysis of the process is employed to formulate the optimization problem. The actual time varying control variables in the reactor system, the recycle rate and coolant temperature, are optimized with regard to an economic objective, and path constrains on the reactor temperature are considered. A optimal operation strategy for the methanol synthesis has not been published before. Similar studies have probably been performed in industry without being published.

7.2 Directions for future work

Modelling

The methanol synthesis loop model should be validated against process data, and if necessary updated. The binary interaction coefficients in the phase separation are good candidates for updating. A better deactivation model for the methanol synthesis catalyst is needed. A good model should: 1) predict the correct deactivation rate under industrial conditions 2) include the effect of temperature variations 3) include the effect of water content variations. Accelerated laboratory experiments can probably be used to find the effect of temperature and water. Catalyst deactivation experiments in the laboratory require very clean gases to avoid catalyst poisoning. Process data from several years should be used to find the deactivation rate and order. The confidential policy of the companies manufacturing the catalyst is also an issue. Maybe these companies could publish deactivation models; as a slow rate of deactivation is an important competitive advantage.

Estimation

Data from a longer period of time should be used in the estimation. The method used to estimate the activity distribution in the reactor at a given time needs improvement.

Optimization

The optimization problem can be expanded to include pressure in the reactor, feed composition and feed flow rate as optimization variables.

Performance and robustness

The computation times for both estimation and optimization are too long for implementation in a control system. To improve computation efficiency the following two strategies are recommended: Several distributed intermediate variables in the reactor and pellet model can be eliminated by substitution. This will, however, reduce the logic structure and readability of the model. Second, the phase equilibrium calculation in the separator can be performed by an external thermodynamic package. *gPROMS* has an interface to the thermodynamic packages Multiflash and IK-CAPE, and Multiflash is licensed to academic users. This would improve both performance and robustness. A large number of auxiliary variables are needed to model the SRK equation of state in *gPROMS*. Since many of these variables have no direct physical meaning, it is difficult to obtain good initial guesses for them. Multiflash was not used in this work because the package was not available to academic when my reseach was being done.

7.3 Implementation issues

This section discusses how the dynamic optimization presented in Chapter 4 may be implemented in the control system of a methanol plant. It is not recommended to implement the calculated optimal control strategies presented in Chapter 4 directly. The work presented in this thesis can serve as a framework for implementing dynamic optimization in the control system of a methanol synthesis plant with feedback.

A control system of a chemical plant can be divided in an optimization layer and a control layer as shown in Figure 7.1. The optimization layer computes the desired reference values of the controlled variables (set points), and the control layers implement these set points. The purpose of the control layer is to stabilize

the plant at the optimal operation point and suppress short-term disturbances, while the optimization layer handles long-term disturbances and moves the plant to new optimal operating points. The control layer may consist of several layers, and a scheduling layer above the optimization layer often exists. The optimization usually consists of linear or nonlinear steady state models, with limited use of feedback (Skogestad and Postlethwaite 1996).

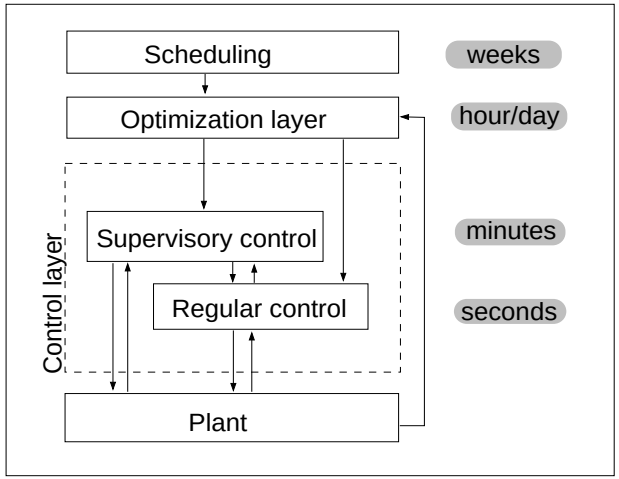

Figure 7.1. Typical control system hierarchy in a general plant.

The dynamic optimization should be implemented in the optimization layer with feedback to update the activity. The catalyst lifetime should be determined in the scheduling layer. A new catalyst deactivation model should also be estimated whenever the commercial catalyst type is changed. A shrinking horizon algorithm is proposed:

Optimization Algorithm
For each time step Δt:

- The catalyst activity is estimated from process measurements.
- The horizon is reduced by Δt .
- Optimal T_c and R profile is calculated and the first Δt part of the profile implemented.

The time step Δt in the optimization can be quite large; weeks or months. It is not necessary to implement the control variable profiles on-line because the time step is large. An uneven discretization of the control variables, with smaller intervals in the fist part, is beneficial in a shrinking horizon algorithm. The model with optimization routine can be interfaced to the control system by the *foreign process* option in *gPROMS*.

Appendix A

Estimation of Optimization Accuracy

Accuracy parameters used in the optimization are given in Table A.1. The optimization accuracy in Table A.1 is the absolute optimization accuracy of the objective function, which is a good estimate of the standard deviations of the objective function. The optimization accuracy in Tc was estimated by comparing the original optimization (a) with an optimization with increased accuracy (b).

$$s = \sqrt{\sum_{i=1}^{8} (Tc_i^a - Tc_i^b)/7} \tag{A.1}$$

Variance and standard deviation of the effects and mean of a response y with standard deviation s in a 2^2 design are calculated from the following equations:

$$V(mean) = \frac{s^2}{4} \tag{A.2}$$

$$V(effect) = V(\overline{y_+} - \overline{y_-}) = (\frac{1}{2} + \frac{1}{2})s^2 = s^2 \tag{A.3}$$

Estimates of the standard deviation in the optimization results, effects and means are given in Table A.2.

Table A.1
Optimization accuracy.

Optimization	Accuracy		
	Optimization	Simulation(relative)	Simulation (absolute)
a	1e-3	1e-5	1e-7
b	1e-3	1e-6	1e-7

Table A.2
Estimated standard deviation of optimization results, effects and means.

Response	s(response)	s(effect)	s(mean)
Obj	1e-3	1e-3	5e-3
Tc	0.35	0.35	0.18

References

Aksgaard, T.S., J.K. Nørskov, C.V. Ovesen and P. Stoltze (1995). A kinetic model of methanol synthesis. *Journal of Catalysis* **156**, 1995.

Asp (2000). *ASPEN PLUS*. 9.3-1 ed.

Asrar, M.T. and A.S. Moharir (1991). Optimal temp-time policy for a packed-bed adiabatic reactor using a deactivated catalyst. *Computers and Chemical Engineering*.

Bart, J.C.J. and R.P.A. Sneeden (1987). Copper-zinc oxide-alumina methanol catalysts revisited. *Catalysis Today* **2**, 1–124.

Bartholomew, C.H. (1993). Sintering kinetics of supported metals: New perspectives from a unifying GPLE treatment. *Applied Catalysis A: General* **107**, 1.

Barton, P.I. (1998). Dynamic optimization in a discontinuous word. *Industrial Engineering Chemical Research* **37**, 996–981.

Bequette, W. (1991). Nonlinear control of chemical processes. *Industrial Engineering Chemical Research* **30**, 1391.

Biegler, L.T. (1984). Solution of dynamic optimization problems by successive quadratic programming and orthogonal collocation. *Computers and Chemical Engineering* **8**(3/4), 243–248.

Biegler, L.T., I.E. Brossmann and A.W. Westerberg (1997). *Systematic Methods of Chemical Process Design*. Prentice Hall International Series in the Physical and Chemical Engineering Sciences. Prentice Hall, Inc.

Box, G.E.F., W.S. Hunter and J.S. Hunter (1975). *Statistics for experimenters*. John Wiley. New York.

Bozga, G. (1999). Optimization of direct and indirect cooled multiple-bed reactors experiencing catalyst decay. *Chemical Engineering Technology* **22**(1), 57–63.

Buzzi-Ferraris, G., E. Facchi, P. Forzatti and E. Tronconi (1984). Control optimization of tubular catalytic reactors with catalyst decay. *Industrial and Engineering Chemical Process Development* **23**, 126.

Chinchen, G.C., P.J. Denny, D.G. Parker, M.S. Spencer, K.C. Waugh and D.A. Whan (1987). Mechanism of methanol synthesis from $CO_2/CO/H_2$ mixtures over copper/zinc oxide/alumina catalysts - Use of C-14-labeled reactants. *Applied Catalysis* **30**, 330.

Cussler, E.L. (1984). *Diffusion, Mass transfer in fluid systems*. Cambridge University Press.

Cybulski, A. (1994). Liquid-phase methanol synthesis: Catalysts, mechanism, kinetics, chemical equilibrium, vapor-liquid equilibria, and modeling - a review. *Catalysis Review: Science and Engineering* **36**(4), 557–613.

Dixit, R.S. and N. Grant (1996). Dynamic operation of a butadiene dimerization reactor undergoing catalyst deactivation. *Canadian Journal of Chemical Engineering* **74**(5), 652.

Edgar, T.F. and D.H. Himmelblau (1989). *Optimization of Chemical Processes*. McGraw-Hill.

Elnashaie, S.S.E.H and M.N. Abdel-Hakim (1988). Optimal feed temperature control for fixed bed catalytic reactors experiencing catalyst deactivation - a heterogeneous model. *Computers and Chemical Engineering* **12**(8), 787–790.

Forzatti, P. and L. Lietti (1999). Catalyst deactivation. *Catalysis Today* **52**, 165–181.

Froment, G.F. and K.B. Birchoff (1990). *Chemical Reaction Analysis and Design*. John Wiley and Son.

Gonzalez-Velasco, J.R., M.A. Gutierrez-Ortiz and A. Romero (1985). Optimization by lumped control of reactors with Langmuir-Hinshelwood catalyst deactivation. *The Canadian Journal of Chemical Engineering* **63**, 314–321.

Gonzalez-Velasco, J.R., M.A. Gutierrez-Ortiz, J.A. Gonzalez-Marcos, N. Amadeo, M-A. Laborde and M. Paz (1992). Optimal inlet temperature trajectories for adiabatic packed reactors with catalyst decay. *Chemical Engineering Science* **47**(2), 105–112.

Gonzalez-Velasco, J.R., M.A. Gutierrez-Ortiz, J.I. Gutierrez-Ortiz and J.A. Gonzalez-Marcos (1987). Optimal temperature policies by distributed control of reactors with LHHW catalyst deactivation. *The Canadian Journal of Chemical Engineering* **65**, 36–41.

Gonzalez-Velasco, J.R., M.A. Gutierrez-Ortiz, J.I. Gutierrez-Ortiz and J.A. Gonzalez-Marcos (1990). Analysis of the lumped and distributed optimal temperature trajectories for paced-bed reactors with concentration dependent catalyst deactivation. *The Canadian Journal of Chemical Engineering* **68**(5), 860–866.

Gonzalez-Velasco, J.R., M.A. Gutierrez-Ortiz, J.I. Gutierrez-Ortiz and J.A. Gonzalez-Marcos (1991). Analysis of combined temperature and space-time trajectories to maintain constant the exit conversion of fixed-bed reactors with catalyst decay. *The Canadian Journal of Chemical Engineering* **47**(2), 105–112.

Graaf, G.H., E.J. Stamhuis and A.A.C.M. Beenackers (1988). Kinetics of low-pressure methanol synthesis. *Chemical Engineering Science* **43**, 3185–3195.

Graaf, G.H., P.J.J.M. Sijtsema, E.J. Stamhuis and G.E.H. Joosten (1986). Chemical equilibria in methanol synthesis. *Chemical Engineering Science* **41**(11), 2883–2890.

Hansen, J.E. (1998). Plant Wide Dynamic Simulation and Control of Chemical Processes. PhD thesis. Technical University of Denmark.

Hillestad, M. (1995). Fixed bed reactor modelling, methanol synthesis. Internal Report, Statoil.

Holmen, A. (1996). *Heterogen katalyse*. Department of Industrial Chemistry, Norwegian University of Science and Technology.

Hyp (2000). *Hysys*. 1.2.3 ed.

Islam, K.A. and W.E. Earl (1990). Deactivation of ICI low temperature methanol catalyst in an industrial reactor. *The Canadian Journal of Chemical Engineering*.

Khanna, R. and J.H. Seinfeld (1987). Mathematical modeling of packed bed reactors: Numerical solutions and model development. *Advances in Chemical Engineering*.

Kroner, A., W. Marquart and E.D. Gilles (1997). Getting around consistent initialization of DAE systems?. *Computers and Chemical Engineering* **21**(2), 145–158.

Kuechen, C. and U. Hoffmann (1993). Investigation of simultaneous reaction of carbon monoxide and carbon dioxide with hydrogen on a commercial copper/zinc oxide catalyst. *Chemical Engineering Science* **48**(22), 3767–3776.

Kung, H.H. (1992). Deactivation of methanol synthesis catalyst - a review. *Catalysis Today* **11**, 443–453.

Ladebeck, J. (1993). Improve methanol synthesis. *Hydrocarbon Processing* pp. 89–91.

Lange, J.-P. (2001). Methanol synthesis: a short review of technology improvements. *Catalysis Today* **64**(1-2), 3.

Løvik, I., M. Hillestad and T. Hertzberg (1998). Long term dynamic optimization of a catalytic reactor system. *Computers and Chemical Engineering* **22**, 707. Supplement.

Løvik, I., M. Hillestad and T. Hertzberg (1999). Modeling and optimization of a reactor system with deactivating catalyst. *Computers and Chemical Engineering* **23**, 839. Supplement.

Løvik, I., M. Hillestad and T. Hertzberg (2000). Sensitivity in optimization of a reactor system with deactivating catalyst. In: *European Symposium of Computer Aided Process Engineering -10* (S.Pierucci, Ed.). p. 517.

Løvik, I., M. Rønnekleiv, O. Olsvik and T. Hertzberg (2001). Estimation of a deactivation model for the methanol synthesis catalyst from historic process data. In: *Computer Aided Process Engineering: The* 11^{th} *European Symposium* (S. Jorgensen and R. Gani, Eds.).

Lurgi (1995). Integrated low pressure methanol process. Technical report. Lurgi Öl Gas Chemie BmbH. Frankfurt am Main, Germany.

Majer, C., W. Marquart and E.D. Gilles (1995). Reinitialization of DAE's after discontinuities. *Computers and Chemical Engineering* **19**, 507–512. Supplement.

Methanex (1998). Current methanol price. http://www.methanex.com.

Methanex (2000*a*). Emerging energy. http://www.methanex.com.

Methanex (2000*b*). Methanol. http://www.methanex.com.

Methanol (1997). *Hydrocarbon Processing* **Petrochemical Processes '97**, 139.

Muhler, M., E. Törnquist, L.P. Nielsen, B.S. Clausen and H. Topsøe (1994). On the role of adsorbed atomic oxygen and CO_2 in copper-based methanol synthesis catalysts. *Catalysis Letter* **25**(1-2), 1–2.

Naess, L., A. Mjaavatten and J.-O. Li (1993). Using dynamic process simulation from conception to normal operation of process plants. *Computers and Chemical Engineering* **17**, 585–600.

Natta, G. (1955). Synthesis of methanol. In: *Catalysis* (P.H. Emmett, Ed.). Vol. III. Chap. 8, p. 349. Reinhold.

NFR (2000). Kjemisk konvertering av naturgass - sluttrapport. Research Council of Norway. Oslo.

Ognue, A.F. and W.H. Ray (1971). Optimal control policies for tubular reactors experiencing catalyst decay. *AIChE Journal* **17**(1), 43.

Oh, M. and C.C. Pantelides (1996). A modelling and simulation language for combined lumped and distributed parameter systems. *Computers and Chemical Engineering* **20**, 661–663.

Øverli, J. M. (1992). Compendium in course no. 62024 Gassturbiner og turbokompressorer. Department of Thermal Energy, Norwegian Institute of Technology.

Ovesen, C.V., B.S. Clausen, J. Schiøtz, P. Stoltze, H. Topsøe and J.K. Nørskov (1997). Kinetic implications of dynamical changes in catalyst morphology during methanol synthesis over Cu/ZnO catalyst. *Journal of Catalysis* **168**, 133–142.

Pantelides, C.C. and P.I. Barton (1993). Equation oriented dynamic simulation: Current status and future perspectives. *Computers and Chemical Engineering* **17S**, 263–285.

PSE (1998). *gPROMS Training Course I.*

PSE (2000*a*). *gPROMS Advaced Users's Guide.* 1.8.0 ed.

PSE (2000*b*). *gPROMS Users's Guide.* 1.8.0 ed.

Rahimpour, M.R., J. Fathikalajahi and A. Jahanmiri (1998). Selective kinetic deactivation model for methanol synthesis from simultaneous reaction of CO_2 and CO with H_2 on a commercial copper/zinc oxide catalyst. *The Canadian Journal of Chemical Engineering* **76**, 153–761.

Reid, R.C., J.M. Prausnitz and B.E. Poling (1988). *Properties of gases and liquids.* McGraw-Hill.

Roberts, G.W., D.M. Brown, T.H. Hsiung and J.J. Lewnard (1993). Deactivation of methanol synthesis catalyst. *Industrial & Engineering Chemistry* **32**, 1610–1621.

Sahibzada, M., D. Chadwick and I.S. Metcalfe (1997). Methanol synthesis from CO_2/H_2 over Pd-promoted $Cu/ZnO/Al_20_3$ catalyst: kinetics and deactivation. In: *Natural Gas Conversion IV* (M. de Pontes, R.L Espinoza, C.P. Nicolaides, J.H. Scholz and M. Surell, Eds.). Vol. 107 of *Studies in Surface Science and Catalysis.* Elsevier Science B. V.

Satterfield, C.N. (1980). *Heterogeneous Catalysis in Practice.* McGraw-Hill.

Schiesser, W.E. (1991). *The Numerical Method of Lines.* Academic Press.

Skogestad, S. and I. Postlethwaite (1996). *Multivariable Feedback Control - Analysis and Design.* Wiley.

Skrzypek, J., J. Sloczynski and S. Ledakowicz (1994). *Methanol Synthesis.* Polish Scientific Publishing.

Skrzypek, J., M. Lachowska and H. Moroz (1991). Kinetics of methanol synthesis over commercial copper/zinc oxide/alumina catalysts. *Chemical Engineering Science* **46**(11), 2809–2813.

Statoil (2000*a*). Allianse for metanol. http://www.statoil.com.

Statoil (2000*b*). Industrianlegg p tjeldberodden. http://www.statoil.com.

Statoil (2000*c*). Samarbeid om brenselsceller. http://www.statoil.com.

Strand, S. (1991). Dynamic optimization in state space predictive control. Dr.Ing. Thesis, Norwegian Institute of Technology.

Supp, E. (1981). Improved methanol process. *Hydrocarbon Processing.*

Vanden Bussche, K.M. and G.F. Froment (1996). A steady-state kinetic model for methanol synthesis and the water gas shift reaction on a commercial $Cu/ZnO/Al_2O_3$ catalyst. *Journal of Catalysis* **161**, 1–10.

Vassiliadis, V.S. (1993). Computational Solution of Dynamic Optimization Problems with General Differential-Algebraic Constrains. PhD thesis. Imperial College. London.

Vassiliadis, V.S., R.W.H. Sargent and C. Pantelides (1994*a*). Solution of a class of multistage dynamic optimization problems, Part II - Problems with path constrains. *Industrial Engineering Chemical Research* **33**, 2123–2133.

Vassiliadis, V.S., R.W.H. Sargent and C.C. Pantelides (1994*b*). Solution of a class of multistage dynamic optimisation problems, part i - problems without path constraints. *Industrial Engineering Chemical Research* **33**, 2111–2122.